

A SIMPLE NEW ELEMENT FOR LINEAR AND  
NONLINEAR ANALYSIS OF PIPING SYSTEMS

by

CARLOS ALBERTO DE ALMEIDA

B.S., Pontifícia Universidade Católica, RJ, Brasil  
(1972)

M.S., Pontifícia Universidade Católica, RJ, Brasil  
(1976)

SUBMITTED TO THE DEPARTMENT OF  
MECHANICAL ENGINEERING IN PARTIAL FULFILLMENT  
OF THE REQUIREMENTS FOR THE DEGREE OF

DOCTOR OF PHILOSOPHY

at the

MASSACHUSETTS INSTITUTE OF TECHNOLOGY

February 1982

© Carlos Alberto de Almeida, 1982

The author hereby grants to M.I.T. permission to reproduce  
and distribute copies of this thesis document in whole or in  
part.

Signature of Author \_\_\_\_\_  
Department of Mechanical Engineering

Certified by \_\_\_\_\_  
Klaus-Jürgen Bathe  
Thesis Supervisor

Accepted by \_\_\_\_\_  
Warren Rohsenow  
Chairman, Departmental Graduate Committee

Archives  
MASSACHUSETTS INSTITUTE  
OF TECHNOLOGY

JUN 7 1982

LIBRARIES

A SIMPLE NEW ELEMENT FOR LINEAR AND NONLINEAR ANALYSIS  
OF PIPING SYSTEMS

by

Carlos Alberto de Almeida

Submitted to the Department of Mechanical Engineering on November 20, 1981 in partial fulfillment of the requirements for the Degree of Doctor of Philosophy.

ABSTRACT

The formulation of a simple and effective displacement based pipe bend element is presented. The displacement assumptions are cubically varying axial, bending and torsional beam displacements along the axis of the elbow with plane sections remaining plane, and pipe radial displacement patterns to include ovalization effects. The amount of cross-sectional ovalization is assumed to vary cubically along the length of the element. The element can be employed to model elbows (with or without internal pressure) of different curvatures, elbows joining straight pipe sections and elbows connected to flanges. The appropriate strain terms required for the element formulation are identified using Novozhilov's shell theory. To enforce the required continuity conditions between elements a penalty procedure is developed, and the internal pressure effects are accounted for by including in the formulation the work performed by the pressure. A total Lagrangian formulation is adopted to include some geometric nonlinear effects, while a bilinear elastic-plastic material model is employed for material nonlinear analysis. The results of various sample solutions are presented, in which the response predicted using the new element is compared and evaluated with other available experimental and analytical/numerical solutions. These sample analyses illustrate the general effectiveness and applicability of the element.

Thesis Supervisor: Dr. Klaus-Jürgen Bathe  
Title: Associate Professor of Mechanical Engineering

## ACKNOWLEDGMENTS

I wish to express my appreciation to Professor K.J. Bathe for his continued interest, encouragement and guidance during the course of this research. Through his active support I was able to experience the challenge and the excitement of working in the field of finite element analysis. I am also grateful to the other members of my thesis committee, Professor M.P. Cleary and Professor J.E. Meyer, for their valuable help during this study.

I would like to thank the "Comissão Nacional de Energia Nuclear - CNEN" and the "Pontifícia Universidade Católica do Rio de Janeiro - PUC/RJ", of Brazil, for their financial support during my doctoral program. To Ms. T. Nolan my special thanks for her accurate typing of this thesis.

Finally, but not least, I am extremely grateful to my wife Nair, who with her love and continued understanding supported these years of study at M.I.T. This thesis is dedicated to our children Veronica, Igor and Priscilla.

## TABLE OF CONTENTS

	<u>PAGE</u>
ABSTRACT . . . . .	2
ACKNOWLEDGEMENTS . . . . .	3
TABLE OF CONTENTS . . . . .	4
LIST OF TABLES . . . . .	7
LIST OF FIGURES . . . . .	8
NOTATION . . . . .	12
1. INTRODUCTION . . . . .	13
2. ON THE THEORIES OF PIPE MODELING . . . . .	19
2.1 The Theory of von Kármán . . . . .	19
2.1.1 Von Kármán assumptions . . . . .	19
2.1.2 Von Kármán analysis . . . . .	22
2.2 Novozhilov's Theory of Thin Shells . . . . .	24
2.2.1 General definitions and assumptions . . . . .	26
2.2.2 Kinematic relations . . . . .	27
2.2.3 Deformations of a shell and deformations of its midsurface . . . . .	30
2.2.4 Evaluation of the ovalization strains . . . . .	36
3. FINITE ELEMENT LINEAR FORMULATION OF THE ELBOW ELEMENT	48
3.1 Evaluation of the Strain-Displacement Matrix . . . . .	49
3.1.1 Element geometry and displacement interpolations assuming no ovalization . . . . .	51
3.1.2 Element displacement interpolations including ovalization . . . . .	55
3.1.3 Displacement derivatives . . . . .	56

TABLE OF CONTENTS (Continued)

	<u>PAGE</u>
3.2 Element Constitutive Matrix . . . . .	62
3.3 Element Completeness and Compatibility Considerations, . . . . .	63
4. END-EFFECTS IN THE ELBOW ELEMENT FORMULATION . . . . .	67
4.1 The Penalty-Function Method . . . . .	68
4.2 Imposition of Continuity on Derivative of Pipe Skin Radial Displacement . . . . .	71
4.2.1 Fixity condition . . . . .	73
4.2.2 Continuity condition . . . . .	78
5. INTERNAL PRESSURE EFFECTS IN PIPES . . . . .	82
5.1 The Internal Pressure Work. . . . .	83
5.1.1 Calculation of area change in a deformed pipe section . . . . .	84
5.2 The Elbow Element Formulation with Internal Pressure. . . . .	87
6. ELBOW ELEMENT FORMULATION FOR NONLINEAR ANALYSES . . . . .	90
6.1 A Formulation for Geometric-Nonlinear-Only Analysis. . . . .	90
6.1.1 Finite element formulation (beam displace- ment modes only) . . . . .	97
6.1.2 Finite element discretization. . . . .	99
6.2 Formulation for Elastic-Plastic Analysis. . . . .	105
6.3 Numerical Integration . . . . .	110
7. SAMPLE ANALYSES. . . . .	113

TABLE OF CONTENTS (Continued)

	<u>PAGE</u>
7.1 Linear Analysis of Two Cantilevered Pipe Cross-Section Beams . . . . .	113
7.2 Analysis of a Pipe Bend . . . . .	116
7.3 In-Plane and Out-of-Plane Bending Analysis of a Second Pipe Bend . . . . .	121
7.4 Analysis of Pressurized Bends . . . . .	126
7.5 Convergence of Stress Continuity, and Effect of Penalty Parameter Size - Some Studies with the Elbow Element . . . . .	129
7.6 Analysis of a Flanged Pipe Bend . . . . .	138
7.7 Analyses of a Pipe Bend for Different End Constraints . . . . .	138
7.8 Elastic-Plastic Analysis of Whatham Pipe Bend.	145
7.9 Large Displacement Analysis of a Cantilever Pipe Section Beam . . . . .	151
8. CONCLUSIONS. . . . .	157
REFERENCES . . . . .	160
APPENDIX A . . . . .	167

## LIST OF TABLES

<u>TABLE</u>		<u>PAGE</u>
2.1	NUMBER OF OVALIZATION SHAPE FUNCTIONS TO BE USED IN RITZ ANALYSIS (AND ELBOW FORMULATION)...	25
3.1	THE TWELVE LOWEST EIGENVALUES OF A FOUR-NODE 30 DEG. BEND ELBOW ELEMENT .....	65
4.1	USE AND CONVERGENCE OF THE PENALTY-FUNCTION METHOD .....	70
4.2	SOLUTIONS OF SIMPLY SUPPORTED BEAM FOR DIFFERENT SIZES OF $\alpha$ .....	75
6.1	MATRICES USED IN THE ELBOW ELEMENT FORMULATION (TOTAL LAGRANGIAN FORMULATION).....	101
7.1	STRAIGHT PIPE ELEMENT STIFFNESS MATRIX ASSOCIATED WITH OVALIZATION DEGREES-OF-FREEDOM (1st VON KARMAN MODE) .....	132
7.2	REQUIRED SOLUTION TIMES IN CASE I/FLANGED AT A AND B, ANALYSIS USING THE ELBOW, PLATE AND SHELL ELEMENT IDEALIZATIONS. (SOLUTION TIME LOG IN SECONDS) .....	150

## LIST OF FIGURES

<u>FIGURES</u>		<u>PAGE</u>
2.1	Coordinate Systems and Displacements of Elbow...	21
2.2	The Pipe Bend Treated as a Doubly-curved Shell..	28
2.3	The Shell Displacement Related to Its Midsurface Displacement .....	31
2.4	Longitudinal Strains in Straight and Curved Pipes due to Axial and Bending Displacements....	39
2.5	Stretching and Bending of a Longitudinal Fiber of the Bend due to Cross-Sectional Ovalization.....	41
2.6	Transverse Strains due to Cross-Sectional Deformations.....	43
2.7	Shear Mechanisms in the Pipe-Shell Formulation.....	45
3.1	Geometry of Pipe Elbow Element.....	50
3.2	Degrees-of-freedom and Interpolation Functions of Pipe Without Ovalization.....	53
4.1	The Simply Supported Beam Considered.....	74
4.2	Interactions Considered in Analyses.....	77
5.1	Area Change of an Ovalized Cross-Section.....	85
6.1	Stress-strain Relation in a Simple Tension Test.....	108
7.1	Linear Analysis of Two Cantilvered Pipe Beams..	115
7.2	Pipe Bend and Finite Element Model Used.....	117
7.3	Longitudinal Stresses at Midsurface of Bend in Fig. 7.2 (No End Constraints).....	118
7.4	Longitudinal Stresses at Inside Surface of Bend in Fig. 7.2 (No End Constraints).....	119



LIST OF FIGURES (Continued)

<u>FIGURES</u>		<u>PAGE</u>
7.5	Hoop Stresses at Inside Surface of Bend in Fig. 7.2 (No End Constraints).....	120
7.6	Longitudinal Stresses at Outside Surface and at $\theta=45^\circ$ of Smith & Ford Bend Subjected to an In-plane Bending Moment.....	122
7.7	Hoop Stresses at Outside Surface and at $\theta=45^\circ$ of Smith & Ford Bend Subjected to an In-plane Bending Moment.....	123
7.8	Longitudinal Stresses at Outside Surface and at $\theta=45^\circ$ of Smith & Ford Bend Subjected to an Out-of-Plane Bending Moment.....	124
7.9	Hoop Stresses at Outside Surface and at $\theta=45^\circ$ of Smith & Ford Bend Subjected to an Out-of-Plane Bending Moment.....	125
7.10	Analysis of Pressurized Bends.....	127
7.11	Stiffening Effects on Pipes due to Internal Pressure.....	128
7.12	Straight Cantilever Pipe Test Problem.....	130
7.13	Predicted Response of Cantilevered Pipe Using Four Equal Elements.....	131
7.14	Predicted Response of Cantilevered Pipe Using Fine Finite Element Idealization (same response obtained using 16 elements of length 0.3 in., or 6 elements of 0.3 in, and 1 element of 3.0 in.).....	133
7.15	Element Size Study for the Analysis of Bends.....	134
7.16	Effect of Size of Penalty Parameter on Predicted Response of Straight Cantilevered Pipe.....	136
7.17	Whatham Pipe Bend, $E$ =Young's Modulus, $\nu$ =Poisson's Ratio.....	139
7.18	Predicted Flexibility Factors for Whatham Pipe	

LIST OF FIGURES (Continued)

<u>FIGURES</u>	<u>PAGE</u>
Bend.....	140
7.19 Predicted Longitudinal Stresses at $\theta=45^\circ$ and at Outside Surface in Analysis of Whatham Pipe Bend, $R=250$ mm.....	141
7.20 Predicted Circumferential Stresses at $\theta=45^\circ$ and at Outside Surface in Analysis of Whatham Pipe Bend, $R=250$ mm.....	142
7.21 Predicted Longitudinal Stresses at $\theta=45^\circ$ and at Outside Surface in Analysis of Whatham Pipe Bend, $R=375$ mm.....	143
7.22 Predicted Circumferential Stresses at $\theta=45^\circ$ and at Outside Surface in Analysis of Whatham Pipe Bend, $R=375$ mm.....	144
7.23 Pipe Bends and Finite Element Models Used.....	146
7.24 Predicted Ovalization Response of Bends Defined in Fig. 7.25. Ovalization Measured at $\phi=90^\circ$ .....	147
7.25 Plate Element Model Used in Case II/Flanges at A and B Analysis.....	148
7.26 Shell Element Model Used in Case I/Flanges at A and B Analysis.....	149
7.27 Responses of Elbow and Shell Element Models in the Analysis of Whatham Pipe Bend. $M_0$ is the Limit Load for Yield Initiation.....	152
7.28 Predicted Longitudinal and Circumferential Stresses at $\theta = 45^\circ$ and at Outside Surface ( $M/M_0 = 1.4$ ).....	153
7.29 Predicted Longitudinal and Circumferential Stresses at $\theta=45^\circ$ and at Outside Surface ( $M/M_0 = 2.0$ ).....	154

LIST OF FIGURES (Continued)

<u>FIGURE</u>		<u>PAGE</u>
7.30	Predicted Longitudinal and Circumferential Stresses at $\theta = 45^\circ$ and at Outside Surface ( $M/M_0 = 2.5$ ).....	155
7.31	Large Displacement Response of a Cantilever using One 4-node Element.....	156
A.1	The Pipe Midsurface Normal Along the Lines of Principal Coordinates.....	168

## NOTATION

All notation is defined in the text when first used. The following is only a list of some frequently used conventions.

A bar ( $\bar{\phantom{x}}$ ) on a vector or tensor quantity means that the quantity is referred to or measured in a local coordinate system.

The convention employed for tensor and vector superscripts and subscripts is the following:

(a) a left superscript denotes the time of the configuration in which the quantity occurs.

(b) a left subscript can have two different meanings. If the quantity considered is a derivative, the left subscript denotes the time of the configuration in which is measured the coordinate with respect to which it is differentiated. Otherwise, the left subscript denotes the time of the configuration in which the quantity is measured.

(c) right lower case subscripts denote the components of a tensor or vector referred to a fixed Cartesian coordinate system ( $i, j, \dots = 1, 2, 3$ ). Differentiation is denoted by a right lower case subscript preceded by a comma, with the subscript indicating the coordinate with respect to which it is differentiated.

## 1. INTRODUCTION

The structural integrity and cost of pipelines are of major concern in the nuclear, oil and various other industries. Piping structures can be subjected to severe thermal, seismic and other mechanical loads, and for these reasons, an increasing amount of attention has been given to their analyses [1].

In the analysis of piping structures it is highly desirable to keep the induced loads on pressure vessels and other piping supports as small as possible, i.e., to allow most of the thermal expansion of the piping system to take place without inducing loads. This expansion is accommodated mainly by the curved pipe components (elbows), which have a high degree of flexibility compared to the straight components. Namely, in addition to undergoing the usual beam deformations, the elbows also ovalize. Although this ovalization of the cross-section can occur in both curved and straight pipes, it affects the flexibility of the pipe bend to a great amount and must be properly modeled in the analysis [2-14].

Because of the importance and the difficulties that lie in the analysis and design of pipe bends, much research has been devoted to the study of their structural behavior. In these investigations, during recent years, also various simple to complex finite element models of pipe bends have been proposed. However, all these structural models have serious limitations either with regard to their accuracy in predicting pipe stresses

and displacements or the cost of using them.

The simplest and widely used approach in the linear analysis of pipelines is to model a pipe bend using simple curved beam theory and scale the stiffness constants and calculated stresses using factors that account for the ovalization of the pipe cross-section and the pipe internal pressure [14, 15]. If the effect of the internal pressure can be neglected, the constants used in this analysis are, in essence, the von Kármán flexibility and stress intensification factors [2]. These constants were derived by von Kármán for in-plane loading and later by Vigness using the von Kármán analysis procedure for out-of-plane loading [4] with a number of assumptions. A major point is that von Kármán considered a differential length of the elbow, hence the internal bending moment and the amount of cross-sectional ovalization are assumed constant along the pipe bend. The conditions of a varying magnitude in the internal bending moment, of no ovalization at an end of the elbow (flanged condition) as well as interaction effects between pipes of different radii cannot be taken into account with accuracy.

Because of the limitations of the foregoing beam analysis of pipe bends, various refined analytical and finite element models have been proposed [11, 16-18]. In essence, these models use shell theory to describe the behavior of the pipe bend. Clark and Reissner proposed equations that treat pipe bends as part of a torus and proposed an asymptotic solution for the stress

and flexibility factors [8]. This approach removes some of the assumptions of the von Kármán analysis but is not effective in the analysis of general pipelines. The greatest potential for the general analysis of pipe bends lies in the use of the finite element method [19]. Pipe elbows are currently being modeled using three-dimensional elements, general shell elements and special elbow-shell elements [20-27]. Using either three-dimensional or general shell elements, in theory, any elbow can be modeled very accurately by using a fine enough finite element mesh. However, in practice, such an analysis of a simple elbow involves typically of the order of a thousand finite element equilibrium equations that need be operated upon, which means that the linear analysis of a single elbow is very costly, the nonlinear analysis of a single elbow is prohibitively expensive and the nonlinear analysis of an assemblage of elbows is clearly beyond the current state-of-the-art of computational tools.

In order to reduce the number of finite element variables special elbow-shell elements have been proposed [26]. Although these elements are more cost-effective in use, they still involve a relatively large number of solution variables and are subject to some major shortcomings, for example, the axial variation of the magnitude of ovalization is still neglected [27] or the rigid body mode criterion is not satisfied [24].

#### Scope of Present Study

The above brief overview on different approaches used in

the finite element analysis of pipelines shows that the effectiveness of an analysis is the result of a trade-off between the accuracy required and the computational cost expended. This is particularly the case in nonlinear analysis, and there is much need for more accurate and effective approaches.

The objective of this investigation is to present the formulation of a new elbow element that is simple and effective and predicts accurately the significant displacements and stresses in piping structures. The elbow element is a four-node displacement based finite element with axial, bending, and torsional deformations and the von Kármán ovalization deformations all varying cubically along the elbow length. Basically, in the formulation of the element the deformation in the plane of the cross-section are added to the general beam deformations making the element a very natural extension and generalization of von Kármán's approach. Because of the lack of the digital computer, von Kármán could only perform the Ritz analysis in the hoop direction of the pipe, but it is interesting to note that von Kármán "urges us engineers to become familiar with the Ritz method, because the method is simple and ideal to develop approximate solutions to complex practical problems" (quoted from Ref. [2]). The formulation of the elbow element extends the work of von Kármán in that the Ritz method (the displacement-based finite element method) is used to take also the lengthwise variation of ovalization into account, to include



the appropriate shear and bending deformations coupled with the deformations of the cross-section, and relax some other von Kármán assumptions. The actual analysis presented in this study is only possible because of the availability of high speed digital computers, and it is performed efficiently using finite element numerical procedures [28].

An examination of the important concepts in von Kármán's theory and its generalization to model interaction effects between pipes are presented in Chapter 2. The important strain terms to enhance von Kármán analysis are identified using a thin shell theory specialized to the analysis of elbow geometries.

In Chapter 3, the formulation of the elbow for linear infinitesimal displacement analysis is presented. The formulation of a four-node displacement-based pipe-section beam element is extended by including the ovalization terms in the displacement description.

The additional terms to be included show that it is necessary to enforce the continuity of the derivatives in the pipe skin radial displacements with respect to the longitudinal coordinate of the pipe. This continuity between elements is imposed using a penalty procedure discussed in Chapter 4.

In Chapter 5, the effects of internal pressure are taken into account in the formulation of the element by adding to its total strain energy the work done by the internal

pressure during the deformation of the cross-section. This formulation is applicable to the elbow element with or without end constraints.

In Chapter 6, we consider the derivation of the elbow element matrices for large displacement and materially nonlinear analyses. A total Lagrangian formulation is developed, in which, however, a number of assumptions are made as discussed in Chapter 6. This formulation represents a fine step towards an effective large displacement analysis capability using the basic concepts already employed in linear analysis.

The numerical results obtained in the analyses of some sample problems are presented in Chapter 7. The analyses demonstrate the validity of the employed formulation and the capabilities of the element. The numerical responses obtained using the element are compared to analytical, experimental and other available numerical solutions.

Finally the conclusions of this study are drawn and recommendations for further investigations are given.

## 2. ON THE THEORIES OF PIPE MODELING

Since the success of von Kármán's theory including the effect of the ovalization of the cross-section in the analysis of a bend, either very simple or quite refined analytical models have been proposed to account for end (interaction) effects such as produced by flanges or tangent pipes. In the search for a more general formulation to include the interaction effects, shell solutions have been widely used in the recently proposed models. In this chapter, first, the theory of von Kármán is reviewed and then the theory of Novozhilov of general thin shells is presented for piping analysis. The objective is to summarize the various assumptions used in von Kármán's pioneering work and to identify the additional strain terms that are important when interaction effects are to be included in the model.

### 2.1 The Theory of von Kármán

The formulation of the pipe elbow element that includes the effects of cross-sectional ovalization can be regarded as an extension of von Kármán analysis. For the sake of completeness of this presentation, the major concepts of von Kármán's model are briefly summarized in this section.

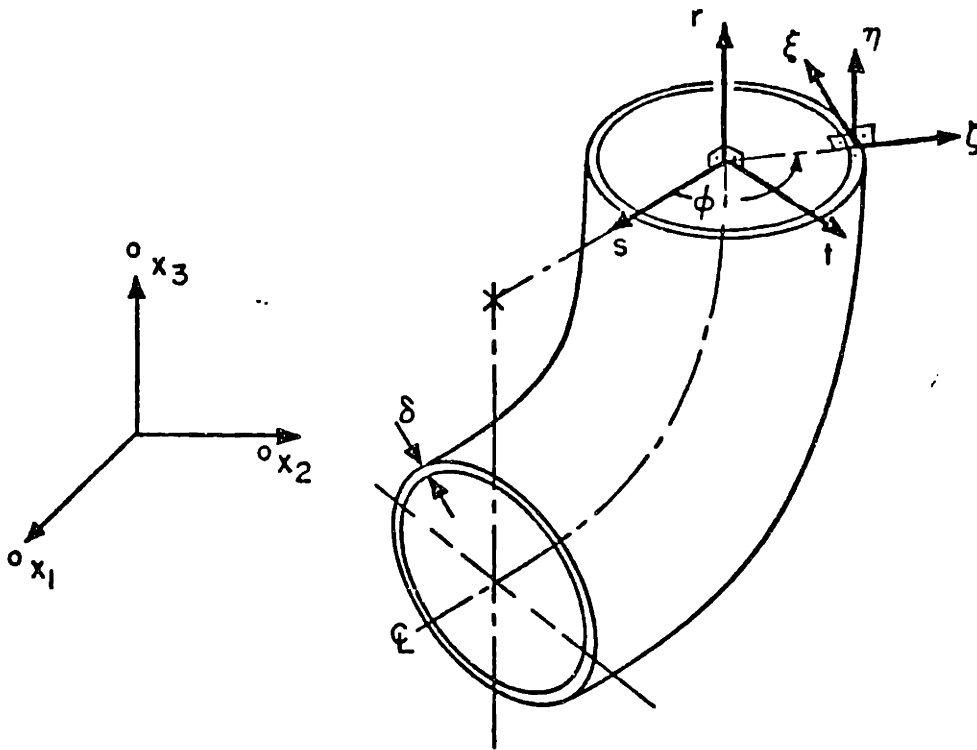
#### 2.1.1 Von Kármán assumptions

In his analysis of pipe elbows von Kármán recognized that in addition to the usual curved beam theory strain components, two additional strain components also need be considered

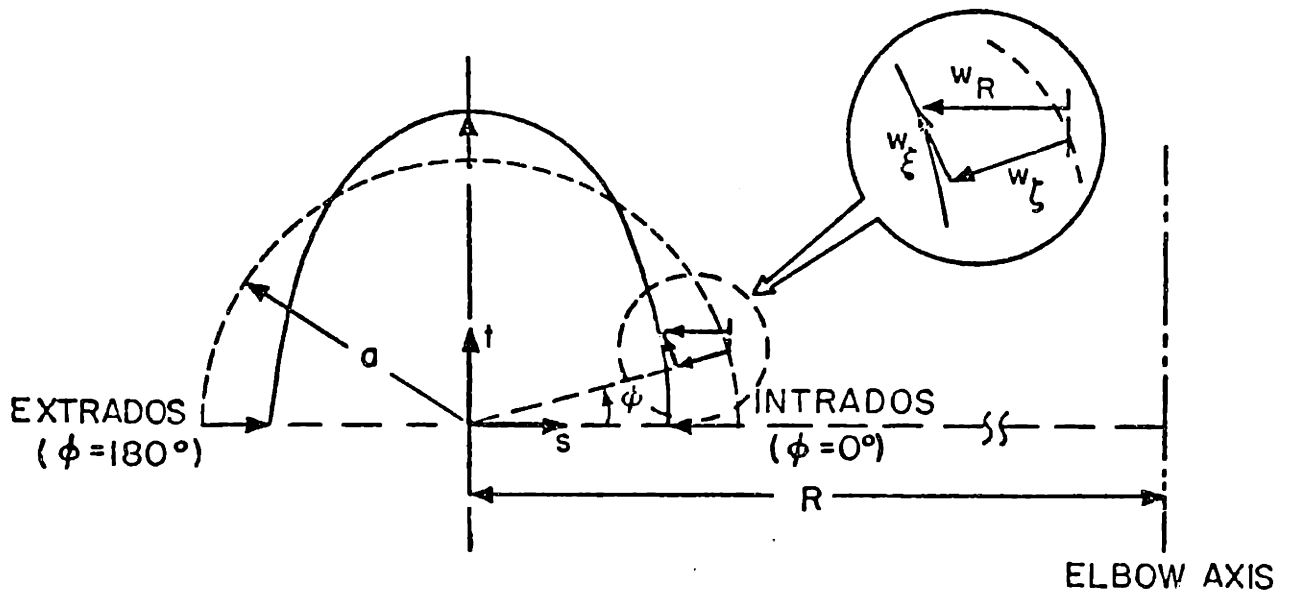
that are due to the ovalization of the cross-section, see Fig. 2.1 These strain components are a pipe cross-sectional circumferential strain,  $(\epsilon_{\xi\xi})_{ov}$ , which is due to the deformation of the cross-section, and a longitudinal strain,  $(\epsilon_{\eta\eta})_{ov}$ , which is due to the change in the curvature of the pipe itself. Corresponding to the usual strain components of curved beam theory and the above two additional strain components, the von Kármán analysis is based on the following major assumptions:

- (a) Plane sections originally plane and normal to the neutral axis of the pipe are assumed to remain plane and normal to the neutral axis;
- (b) The longitudinal strains are assumed to be of constant magnitude through the pipe wall thickness;
- (c) The circumferential strains are assumed to vanish at the middle surface of the pipe wall, and are due to pure transverse bending of the pipe wall. Hence the pipe wall thickness is assumed to be small in comparison to the pipe mean-radius; i.e.
 
$$\delta/a \ll 1;$$
- (d) The pipe mean-radius is assumed to be much smaller than the radius of the pipe bend; i.e.
 
$$a/R \ll 1;$$
 and
- (e) The effect of Poisson's ratio is neglected.

Using the assumption in (c) a relation can be written between the radial and circumferential displacements of the



(a) COORDINATE SYSTEMS USED



(b) DISPLACEMENTS OF DEFORMED CROSS-SECTION (FIRST VON KÁRMÁN MODE;  $w_s$  IS SHOWN NEGATIVE)

FIGURE 2.1 - Coordinate Systems and Displacements of Elbow

middle surface of the pipe wall,

$$w_{\xi} = - \frac{dw_{\xi}}{d\phi} \quad (2.1)$$

where  $w_{\xi}$  is the radial displacement,  $w_{\xi}$  is the tangential displacement and  $\phi$  measures the angular position considered as shown in Fig. 2.1.

### 2.1.2 Von Kármán analysis

In his analysis von Kármán established the strain energy in an element of pipe that is subjected to a constant bending moment, and used the Ritz method to estimate the amount of ovalization.

Using the assumptions summarized above, the longitudinal strains due to the distortion of the cross-section are

$$(\epsilon_{rr})_{ov} = \frac{w_R}{R} \quad (2.2)$$

where  $R$  is the pipe bend radius and  $w_R$  is the local displacement of the pipe wall in the bend radial direction, see Fig. 1.

Also, the circumferential strain component is

$$(\epsilon_{\xi\xi})_{ov} = - \frac{1}{a^2} \left[ w_{\xi} + \frac{d^2 w_{\xi}}{d\phi^2} \right] \xi \quad (2.3)$$

where  $a$  is the mean-radius of the pipe and  $\xi$  is the local radial coordinate in the pipe wall, see Fig. 2.1.

Using Eqs. (2.1) to (2.3) and assumptions (a) to (e) above, the total strain energy of an elbow of angle  $\theta_c$  is

$$\begin{aligned}
V = \frac{E \alpha \delta R}{2} \int_0^{\theta_0} \left\{ \int_0^{2\pi} \left[ \underbrace{-\left(\frac{\Delta\theta}{R\theta}\right) a \cos \phi}_{\text{TERM 1}} + \underbrace{\frac{1}{R} \left( w_{\xi} \sin \phi + \frac{dw_{\xi}}{d\phi} \cos \phi \right)}_{\text{TERM 2}} \right]^2 d\phi \right. \\
\left. + \int_0^{2\pi} \underbrace{\left( \frac{\delta^2}{12} \right) \left[ \frac{1}{\alpha^2} \left( \frac{dw_{\xi}}{d\phi} + \frac{d^3 w_{\xi}}{d\phi^3} \right) \right]^2}_{\text{TERM 3}} d\phi \right\} d\theta \quad (2.4)
\end{aligned}$$

where  $\delta$  is the pipe wall thickness,  $E$  is the Young's modulus of the material and  $\Delta\theta$  is the cross-sectional angular rotation. In Eq. (2.4) TERM 1 corresponds to the curved beam theory longitudinal strain, and TERM 2 and TERM 3 correspond to the straining that is due to ovalization.

In Eq. (2.4) the only variable corresponding to the ovalization of the cross-section is the displacement  $w_{\xi}$ . To estimate this displacement von Kármán assumed for in-plane bending of the elbow

$$w_{\xi} = \sum_{n=1}^N c_n \sin 2n\phi \quad (2.5)$$

and performed a Ritz analysis to obtain the parameters  $c_n$ . The validity of the von Kármán trial functions in Eq. (2.5) has been substantiated by experiments [4-6, 10].

Considering the von Kármán analysis, a pipe geometric factor  $\lambda$ , where  $\lambda = \frac{R\delta}{\alpha^2}$ , plays an important role in the determination of the number  $N$  of trial functions that should be

included in the analysis. Table 2.1 summarizes the number of trial functions that need be used for different values of  $\lambda$  in order to obtain satisfactory results.

Considering the von Kármán analysis, it may be noted that assumptions (b), (d) and (e) are not used in the formulation of the elbow element presented in Chapter 3.

The basic assumption using the strain components in Eqs. (2.2) and (2.3) is that, in essence, each differential length of the elbow can ovalize independently. Therefore, the interaction effects in the ovalization between elbows of different bend curvatures, an elbow and a straight pipe section, and an elbow and a rigid flange cannot be properly modeled. To render the formulation applicable to such situations it is necessary to extend the von Kármán analysis.

In the next section the formulation of a general theory for thin shells is specialized to the analysis of thin pipe shell surfaces. The important additional strain terms found are such that the von Kármán analysis is naturally extended to model interaction effects in piping structures.

## 2.2 Novozhilov's Theory of Thin Shells

A curved elbow subjected to external loading that leads to ovalization of the cross-section can be regarded as a doubly-curved thin shell. Despite the completeness of some currently available thin shell theories used in the analysis of pipes, they have lead to rather cumbersome formulations



TABLE 2.1 - NUMBER OF OVALIZATION SHAPE FUNCTIONS  
TO BE USED IN RITZ ANALYSIS (AND  
ELBOW FORMULATION)

Geometric Range	Number of Functions N
$\lambda \geq .5$	1
$.16 \leq \lambda \leq .5$	2
$.08 \leq \lambda \leq .16$	3
$.04 \leq \lambda < .08$	4

while presenting difficulties in their physical interpretation [9, 25, 26]. A relatively simple and effective theory for thin shells was introduced by Novozhilov [29]. In this theory, which is based on Kirchhoff's method [30], the deformations at any point of the shell are referred to the deformations of the shell midsurface. The objective in this section is to summarize Novozhilov's theory in order to identify the important strain terms applicable to the analysis of pipe elbows.

### 2.2.1 General definitions and basic assumptions

The shell is defined as a body bounded by two curved surfaces where the distance between the surfaces is small compared with other dimensions. The locus of points mid-way between these surfaces defines the middle surface of the shell. The thickness  $\delta$  of the shell is the distance between the two surfaces measured along the normal to the mid-surface.

The formulation of Novozhilov's theory of thin shells<sup>†</sup> is basically an extension of the well-accepted theory of beam bending with the following basic assumptions:

(a) the straight fibers of the shell that are perpendicular to the mid-surface before deformation remain so after

---

<sup>†</sup>A shell is called "thin" if the ratio  $\delta/\bar{R}$  (where  $\bar{R}$  is the radius of curvature of the midsurface) is very small compared with unity. Considering general applications with an admissible relative error of 5%, Novozhilov suggests that for thin shells this condition corresponds to  $.001 \leq (\delta/\bar{R}) \leq .05$ .

deformation and do not change their lengths; and

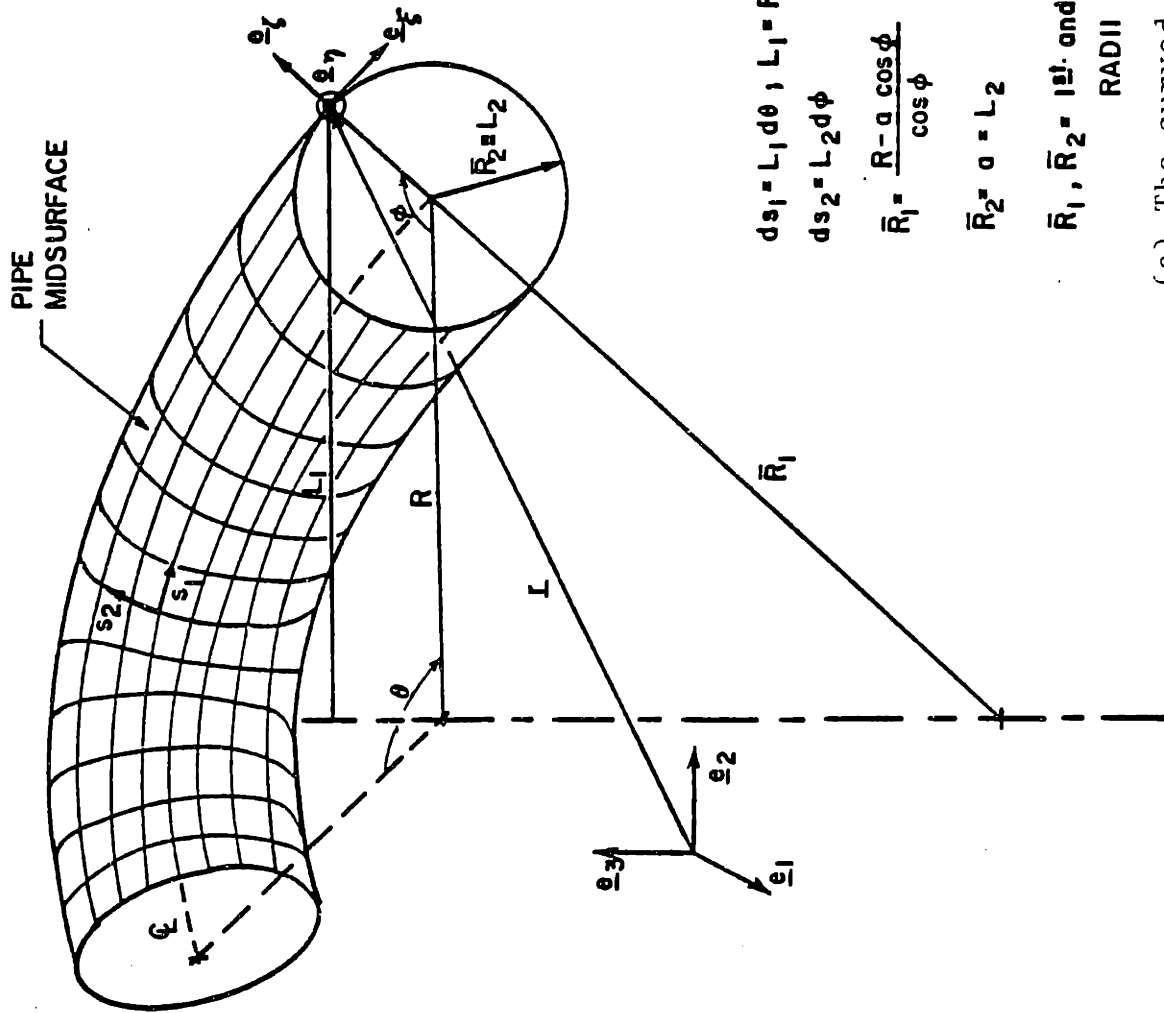
(b) the normal stresses acting perpendicular to the mid-surface are neglected in comparison with other stresses.

Using the above assumptions, transverse shear deformations to the midsurface are neglected. Therefore, the state of deformations assumed in the theory corresponds to a plane stress condition, namely, an in-plane shear stress and two normal stresses all parallel to the shell midsurface, see Fig. 2.2(b).

Basically these hypotheses reduce the problem of the deformation of a shell to the study of the deformation of its midsurface, in the same way as the hypothesis regarding plane sections in the bending of a beam reduces that problem to the study of the bending of its neutral axis.

### 2.2.2 Kinematic relations

In the Novozhilov theory of thin shells, which is based on the Kirchhoff's hypotheses, the total shell deformations are the sum of three basic deformation components of its midsurface: stretching, distortion and bending. To simplify the study of these deformations it is convenient to define a local set of curvilinear coordinates in which the formulae for the surface of the shell attain a simple form [31]. Recalling basic concepts of differential geometry, such set of coordinates is formed by two families of orthogonal curves, Fig. 2.2 (a), which are the lines of principal curvature of the surface. These curves define a local system of curvilinear coordinates  $S_1$  and  $S_2$  where



$$ds_1 = L_1 d\theta, \quad L_1 = R - a \cos \phi$$

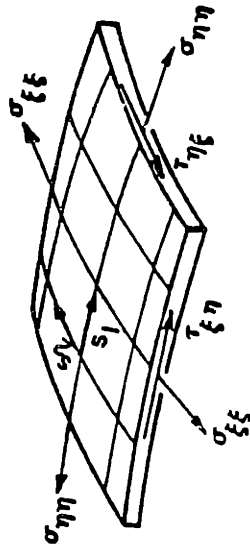
$$ds_2 = L_2 d\phi$$

$$\bar{R}_1 = \frac{R - a \cos \phi}{\cos \phi}$$

$$\bar{R}_2 = a = L_2$$

$\bar{R}_1, \bar{R}_2 = 1^{st}$  and  $2^{nd}$  PRINCIPAL MIDSURFACE  
RADIi OF CURVATURE

(a) The curved pipe geometry.



(b) Plane stress condition assumed in the formulation.

FIGURE 2.2 The Pipe Bend Treated as a Doubly-curved Shell.

a position vector

$$\underline{r} = \underline{r}(s_1, s_2) \quad (2.6)$$

defines the entire surface.

From the geometry of the bend in Fig. 2.2(a), independent variations of each curvilinear coordinate give

$$ds_1 = L_1 d\theta = (R - a \cos \phi) d\theta \quad (2.7)$$

$$ds_2 = L_2 d\phi = a d\phi \quad (2.8)$$

where  $ds_1$  and  $ds_2$  are increases in arc lengths along principal coordinate lines,  $R$  and  $a$  are the bend radius and the mean-radius of the bend, and  $\theta$  and  $\phi$  are natural angular parameters of the pipe bend. In theory of surfaces, the quantities  $L_1$  and  $L_2$  are called Lamé parameters and in general they are not the principal radii of curvature.

During the calculation of deformations, all vectors defining points of the pipe midsurface will be given in terms of their projections on the directions of the tangents of the curvilinear coordinate lines and on the normal to the midsurface of the pipe at the point considered. These two tangents and the normal form a local set of Cartesian coordinates defined by the following set of orthogonal unit vectors, see Fig. 2.2(a),

$$\underline{e}_\eta = \frac{\partial \underline{r}}{\partial s_1} = \frac{1}{L_1} \frac{\partial \underline{r}}{\partial \theta} \quad (2.9)$$

$$\underline{e}_\xi = \frac{\partial \underline{r}}{\partial s_2} = \frac{1}{L_2} \frac{\partial \underline{r}}{\partial \phi} \quad (2.10)$$

$$\underline{e}_\zeta = \underline{e}_\eta \times \underline{e}_\xi \quad (2.11)$$

where  $r$ ,  $s_1$  and  $s_2$  are as defined in Eqs. (2.6) to (2.8).

Also, the geometry of the midsurface of the pipe gives rise of the following Gauss-Weingarten relations,

$$\frac{\partial}{\partial s_1} [\underline{e}] = \left(\frac{1}{L_1}\right) \begin{bmatrix} 0 & -\sin \phi & \cos \phi \\ \sin \phi & 0 & 0 \\ -\cos \phi & 0 & 0 \end{bmatrix} [\underline{e}] \quad (2.12)$$

$$\frac{\partial}{\partial s_2} [\underline{e}] = \left(\frac{1}{L_2}\right) \begin{bmatrix} 0 & 0 & 0 \\ 0 & 0 & -1 \\ 0 & 1 & 0 \end{bmatrix} [\underline{e}] \quad (2.13)$$

with  $[\underline{e}]^T = [e_r \quad e_\xi \quad e_\zeta]$ .

Details of the derivation of the foregoing equations are given in Appendix A as they represent the transformations of local unit vectors along the lines of principal curvilinear coordinates.

### 2.2.3 Deformations of a shell and deformations of its midsurface

Consider a point  $O$ , see Fig. 2.5, at a distance  $\zeta$  from the midsurface of the pipe. If during the process of deformation point  $O$  moves to point  $O_1$  through a displacement  $\underline{u}$ , by virtue of assumptions (a) and (b) in Sec. 2.2.1, a point  $O'$  of the midsurface undergoes a displacement  $\underline{u}'$  and reaches a point  $O'_1$ . Therefore, the total displacement of point  $O$  in terms of the

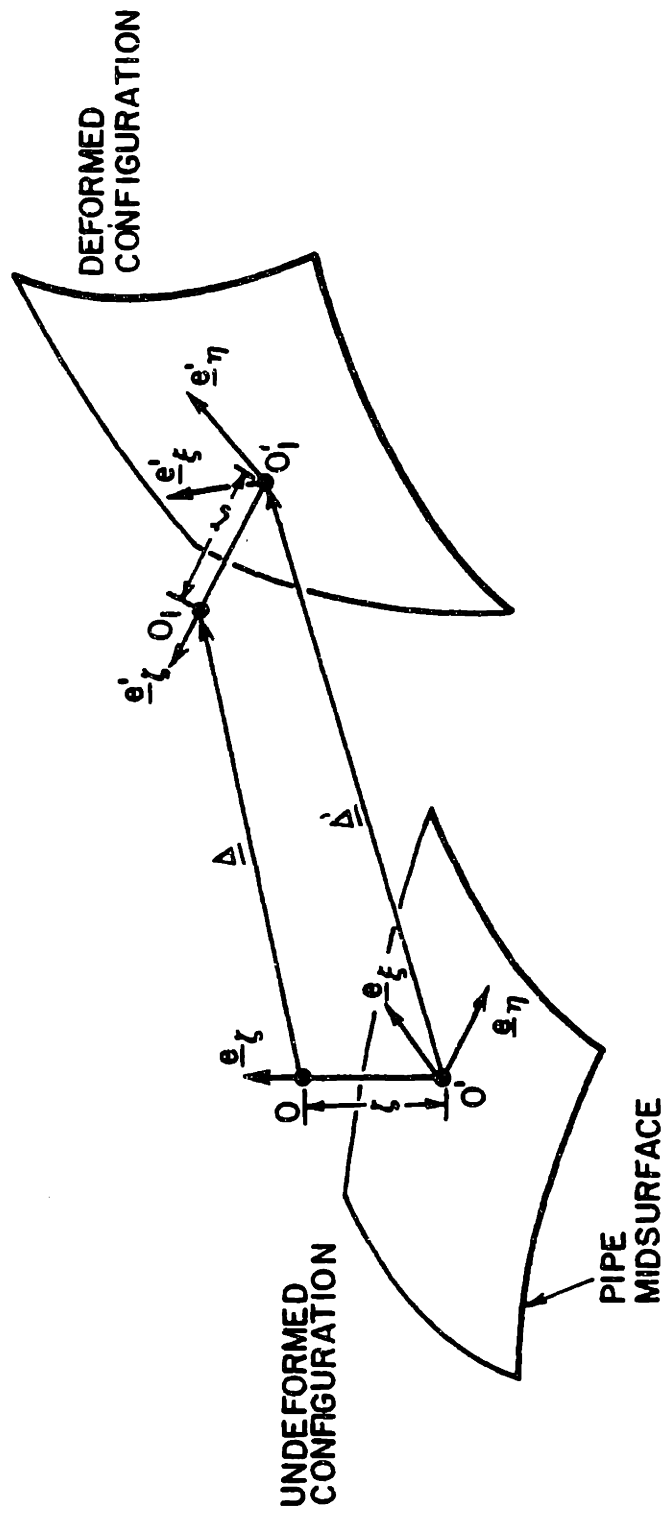


FIGURE 2.3 The Shell Displacement Related to its Midsurface Displacement.

midsurface displacement is

$$\underline{\Delta} = \underline{\Delta}' + (\underline{e}'_s - \underline{e}_s) \xi \quad (2.14)$$

with,

$$\underline{\Delta}' = w_\eta \underline{e}_\eta + w'_s \underline{e}'_s + w_s \underline{e}_s \quad (2.15)$$

where  $\underline{e}'_s$  is the normal to the deformed midsurface and  $w_\eta$ ,  $w'_s$  and  $w_s$  are the longitudinal, the circumferential and the radial local displacements of the midsurface point  $O'$ .

Stretching and distortional displacements of the midsurface are accounted by the displacement vector  $\underline{\Delta}'$  while the position dependent term in Eq. (2.14) is the displacement due to bending of the midsurface. Noting that,

$$\frac{\partial \underline{\Delta}}{\partial s_1} = \frac{\partial \underline{\Delta}'}{\partial s_1} + \frac{\partial}{\partial s_1} (\underline{e}'_s - \underline{e}_s) \xi, \quad i = 1, 2 \quad (2.16)$$

and using Eqs. (2.12), (2.13) and (2.15), the derivative of displacements at the midsurface reduces to,

$$\frac{\partial \underline{\Delta}'}{\partial s_1} = \hat{\epsilon}_{\eta\eta} \underline{e}_\eta + \hat{\omega}_1 \underline{e}'_s + \hat{\lambda}_1 \underline{e}_s \quad (2.17)$$

where,

$$\hat{\epsilon}_{\eta\eta} = \frac{1}{L_1} \left[ \frac{\partial w_\eta}{\partial \theta} + w'_s \sin \phi - w_s \cos \phi \right] \quad (2.18)$$



$$\hat{\omega}_1 = \frac{1}{L_1} \left[ \frac{\partial w_\xi}{\partial \theta} - w_\eta \sin \phi \right] \quad (2.19)$$

$$\hat{\chi}_1 = \frac{1}{L_1} \left[ \frac{\partial w_\xi}{\partial \theta} + w_\eta \cos \phi \right] \quad (2.20)$$

and similarly,

$$\frac{\partial \Delta'}{\partial \phi_2} = \hat{\omega}_2 e_\eta + \hat{\xi}_{\xi\xi} e_\xi + \hat{\chi}_2 e_\tau \quad (2.21)$$

where,

$$\hat{\omega}_2 = \frac{1}{L_2} \frac{\partial w_\eta}{\partial \phi} \quad (2.22)$$

$$\hat{\xi}_{\xi\xi} = \frac{1}{L_2} \left[ \frac{\partial w_\xi}{\partial \phi} + w_\tau \right] \quad (2.23)$$

$$\hat{\chi}_2 = \frac{1}{L_2} \left[ \frac{\partial w_\xi}{\partial \phi} - w_\tau \right] \quad (2.24)$$

The quantities  $\hat{\omega}_1$ ,  $\hat{\omega}_2$ ,  $\hat{\chi}_1$  and  $\hat{\chi}_2$  are identified with rotation angles by which the unit vectors  $e_\eta$ ,  $e_\xi$  and  $e_\tau$  rotate as the result of midsurface deformations [29]. Namely,  $\hat{\omega}_1$  and  $\hat{\omega}_2$  are respectively the angular changes experienced by  $e_\eta$  and  $e_\xi$  about the normal  $e_\theta$ . The in-plane shear strains at the pipe midsurface are hence,

$$\hat{\omega}_{\eta\xi} = \hat{\omega}_1 + \hat{\omega}_2 \quad (2.25)$$

where  $\hat{\omega}_1$  and  $\hat{\omega}_2$  are given in Eqs. (2.19) and (2.22). Also  $\hat{\chi}_1$  and  $\hat{\chi}_2$  are the rotation angles of the normal  $\underline{e}_\xi$  about the axes  $\underline{e}_\eta$  and  $\underline{e}_\zeta$ , respectively. Hence, the normal to the deformed midsurface is related to the normal in the undeformed configuration by the equation

$$\underline{e}'_\xi = \underline{e}_\xi - (\hat{\chi}_1 \underline{e}_\eta + \hat{\chi}_2 \underline{e}_\zeta) \quad (2.26)$$

where  $\hat{\chi}_1$  and  $\hat{\chi}_2$  are given in Eqs. (2.18) and (2.22). The strain-displacement relations for the bending displacements are then obtained substituting Eq. (2.26) into Eq. (2.16), thus

$$\frac{\partial}{\partial s_i} \left[ \underline{e}'_\xi - \underline{e}_\xi \right]_{\xi} = \left[ \tilde{\epsilon}_{\eta\eta} \underline{e}_\eta + \tilde{\chi}_1 \underline{e}_\xi + \tilde{\chi}_2 \underline{e}_\zeta \right]_{\xi} \quad (2.27)$$

where,

$$\tilde{\epsilon}_{\eta\eta} = -\left(\frac{1}{L_1}\right)^2 \frac{\partial^2 w_\xi}{\partial \theta^2} - \frac{1}{L_2} \left( \frac{\partial w_\xi}{\partial \theta} - w_\xi \right) \frac{\sin \phi}{L_1} - \frac{\cos \phi}{L_1^2} \frac{\partial w_\eta}{\partial \theta} \quad (2.28)$$

$$\tilde{\omega}_1 = -\frac{1}{L_1 L_2} \frac{\partial}{\partial \theta} \left[ \frac{\partial w_\xi}{\partial \theta} - w_\xi \right] + \left(\frac{1}{L_1}\right)^2 \left[ \frac{\partial w_\xi}{\partial \theta} + w_\eta \cos \phi \right] \sin \phi \quad (2.29)$$

$$\tilde{\chi}_2 = -\left(\frac{1}{L_1}\right)^2 \left[ \frac{\partial w_\xi}{\partial \theta} + w_\eta \cos \phi \right] \cos \phi \quad (2.30)$$

and similarly,

$$\frac{\partial}{\partial s_2} [\underline{e}'_s - \underline{e}_z] \zeta = [\tilde{\omega}_2 \underline{e}_\eta + \tilde{\epsilon}_{\xi\xi} \underline{e}_\xi + \tilde{\chi}_2 \underline{e}_z] \zeta \quad (2.31)$$

where,

$$\tilde{\omega}_2 = -\frac{1}{L_1 L_2} \frac{\partial}{\partial \phi} \left[ \frac{\partial w_\eta}{\partial \theta} + w_\eta \cos \phi \right] \quad (2.32)$$

$$\tilde{\epsilon}_{\xi\xi} = -\left(\frac{1}{L_2}\right)^2 \frac{\partial}{\partial \phi} \left[ \frac{\partial w_\xi}{\partial \phi} - w_\xi \right] \quad (2.33)$$

$$\tilde{\chi}_2 = \left(\frac{1}{L_2}\right)^2 \left[ \frac{\partial w_\xi}{\partial \phi} - w_\xi \right] \quad (2.34)$$

Finally, substituting from Eqs. (2.27) and (2.31) into Eq. (2.16) the total strains for a pipe geometry shell using Novozhilov thin shell theory gives

$$\begin{aligned} \epsilon_{\eta\eta} &= \hat{\epsilon}_{\eta\eta} + \tilde{\epsilon}_{\eta\eta} \zeta \\ \epsilon_{\xi\xi} &= \hat{\epsilon}_{\xi\xi} + \tilde{\epsilon}_{\xi\xi} \zeta \end{aligned} \quad (2.35)$$

$$\epsilon'_{\eta\xi} = \hat{\epsilon}'_{\eta\xi} + \tilde{\epsilon}'_{\eta\xi} \zeta$$

where in-plane midsurface deformations and midsurface bending parameters are defined by only three linear midsurface displacements  $w_\eta$ ,  $w_\xi$  and  $w_\zeta$ . As in Euler's theory of beams where

the bending strains result from the change of curvature of the beam neutral axis, the bending parameters  $\tilde{\epsilon}_{\eta\eta}$  and  $\tilde{\epsilon}_{\xi\xi}$  are also changes of middle surface curvature of the shell during deformation.

#### 2.2.4 Evaluation of the ovalization strains

The linear strain components derived in Eqs. (2.35) are applicable to very general deformation patterns of the pipe, such as localized deformations of its midsurface. Considering the important effects in the behavior of a piping structure, two deformation mechanisms take place in the overall response of the bend under external loading: (a) the deformation of a beam with circular cross-section which does not distort either in its plane or out of its plane, and (b) the deformation due to the ovalization of the pipe cross-section. Therefore, in the formulation of the elbow element presented in the next chapter we consider the axial, bending and torsional beam displacements and the cross-sectional ovalization displacements. The corresponding pipe-shell deformations resulting from these displacements are physically identified in Eqs. (2.35) and written as follows,

$$\begin{aligned}
 \varepsilon_{\eta\eta} = & \underbrace{\frac{\partial w_\eta}{L_1 \partial u} \left[ 1 + \frac{z}{R_1} \right]}_{\text{TERM 1}} + \underbrace{\frac{w_\xi \sin \phi - w_\xi \cos \phi}{L_1}}_{\text{TERM 2}} - \underbrace{\left[ \frac{\partial^2 w_\xi}{L_1^2 \partial \theta^2} + \frac{1}{L_2} \left( \frac{\partial w_\xi}{\partial \phi} - w_\xi \right) \frac{\sin \phi}{L_1} \right]}_{\text{TERM 3}} z \\
 & \hspace{15em} \text{TERM 3} \\
 & \hspace{15em} \text{TERM 2} \\
 & \hspace{15em} \text{TERM 1}
 \end{aligned} \tag{2.36}$$

$$\varepsilon_{\xi\xi} = \underbrace{\frac{1}{L_2} \left( w_\xi + \frac{\partial w_\xi}{\partial \phi} \right)}_{\text{TERM 4}} - \underbrace{\frac{\partial}{L_2 \partial \phi} \left[ \frac{1}{L_2} \left( \frac{\partial w_\xi}{\partial \phi} - w_\xi \right) \right]}_{\text{TERM 5}} z \tag{2.37}$$

$$\begin{aligned}
 \gamma_{\eta\xi} = & \underbrace{\frac{\partial w_\eta}{L_2 \partial \phi} \left[ 1 + \frac{z}{R_1} \right]}_{\text{TERM 6}} - \underbrace{\frac{w_\eta \sin \phi}{L_1}}_{\text{TERM 7}} + \underbrace{\frac{dw_\xi}{L_1 \partial u} \left[ 1 + \frac{z}{R_2} \right]}_{\text{TERM 7}} + \underbrace{\frac{\partial}{L_1 \partial \theta} \left[ \frac{w_\xi \sin \phi}{L_1} - 2 \frac{\partial w_\xi}{L_2 \partial \phi} \right]}_{\text{TERM 8}} z \\
 & \hspace{15em} \text{TERM 6} \\
 & \hspace{15em} \text{TERM 7} \\
 & \hspace{15em} \text{TERM 8}
 \end{aligned} \tag{2.38}$$

Straining due to beam displacements

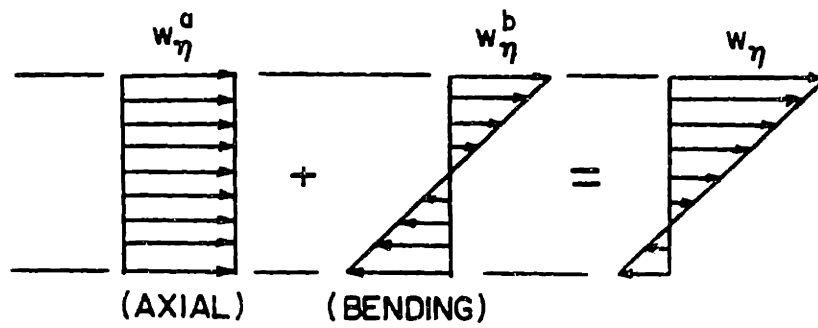
Straining due to ovalization displacements

where,

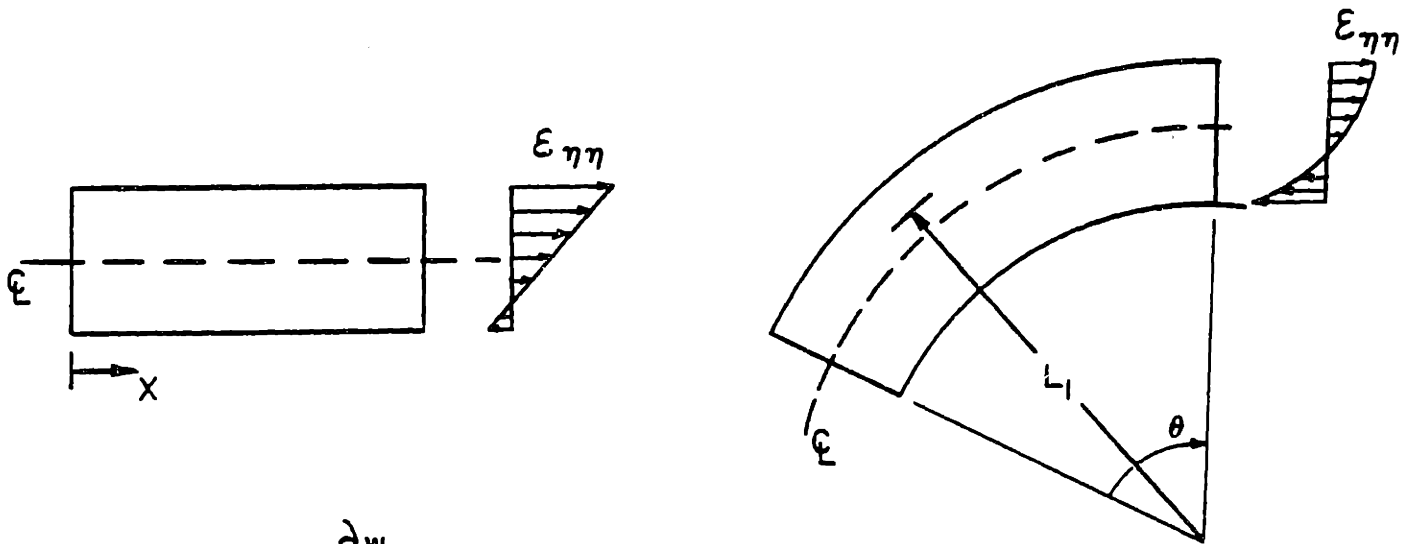
TERM 1 is the longitudinal straining due to both axial and bending beam displacements of the tube. For thin pipes, the expression in parenthesis is approximated by unity and this term reduces to the derivative of the displacement  $w_\gamma$  with respect to the longitudinal curvilinear coordinate. Displacements and strains in both straight and curved pipes are shown in Fig. 2.4.

TERM 2 is the contribution to the longitudinal strains due to the stretching of a longitudinal fiber of the elbow whose cross-section ovalizes. This term is identical to von Kármán's longitudinal strain in Eq. (2.2), except for the von Kármán assumption that all longitudinal fibers have the same bend radius. Consequently, using the shell equations, the assumption (d) of the von Kármán analysis is not used in the elbow formulation. This strain term, shown in Fig. 2.5 (a), is basically the ratio of the radial displacement  $w_\lambda$  of the longitudinal fiber to its bend radius. Hence, for the straight pipe geometry this term vanishes.

TERM 3 is the longitudinal bending strains due to the ovalization of the pipe cross-section. The first component of this term is due to the longitudinal bending of the pipe skin while the second component is the result of the shell double curvature. In this study we are only concerned with thin pipes, hence, the second bending component is neglected comparing with other



(a) beam displacements

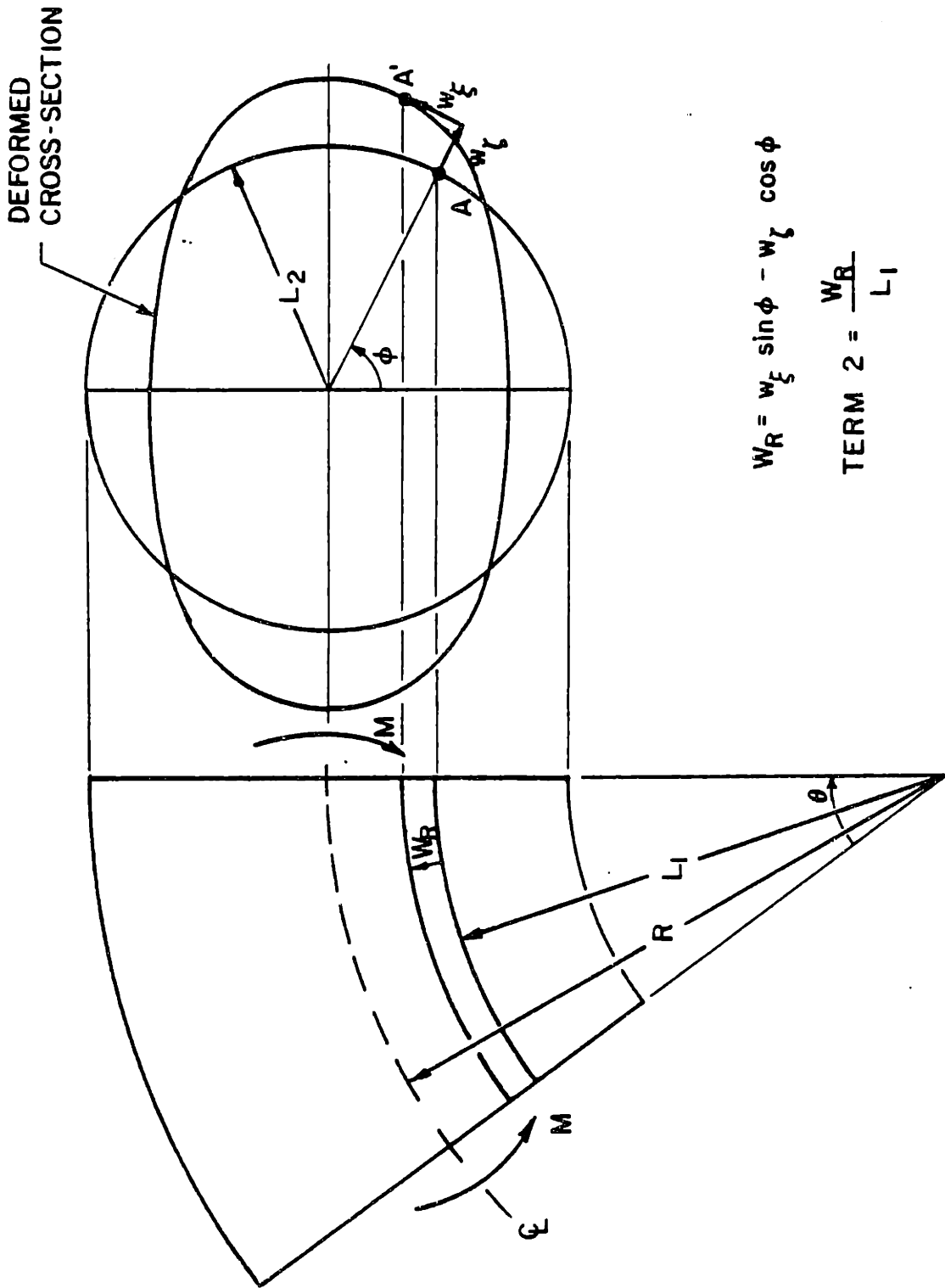


$$\text{TERM I} = \frac{\partial w_{\eta}}{\partial x}$$

$$\text{TERM I} = \frac{\partial w_{\eta}}{L_1 \partial \theta}$$

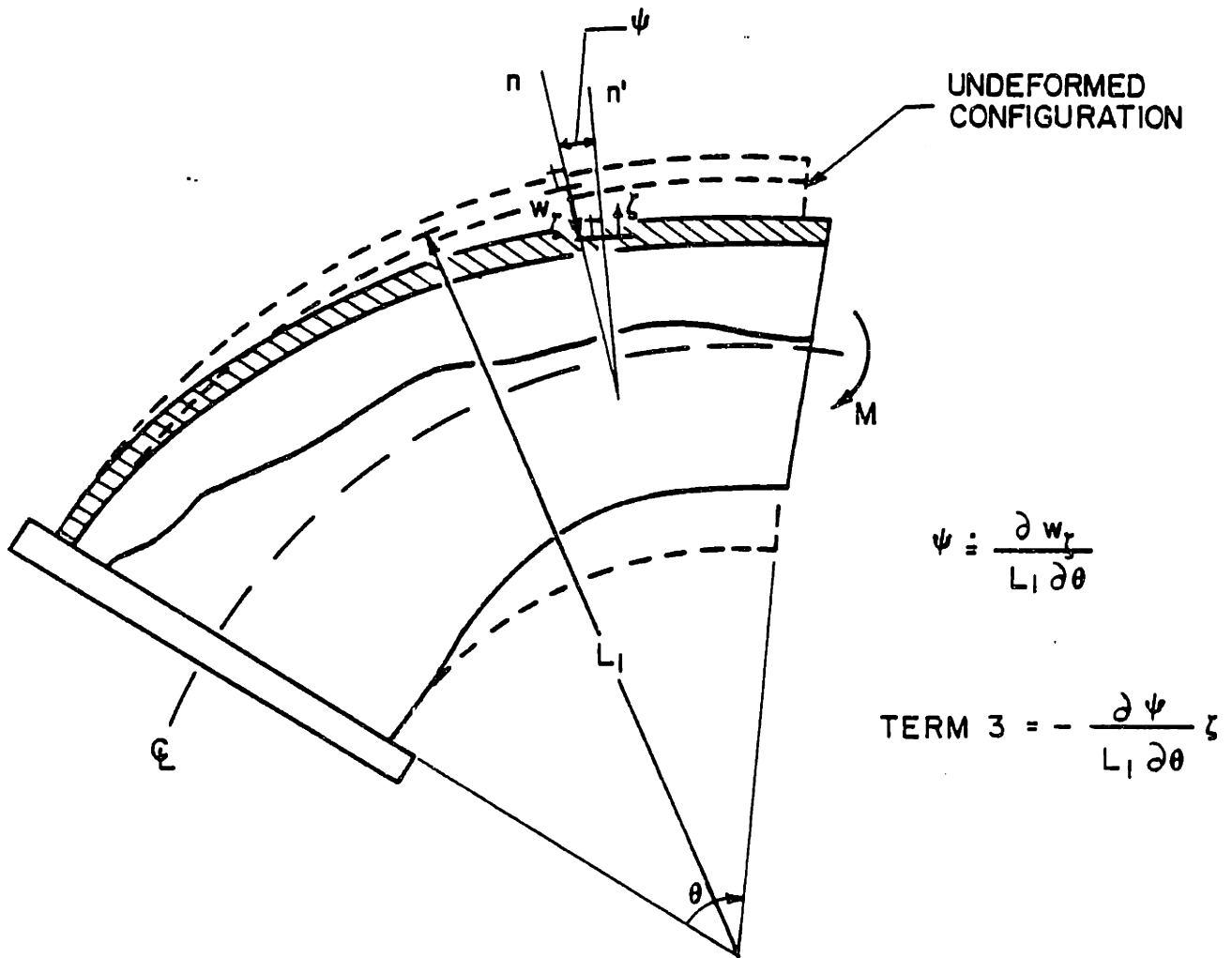
(b) beam longitudinal strains

FIGURE 2.4 Longitudinal Strains in Straight and Curved Pipes due to Axial and Bending Displacements.



(a) Stretching of a midsurface longitudinal fiber due to the ovalization of the elbow cross-section.





(b) Longitudinal pipe skin bending of a flanged elbow<sup>†</sup>.  
 ( $w_z$  is shown negative).

FIGURE 2.5 Stretching and Bending of a Longitudinal Fiber of the Bend Due to Cross-sectional Ovalization.

<sup>†</sup> Figure not to scale. Cross-sectional ovalization exaggerated to show longitudinal bending of the pipe skin.

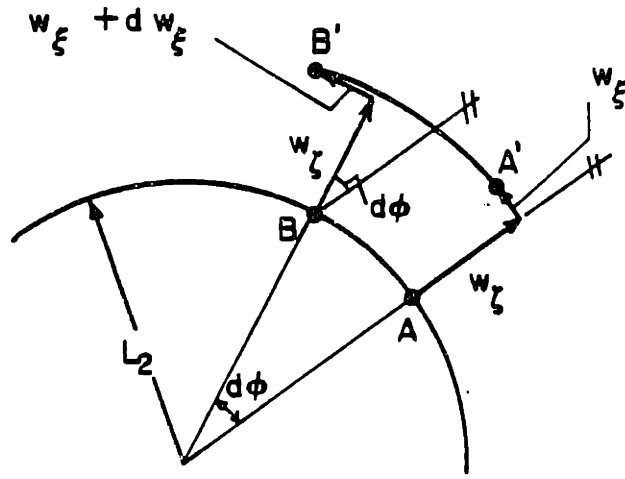
terms in Eq. (2.36). The remainder of TERM 3 represents the straining due to the variation of the ovalization along the pipe length, shown in Fig. 2.5(b).

TERM 4 corresponds to the circumferential strains due to the stretching of the pipe midsurface, see Fig. 2.6(a). Using von Kármán's assumption of pure transverse bending strains due to cross-sectional distortions, this term is set equal to zero and Eq. (2.1) is immediately verified.

TERM 5 is the bending deformation of the elbow midsurface due to distortions of the pipe cross-section. This term, which is equivalent to Eq. (2.3) in von Kármán analysis, contains the change in relative curvature of an ovalized cross-section as in the classical theory of circular beams, see Fig. 2.6(b).

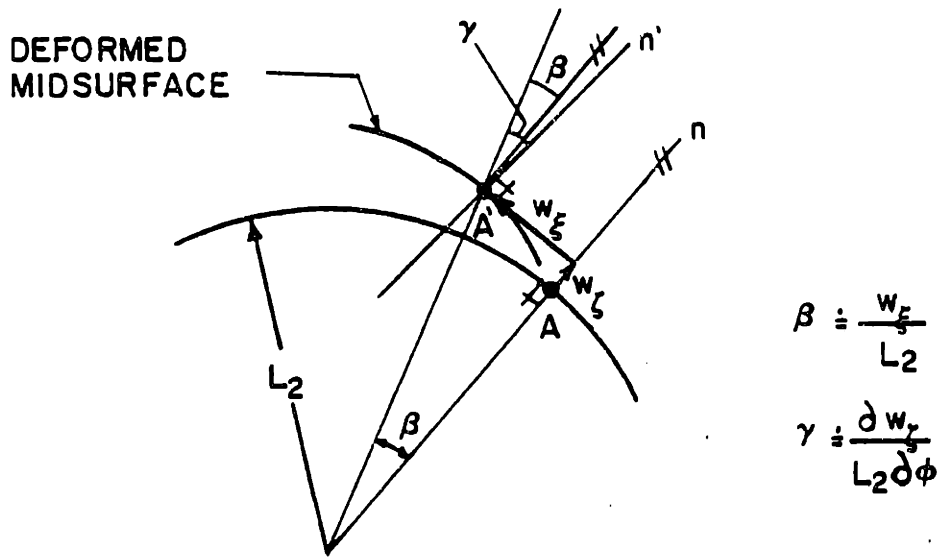
TERM 6 is the shear straining of the elbow midsurface due to axial and bending displacements of a beam. For thin pipes, the expressions inside the parenthesis are approximated by unity. The simplified form then represents the angular distortion of the pipe midsurface measured in the local convected coordinate system, see Fig. 2.7(a).

TERM 7 corresponds to in-plane shear strains due to the circumferential displacements of the cross-section. Hence, this term contains the shearing due to the torsional beam displacement  $w_z^T$  of the elbow as well as the shearing due to the displacement  $w_z^E$  of the ovalized cross-section. Although the expression in parenthesis is assumed equal to unity in the elbow formulation, it accounts for a linear distribution of the



$$\text{TERM 4} = \frac{\widehat{A'B'} - \widehat{AB}}{\widehat{AB}} = \frac{[L_2 d\phi + w_z d\phi + dw_z] - L_2 d\phi}{L_2 d\phi} = \frac{1}{L_2} \left[ w_z + \frac{\partial w_z}{\partial \phi} \right]$$

(a) Transverse deformation due to stretching of the pipe cross-section.



$$\beta = \frac{w_z}{L_2}$$

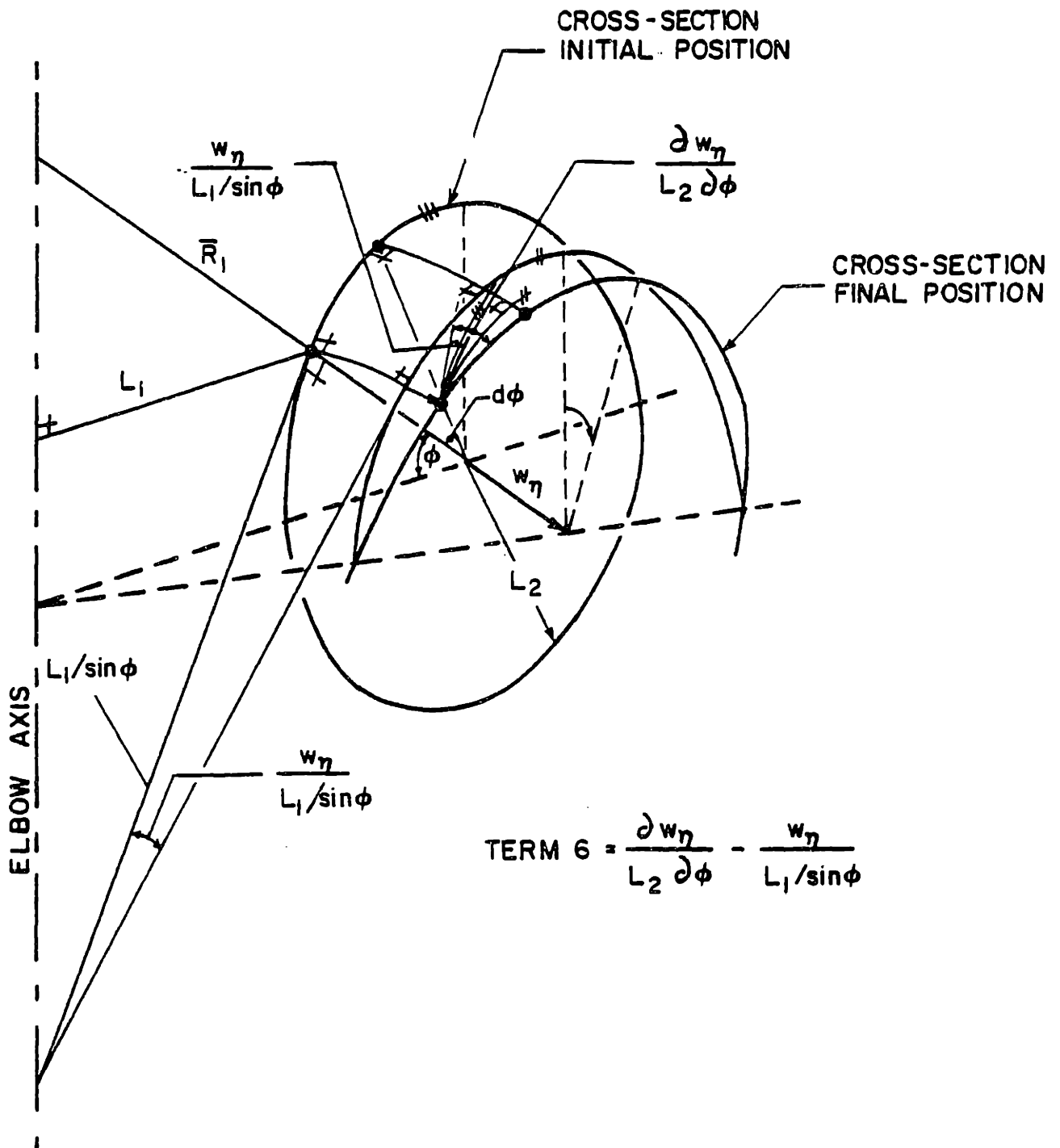
$$\gamma = \frac{\partial w_z}{L_2 \partial \phi}$$

RELATIVE CURVATURE:  $\gamma - \beta$

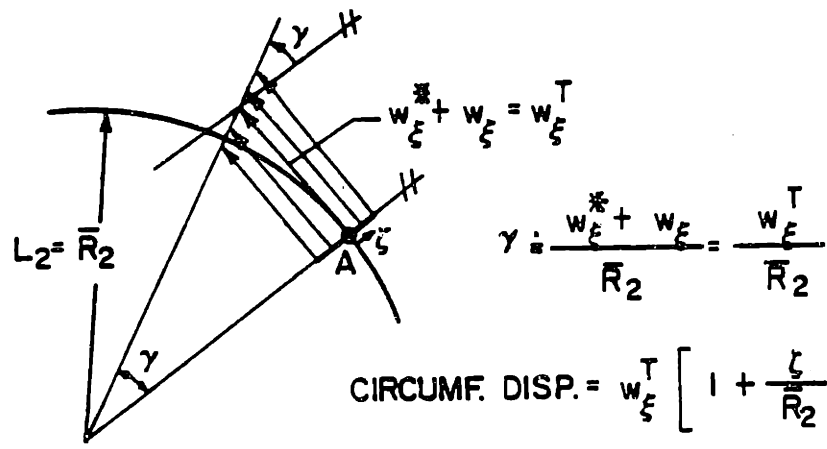
$$\text{TERM 5} = \frac{\partial}{L_2 \partial \phi} \left[ \frac{1}{L_2} \left( \frac{\partial w_z}{\partial \phi} - w_z \right) \right]$$

(b) Bending strains in the ovalized cross-sections.

FIGURE 2.6 Transverse Strains Due to Cross-sectional Deformations.

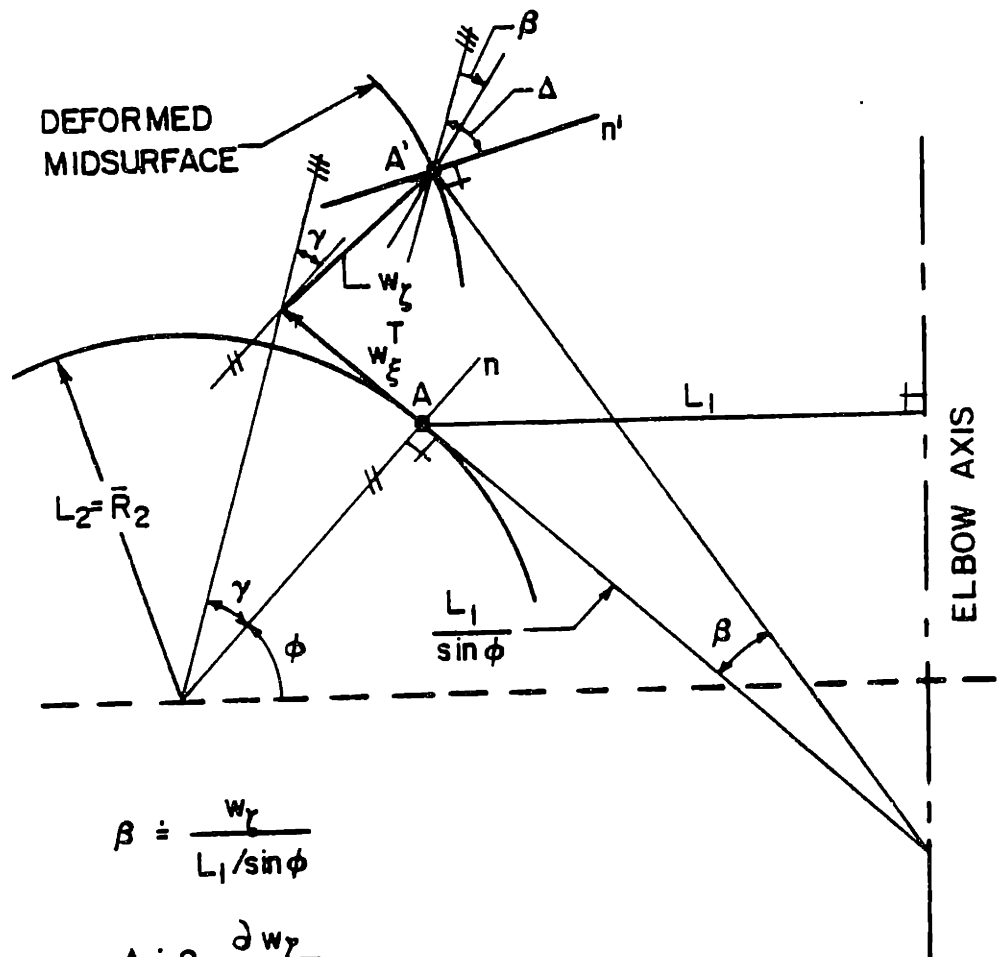


(a) Misurface shear deformation due to axial and bending beam displacements (out-of-plane bending shown).



$$\text{TERM 7} = \frac{\partial}{L_1 \partial \theta} (w_{\xi}^* + w_{\xi}) \left[ 1 + \frac{\xi}{R_2} \right]$$

(b) Shear strains in the elbow due to circumferential displacements.



$$\beta = \frac{w_{\gamma}}{L_1 / \sin \phi}$$

$$\Delta = 2 \frac{\partial w_{\gamma}}{L_2 \partial \phi}$$

$$\text{CIRCUMF. DISP.} = (\beta - \Delta) \xi$$

$$\text{TERM 8} = \frac{\partial}{L_1 \partial \theta} \left[ w_{\gamma} \frac{\sin \phi}{L_1} - 2 \frac{\partial w_{\gamma}}{L_2 \partial \phi} \right] \xi$$

(c) Shear strains in the elbow due to radial displacements.

FIGURE 2.7 Shear Mechanisms in the Pipe-shell Formulation.

shear strains throughout the pipe thickness shown in Fig. 2.7(b). TERM 8 represents the shear straining due to radial displacements in a deformed cross-section. In Fig. 2.7(c) we give a physical significance to the strains in TERM 8 by proceeding from the kinematics presented in Fig. 2.7(b). For thin pipes, this term is negligible compared to other terms in Eq. (2.38).

Introducing the above assumptions and the Lamé parameters (Eqs. (2.7) and (2.8)) into Eqs. (2.36) to (2.38) results in the following important strain terms that include the effects of cross-section ovalization in the formulation of the pipe-bend,

$$(\epsilon_{\theta\theta})_{ov} = \frac{w_{\theta} \sin \phi + \frac{\partial w_{\theta}}{\partial \phi} \cos \phi}{R - a \cos \phi} + \frac{\gamma^2}{(R - a \cos \phi)^2} \left[ \frac{\partial w_{\theta}}{\partial \phi} \right]_{\gamma} \quad (2.39)$$

$$(\epsilon_{\theta\theta})_{ov} = \frac{1}{a^2} \frac{\partial}{\partial \phi} \left[ w_{\theta} + \frac{\partial^2 w_{\theta}}{\partial \phi^2} \right]_{\gamma} \quad (2.39)$$

$$(\sigma_{\theta\theta})_{ov} = \left( \frac{1}{R - a \cos \phi} \right) \frac{\partial w_{\theta}}{\partial \phi} \quad (2.39)$$

In Eqs. (2.39), the strains due to ovalization reduce to a proper evaluation of the displacement  $w_{\theta}$ . As in von Kármán

analysis this feature allows simple parameters, or generalized degrees-of-freedom, per cross-section being used to include the ovalization deformations.

In the next chapter the formulation of a general beam element is presented and modified by Eqs. (2.39) to include the ovalization effects. The resulting formulation is simple and accurate in various piping analyses.

### 3. FINITE ELEMENT LINEAR FORMULATION OF THE ELBOW ELEMENT

The basic analytical shell formulation employed to model a pipe whose cross-section is allowed to deform in its own plane was discussed in the previous chapter. The shell solution, shown as a natural extension of von Kármán's theory for piping analysis, reduces to a general formulation of the beam modified by a few strain terms to include the effects of ovalization of the tube. The identification of both the beam and the ovalization deformations in the shell formulation, was possible by using a convenient local system of coordinates. The separation of these two independent modes of deformation is an important feature of the elbow element formulation, because it allows independent ovalization degrees-of-freedom being added to the conventional beam degrees-of-freedom.

Using standard finite element procedures, the principle of virtual work (or principle of minimum total potential energy) is invoked to derive the equilibrium equations that govern the response of the element [19]. If linear analysis is considered, we have

$$\underline{K}_L \underline{U} = \underline{R} \quad (3.1)$$

where  $\underline{K}_L$  is the element stiffness matrix corresponding to the degrees-of-freedom listed in  $\underline{U}$ ,



$$\underline{K}_L = \int_V \underline{B}^T \underline{C} \underline{B} dV \quad (3.2)$$

and  $\underline{R}$  is the effective nodal point load vector. In Eq. (3.2)  $\underline{B}$  is the strain-displacement matrix,  $\underline{C}$  is the constitutive matrix, and the integration is performed over the element volume  $V$ .

In this chapter, the formulation of the elbow element for linear analysis is presented. First, we discuss the formulation of an isoparametric displacement-based three-dimensional bending element that includes the important axial, bending and torsional displacements of pipe cross-sectional beam elements. Then, the beam element deformations are modified by ovalization deformations with the strains in Eqs. (2.59). This results in the final strain-displacement matrix  $\underline{B}$  of the elbow element, and we discuss also the corresponding stress-strain matrix  $\underline{C}$ .

### 3.1 Evaluation of the Strain-Displacement Matrix

Using the concepts of finite element analysis, we need to describe the geometry and the variations of internal element displacements of a typical pipe element in terms of its nodal point quantities [19, 32]. A generic pipe-elbow element with the assumed four nodal points is shown in Fig. 3.1. To establish the geometry and displacement interpolation functions of the element, we assume first that the pipe cross-section does not

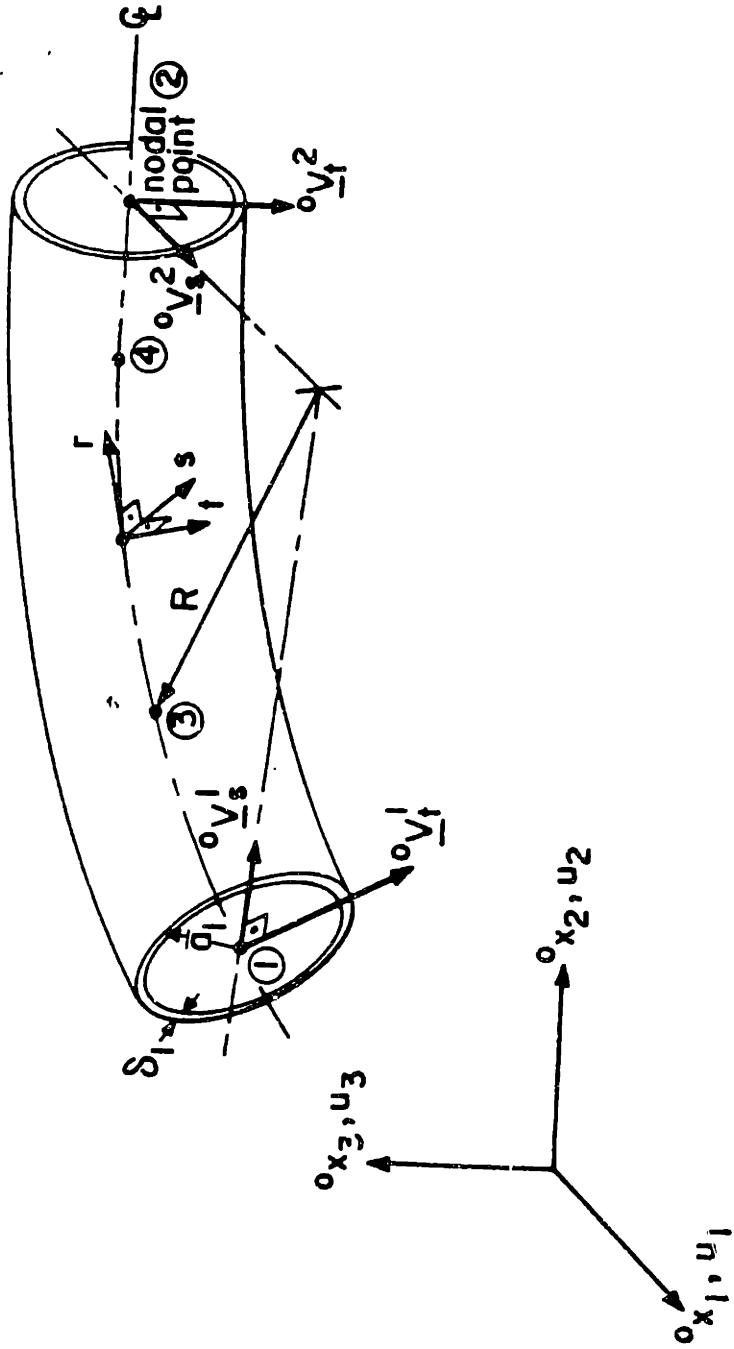


FIGURE 3.1 - Geometry of Pipe Elbow Element

ovalize. In this case the coordinate and displacement interpolations and the degrees-of-freedom are as used in the isoparametric finite element formulations of beam, plate and shell elements recently proposed [28, 33-35].

### 3.1.1 Element geometry and displacement interpolations assuming no ovalization

The basic assumption in this formulation is that plane sections originally normal to the center line axis of the pipe element remain plane but not necessarily normal to the center line axis. Thus, we can write the following equations for the coordinates of a point in the element before and after deformation,

$${}^l x_i(r, s, t) = \sum_{k=1}^4 h_k {}^l x_i^k + t \sum_{k=1}^4 \bar{a}_k h_k {}^l v_{ti}^k + s \sum_{k=1}^4 \bar{a}_k h_k {}^l v_{si}^k \quad (3.3)$$

/  $i = 1, 2, 3$

where,

- $r, s, t$  = isoparametric coordinates [19]
- ${}^l x_i$  = Cartesian coordinate of any point in the pipe element
- $h_k(r)$  = isoparametric interpolation functions
- ${}^l x_i^k$  = Cartesian coordinate of nodal point

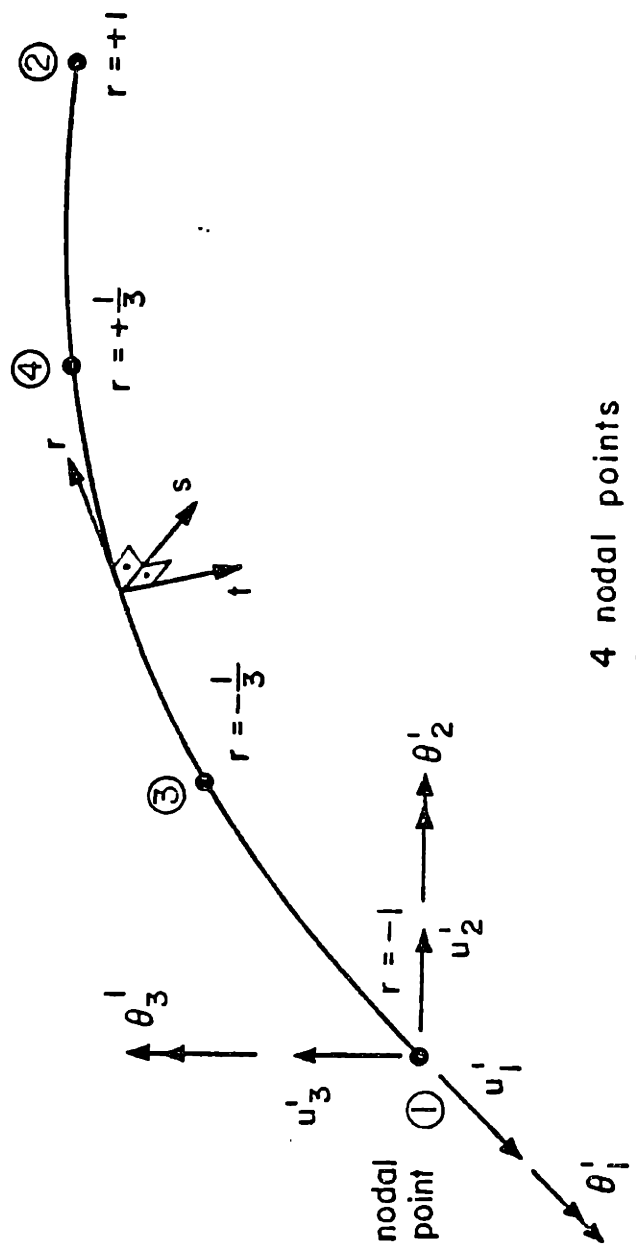
$$\begin{aligned}
\bar{a}_k &= \text{cross-sectional outer radius of element} \\
&\quad \text{at nodal point } k \\
{}^{\ell}V_{ti}^k &= \text{component } i \text{ of unit vector } \underline{V}_t^k, \text{ in} \\
&\quad \text{direction } t \text{ at nodal point } k \\
{}^{\ell}V_{si}^k &= \text{component } i \text{ of unit vector } \underline{V}_s^k, \text{ in} \\
&\quad \text{direction } s \text{ at nodal point } k,
\end{aligned}$$

and the left superscript  $\ell$  denotes the configuration of the element; i.e.,  $\ell = 0$  denotes the original configuration, whereas  $\ell = 1$  corresponds to the configuration in the deformed position.

The interpolation functions  $h_k(r)$  used in Eq. (3.3) are derived in Ref. [19]. In this work we use the high order four node element. The cubic interpolation functions of this element are summarized in Fig. 3.2. In the application of Eq. (3.3) it must be noted that the structural cross-section considered is hollow, meaning that Eq. (3.3) is only applicable for the values of  $s$  and  $t$  that satisfy the equation

$$\left(1 - \frac{\delta_k}{\bar{a}_k}\right)^2 \leq s^2 + t^2 \leq 1 \quad (3.4)$$

where  $\bar{a}_k$  is the outside radius of the element at node  $k$ . This fact is properly taken into account in the numerical integration to calculate the element stiffness matrix.



4 nodal points  
24 degrees-of-freedom

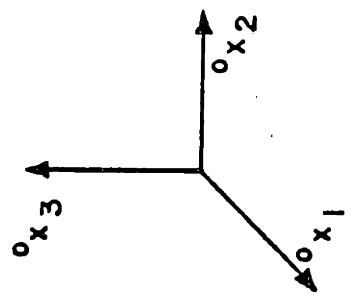
$$h_1 = [-9r^3 + 9r^2 + r - 1] / 16$$

$$h_2 = [9r^3 + 9r^2 - r - 1] / 16$$

$$h_3 = [27r^3 - 9r^2 - 27r + 9] / 16$$

$$h_4 = [-27r^3 - 9r^2 + 27r + 9] / 16$$

FIGURE 3.2 - Degrees-of-freedom and Interpolation Functions of Pipe Without Ovalization



To obtain the displacement components at any point  $r, s, t$  in the pipe we have

$$u_i(r, s, t) = {}^1x_i - {}^0x_i \quad (3.5)$$

Thus, substituting from Eq. (3.3) we have

$$u_i(r, s, t) = \sum_{k=1}^4 h_k u_i^k + t \sum_{k=1}^4 \bar{a}_k h_k V_{ti}^k + s \sum_{k=1}^4 \bar{a}_k h_k V_{si}^k \quad (3.6)$$

where

$$V_{ti}^k = {}^1V_{ti}^k - {}^0V_{ti}^k \quad (3.7)$$

$$V_{si}^k = {}^1V_{si}^k - {}^0V_{si}^k$$

Considering the finite element solution for linear analysis, we express the components  $V_{ti}^k$  and  $V_{si}^k$  in terms of rotations about the global axes  ${}^0x_i$ ,  $i = 1, 2, 3$ . Namely we have

$$\underline{V}_t^k = \underline{\theta}_k \times {}^0\underline{V}_t^k \quad (3.8)$$

$$\underline{V}_s^k = \underline{\theta}_k \times {}^0\underline{V}_s^k$$

where  $\underline{\theta}_k$  is a vector listing the nodal point rotations at nodal point  $k$ , see Fig. 3.2,

$$\underline{\theta}_k = \begin{bmatrix} \theta_1^k \\ \theta_2^k \\ \theta_3^k \end{bmatrix} \quad (3.9)$$

Thus, substituting from Eqs. (3.8) and (3.9) into Eq. (3.6) the displacement components  $u_i(r,s,t)$  are obtained in terms of the nodal point displacements  $u_i^k$ , and rotations  $\theta_i^k$ , for  $i=1,2,3$  and  $k=1,2,3,4$  (cubic interpolation).

### 3.1.2 Element displacement interpolations including ovalization

The beam displacements shown in Eq. (3.6) assume that the cross-section of the pipe does not deform. To include the effect of ovalization we use the displacement patterns suggested by von Kármán and other authors [2, 5 and 6], and interpolate these displacement patterns cubically along the length of the elbow. Then, considering the in-plane and the out-of-plane actions of the pipe we use

$$w_E(r, \phi) = \sum_{m=1}^{N_c} \sum_{k=1}^4 h_k c_m^k \sin 2m\phi + \sum_{m=1}^{N_d} \sum_{k=1}^4 h_k d_m^k \cos 2m\phi \quad (3.10)$$

where the  $c_m^k$  and  $d_m^k$ , and  $k=1,2,3,4$  are the unknown generalized ovalization displacements. Depending on the pipe geometry, and the type of loading, it may be sufficient to include only the first, or first two, terms of one (or both) double summation(s) in Eq. (3.10), as discussed in Section 2.1.2 (Table 2.1). In the implementation of the element we have allowed  $N_c$  to be 0 (no ovalization), 1, 2 or 5 and similarly for  $N_d$ .

The total pipe-elbow displacements are the sum of the displacements given in Eq. (3.6) and Eq. (3.10). Therefore, a typical nodal point of a three-dimensional elbow element can have from six to twelve degrees-of-freedom at each node, depending on whether the ovalization displacements are included and which ovalization patterns are used.

### 3.1.3 Displacement derivatives

With the geometry and displacement interpolations given in Eqs. (3.3) and (3.6), standard procedures are used to evaluate the appropriate displacement derivatives that con-



stitute the strain-displacement transformation matrix referred to the beam displacement. Based on the results presented in Chapter 2 (Eqs. (2.36) to (2.39) and using the displacement interpolations given in Eq. (3.10) the complete strain-displacement relations for in-plane and out-of-plane bending of the elbow element can be written as

$$\begin{bmatrix} \epsilon_{\eta\eta} \\ \delta_{\eta\xi} \\ \delta_{\eta\xi} \\ \hline \epsilon_{\xi\xi} \end{bmatrix} = \sum_{k=1}^4 \begin{bmatrix} \underline{B}_k & \underline{B}_{ov1}^k & \underline{B}_{ov3}^k \\ \hline \underline{0} & \underline{B}_{ov2}^k & \underline{B}_{ov4}^k \end{bmatrix} \underline{u}^k \quad (3.11)$$

where

$$\underline{u}^{kT} = \left[ u_1^k \quad u_2^k \quad u_3^k \quad \theta_1^k \quad \theta_2^k \quad \theta_3^k \quad \middle| \quad c_1^k \quad c_2^k \quad c_3^k \quad \middle| \quad d_1^k \quad d_2^k \quad d_3^k \right] \quad (3.12)$$

and only as many ovalization displacements need be included as deemed necessary.

The displacement derivatives in  $\underline{B}_k$  correspond to the strains that are due to the beam nodal point displacement and rotations. Using Eqs. (3.6) to (3.9) we have

$$\begin{bmatrix} u_{i,r} \\ u_{i,s} \\ u_{i,t} \end{bmatrix} = \sum_{k=1}^N \begin{bmatrix} h_{k,r} [ 1 & (g)_{1i}^k & (g)_{2i}^k & (g)_{3i}^k ] \\ h_k [ 0 & (\hat{g})_{1i}^k & (\hat{g})_{2i}^k & (\hat{g})_{3i}^k ] \\ h_k [ 0 & (\bar{g})_{1i}^k & (\bar{g})_{2i}^k & (\bar{g})_{3i}^k ] \end{bmatrix} \begin{bmatrix} u_i^k \\ \theta_1^k \\ \theta_2^k \\ \theta_3^k \end{bmatrix} \quad (3.13)$$

where we employ the notation

$$(\hat{g})^k = \bar{a}_k \begin{bmatrix} 0 & -{}^0V_{s3}^k & {}^0V_{s2}^k \\ {}^0V_{s3}^k & 0 & -{}^0V_{s1}^k \\ -{}^0V_{s2}^k & {}^0V_{s1}^k & 0 \end{bmatrix} \quad (3.14)$$

$$(\bar{g})^k = \bar{a}_k \begin{bmatrix} 0 & -{}^0V_{t3}^k & {}^0V_{t2}^k \\ {}^0V_{t3}^k & 0 & -{}^0V_{t1}^k \\ -{}^0V_{t2}^k & {}^0V_{t1}^k & 0 \end{bmatrix} \quad (3.15)$$

and

$$(g)_{ij}^k = s (\hat{g})_{ij}^k + t (\bar{g})_{ij}^k \quad (3.16)$$

To obtain the displacement derivatives corresponding to the axes  ${}^0x_i$ ,  $i=1,2,3$  we employ the Jacobian transformation

$$\frac{\partial}{\partial \underline{x}^0} = {}^0\underline{J}^{-1} \frac{\partial}{\partial \underline{r}} \quad (3.17)$$

where the Jacobian matrix,  ${}^0\underline{J}$ , contains the derivatives of the coordinates  ${}^0x_i$ ,  $i=1,2,3$  with respect to the isoparametric coordinates  $r$ ,  $s$  and  $t$  [19]. Then, substituting from Eq. (3.13) into Eq. (3.17) we have

$$\begin{bmatrix} \frac{\partial u_i}{\partial x_1^0} \\ \frac{\partial u_i}{\partial x_2^0} \\ \frac{\partial u_i}{\partial x_3^0} \end{bmatrix} = \sum_{k=1}^N \begin{bmatrix} h_{k,1} & (G1)_{i1}^k & (G2)_{i1}^k & (G3)_{i1}^k \\ h_{k,2} & (G1)_{i2}^k & (G2)_{i2}^k & (G3)_{i2}^k \\ h_{k,3} & (G1)_{i3}^k & (G2)_{i3}^k & (G3)_{i3}^k \end{bmatrix} \begin{bmatrix} u_i^k \\ \theta_1^k \\ \theta_2^k \\ \theta_3^k \end{bmatrix} \quad (3.18)$$

where

$$(G_m)_{in}^k = \left( {}^0J_{n1}^{-1} (g)_{mi}^k \right) h_{k,r} + \left( {}^0J_{n2}^{-1} (\hat{g})_{mi}^k + {}^0J_{n3}^{-1} (\bar{g})_{mi}^k \right) h_k \quad (3.19)$$

With the displacement derivatives defined in Eq. (3.18) we can directly assemble the strain-displacement matrix  $\underline{B}_k$ . Namely, Eq. (3.18) is used to establish the global strain components (corresponding to the  ${}^0x_i$ ,  $i=1,2,3$  axes), which are then employed to obtain, using a second order tensor transformation, the local strain components  $\epsilon_{\eta\eta}$ ,  $\delta_{\eta\xi}$  and  $\delta_{\eta\xi}$  corresponding to the elements of the matrix  $\underline{B}_k$ .

The elements of the matrices  $\underline{B}_{ov1}^k$ ,  $\underline{B}_{ov2}^k$ ,  $\underline{B}_{ov3}^k$  and  $\underline{B}_{ov4}^k$  are associated to the element ovalization degrees-of-freedom as they correspond to the ovalization deformations in Eqs. (2.39). Thus, substituting  $w_{\xi}$  from Eq. (3.10) into Eqs. (2.39) we obtain

$$\underline{B}_{ov1}^k = \frac{h_k}{R - a \cos \phi} \begin{bmatrix} a_1 & a_2 & a_3 \\ 0 & 0 & 0 \\ 0 & 0 & 0 \end{bmatrix} + \frac{d}{dr} \begin{bmatrix} h_{k,r} & (a_1^I & a_2^I & a_3^I) \\ h_k & (b_1^I & b_2^I & b_3^I) \\ 0 & 0 & 0 \end{bmatrix} \quad (3.20)$$

where

$$a_\ell = m \cos(m\phi) \cos\phi + \sin(m\phi) \sin\phi \quad (3.21)$$

$$a_\ell^i = \left[ \frac{2}{(R - a \cos\phi)\theta} \right]^2 m \cos(m\phi) \xi \quad (3.22)$$

$$b_\ell^I = \left[ \frac{2}{(R - a \cos\phi)\theta} \right] \sin(m\phi) \quad (3.23)$$

$m = 2\ell$  ;  $R\theta =$  length of elbow at center line

and

$$\underline{B}_{ov2}^k = \frac{h_k}{a^2} \begin{bmatrix} b_1 & b_2 & b_3 \end{bmatrix} \quad (3.24)$$

where

$$b_\ell = -m(m^2 - 1) \cos(m\phi) \xi, \quad (3.25)$$

and

$$\underline{B}_{ov3}^k = \frac{h_k}{R - a \cos\phi} \begin{bmatrix} \tilde{a}_1 & \tilde{a}_2 & \tilde{a}_3 \\ 0 & 0 & 0 \\ 0 & 0 & 0 \end{bmatrix} + \frac{d}{dr} \begin{bmatrix} h_{k,r} (\tilde{a}_1^I & \tilde{a}_2^I & \tilde{a}_3^I) \\ h_k (\tilde{b}_1^I & \tilde{b}_2^I & \tilde{b}_3^I) \\ 0 & 0 & 0 \end{bmatrix} \quad (3.26)$$

where

$$\tilde{a}_1 = -m \sin(m\phi) \cos\phi + \cos(m\phi) \sin\phi \quad (3.27)$$

$$\tilde{a}_2^I = - \left[ \frac{2}{(R - a \cos\phi)\theta} \right]^2 m \sin(m\phi) \zeta \quad (3.28)$$

$$\tilde{b}_2^I = \left[ \frac{2}{(R - a \cos\phi)\theta} \right] \cos(m\phi) \quad , \quad (3.29)$$

and

$$\underline{B}_{ov4}^k = \frac{h_k}{a^2} \left[ \tilde{b}_1 \quad \tilde{b}_2 \quad \tilde{b}_3 \right] \quad (3.30)$$

where,

$$\tilde{b}_1 = m(m^2 - 1) \sin(m\phi) \zeta \quad (3.31)$$

The expressions given above are for a curved pipe. If a straight pipe is considered the term  $\left[ \frac{2}{(R - a \cos\phi)\theta} \right]$  need be replaced by  $\left[ \frac{2}{L} \right]$  where  $L$  is the total length of the element. Also, the first matrices in Eqs. (3.20) and (3.26) vanish and only the second matrices remain in the formulation of the straight elements.

### 3.2 Element Constitutive Matrix

The stress-strain matrix employed in the formulation cor-

responds to plane stress conditions in the  $\eta$ - $\xi$  plane (Kirchhoff's hypotheses). In linear analysis we use

$$\begin{bmatrix} \sigma_{\eta\eta} \\ \sigma_{\eta\xi} \\ \sigma_{\xi\eta} \\ \sigma_{\xi\xi} \end{bmatrix} = \frac{E}{1-\nu^2} \begin{bmatrix} 1 & 0 & 0 & \nu \\ 0 & \frac{1-\nu}{2} & 0 & 0 \\ 0 & 0 & \frac{1-\nu}{2} & 0 \\ \nu & 0 & 0 & 1 \end{bmatrix} \begin{bmatrix} \epsilon_{\eta\eta} \\ \gamma_{\eta\xi} \\ \gamma_{\xi\eta} \\ \epsilon_{\xi\xi} \end{bmatrix} \quad (3.32)$$

where  $E$  is the Young's modulus and  $\nu$  is the Poisson's ratio of the material.

### 3.5 Element Completeness and Compatibility Considerations

In the idealization of an actual physical problem by finite elements, the accuracy of the solution depends mainly on the number of elements used in the model and on the order of interpolation functions employed within the element domains. To assure the solution converges monotonically, the elements must be complete and compatible [19]. If these conditions are satisfied the analysis results will approximate the analytical ("exact") solution increasingly better as we continue to refine the finite element mesh. In this section we investigate whether the formulation of the elbow element,

which is a degenerated isoparametric (or superparametric) element, satisfies these convergence criteria.

The requirement of completeness means that the rigid body displacements and the constant strain states must be represented by the element displacement functions. Considering the superparametric elbow element, this condition is effectively verified by representing the stiffness matrix in the basis of its eigenvectors, which must contain the rigid body modes and the constant straining modes [19]. Namely, we want to diagonalize the element stiffness matrix  $\underline{K}_L$  by using the transformation,

$$\underline{\Lambda} = \underline{\Phi}^T \underline{K}_L \underline{\Phi} \quad (3.33)$$

with,

$$\underline{\Phi} = \left[ \begin{array}{c|c|c|c} \underline{\phi}_1 & \underline{\phi}_2 & \dots & \underline{\phi}_n \end{array} \right] \quad (3.34)$$

where  $\underline{\phi}_1, \dots, \underline{\phi}_n$  are the matrix eigenvectors and  $\underline{\Lambda}$  is a diagonal matrix storing the corresponding eigenvalues  $\lambda_i$ . Table 3.1 presents element lowest twelve eigenvalues and the physical meaning of the associated eigenvectors. The first six eigenvalues demonstrate the presence of six rigid body modes in the element displacement functions. Also, the remaining eigenvalues show that the element can represent torsional and flexural modes of the bend.

To satisfy the compatibility condition, the displacements



TABLE 3.1 THE TWELVE LOWEST EIGENVALUES OF A FOUR-NODE  
50 DEG. BEND ELBOW ELEMENT ( $\lambda = .165$ ,  $\nu = .3$ )

i	$\lambda_i/E$	Eigenvector representations
1 - 6	0.0	Three rigid body displacements and three rigid body rotations
7	.76806	torsional mode
8	.81707	in-plane bending mode
9	2.7167	torsional mode
10	2.9683	torsional plus out-of-plane bending mode
11	2.9806	in-plane bending mode
12	5.0741	in-plane bending mode

within the elements and across the element boundaries must be continuous. In the finite element models for beams where elements are connected at end nodes, the continuity in displacements between elements is always preserved. In the elbow element formulation, however, additional compatibility in the ovalization degrees-of-freedom must be preserved because of the longitudinal bending of the pipe skin included here. Hence, it is also necessary to enforce in the finite element formulation continuity on the first derivatives of the cross-sectional local displacements at the element boundaries. The longitudinal pipe skin bending strain in Eq. (2.39a) requires that continuity in  $\left(\frac{\partial w_{\xi}}{\partial \theta}\right)$  must be imposed, which is achieved using the penalty procedure presented in Chapter 4. It is interesting to notice, however, that the shear strain in Eq. (2.39c), which is a function of  $\left(\frac{\partial w_{\xi}}{\partial \theta}\right)$ , requires only continuity in  $w_{\xi}$  that is already assured in the formulation.

#### 4. END-EFFECTS IN THE ELBOW ELEMENT FORMULATION

The initial interest in end-effects on elbows was motivated by Purdue and Vigness [6] who reported a series of tests on bends of different sizes. In their work the authors show that for a 90° flanged elbow, a theory which does not account for the end-effects overestimates the flexibility and the stress intensification of the bend by a factor of two or more. Additional experimental results on 180° bends with or without flanges [36], on 90° flanged elbows [37], and on curved-straight pipe assemblages [38-40] further confirmed these conclusions:

(a) the flexibility and stress intensification factors of a flanged elbow depend on the total bend angle of the pipe and, (b) in a straight-curved pipe configuration, the amount of the cross-sectional ovalization decays monotonically from the elbow into the attached tangent portions, somehow stiffening the bend.

On the basis of these experimental evidences, various attempts have been made to devise analytical or numerical models that include these end effects [37, 41-43]. Apart from the limited success of these models in the analyses of bends, they are not general in use presenting some deficiencies such as being only applicable to flanged elbows or considering only constant in-plane bending loadings. Therefore, it is needed that a proposed model for general piping analysis is applicable to configurations involving assemblages of straight and curved tube sections while accounting for the important end-effects

such as flanges and continuity constraints.

In the preceding chapter we presented the finite element formulation of the pipe-elbow element. As we already pointed out, the elbow formulation is a natural enhancement of von Kármán's analysis. It includes the interaction effects (or end-effects) of the cross-sectional ovalization between elbows of different curvatures, elbows and straight pipe sections, and elbows with rigid flanges. The strain terms included in this formulation, beyond those considered in von Kármán's formulation, are due to the variation of ovalization along the longitudinal axis of the elbow. However, it was shown that to assure compatibility between the elements it is now also necessary to enforce continuity on the derivatives of the radial displacement with respect to the longitudinal membrane coordinate  $\eta$ . In this chapter a penalty procedure is introduced to impose this continuity. Two basic cases are considered: a fixity condition, when an element is clamped to a rigid flange, and a continuity condition, when two elements are joined.

#### 4.1 The Penalty-Function Method

The method of penalty-functions, used in applications of mathematical programming [44], is a reliable technique for solving constrained problems. The technique consists of transforming a constrained problem into a sequence of unconstrained minimization problems using a penalty-function. If for instance, we consider the problem of uni-dimensional

minimization of an objective function  $\mathbf{W}(\mathbf{x})$  subjected to equality constraint equations  $\mathbf{g}_i(\mathbf{x})=0$  ,  $i = 1, \dots, N$  , a possible penalty function for its solution is

$$\Phi(\mathbf{x}, \alpha) = \mathbf{W}(\mathbf{x}) + \alpha \sum_{i=1}^N [\mathbf{g}_i(\mathbf{x})]^2 \quad (4.1)$$

For each chosen value of  $\alpha$  , typically  $\alpha = 1, 10, 100, \dots$  , a solution that minimizes  $\Phi(\mathbf{x}, \alpha)$  is found. As  $\alpha$  gets larger, the solution will more closely satisfy the imposed constraints. Subject to certain conditions on the functions  $\mathbf{W}(\mathbf{x})$  and  $\mathbf{g}_i(\mathbf{x})$  , the penalty method has been shown to be a very reliable technique provided the value of  $\alpha$  is sufficiently large [45]. The choice of the appropriate size of  $\alpha$  must, in general, be left to an empirical test. In Table 4.1, an example illustrates the convergence of the method and shows how easily it can be applied in the solution of a constrained problem.

Considering the finite element discretization of the pipe elbow element presented in Chapter 3, it was shown that to assure the compatibility between adjoining elements it is necessary to impose equality constraints on the variational principle governing the element. The usual procedure of imposing such constraints is through the use of Lagrange multipliers but this technique increases the number of unknown parameters to solve for and results into a non-positive definite stiffness matrix. For these reasons, an increasing amount of attention has been paid to recent applications of

TABLE 4.1 USE AND CONVERGENCE OF THE PENALTY-FUNCTION METHOD

Objective Function: $W(x,y) = x^2 + y^2$				
Constraint Function: $g(x,y) = 2x + y - 2=0$				
Penalty Function: $\phi(x,y,\alpha) = x^2 + y^2 + \alpha(2x+y-2)^2$				
Exact Solution: $W_{\min}=.8$ at $x=.8$ and $y=.4$				
$\alpha$	$x$	$y$	$g$	$W$
0.	0.	0.	-2.	0.
1.	.6667	.3333	-.3333	.5556
10.	.7843	.3921	-.0393	.7689
100.	.7984	.3992	-.0040	.7968
1000.	.7998	.3999	-.0005	.7996

penalty methods in the finite element formulations of a wide range of problems [46-50].

#### 4.2 Imposition of Continuity on Derivative of Pipe Skin Radial Displacement

The objective is to enforce continuity on the first derivative of the ovalization displacement  $w_z$  between elements without introducing additional degrees-of-freedom. In the classical analysis of beam structures this continuity is achieved by introducing beam rotational degrees-of-freedom. However, we can enforce the continuity in the elbow formulation without the use of rotational degrees-of-freedom using a penalty-function procedure.

As we have already indicated, the basic technique in this method is to add the constraint to be achieved in the solution, say

$$\text{CONSTRAINT} = 0 \quad (4.2)$$

to the variational indicator of the problem in the following penalty-function form,

$$\Pi = \mathcal{U} - \mathcal{W} + \frac{\alpha}{2} \int_0^{2\pi} (\text{CONSTRAINT})^2 d\phi \quad (4.3)$$

where  $\mathcal{U}$  and  $\mathcal{W}$  are the total strain energy and total potential of the external loads, respectively, and  $\alpha$  is the penalty parameter. The solution obtained using Eq. (4.3), with  $\delta\Pi=0$ ,

will satisfy the condition in Eq. (4.2) to the required accuracy provided  $\alpha$  is selected sufficiently large [19, 32]. The following example yields some physical insight in the use of the penalty method.

The simply supported straight beam loaded at its mid-span, shown in Fig. 4.1(a), is modeled by two four-noded isoparametric elements. In the formulation only the beam axis transverse displacements are considered, i.e.,

$$w(r) = \sum_{i=1}^4 h_i w_i \quad (4.4)$$

where  $h_i$  are the interpolation functions, see Fig. 3.2, and  $w_i$  are the displacements at the element nodes. If transverse shear deformations are neglected, the cross-sectional rotations are, in linear analysis, the derivatives of the displacements with respect to the coordinate  $y$ . Therefore, to impose the continuity of cross-sectional rotations at the common node it is necessary to use the following compatibility constraint

$$\text{CONSTRAINT} = \frac{2}{L} \left. \frac{dw}{dr} \right|_{r=+1}^{(1)} - \frac{2}{L} \left. \frac{dw}{dr} \right|_{r=-1}^{(2)} \quad (4.5)$$

Bringing into Eq. (4.3) the expressions in Eqs. (4.4) and (4.5) and the usual longitudinal bending strains,

$$\epsilon_{yy} = - \left[ \frac{2}{L} \right]^2 \frac{d^2 w}{dr^2} z, \quad (4.6)$$



the equilibrium equations obtained by invoking the stationarity of the functional  $\Pi$  are

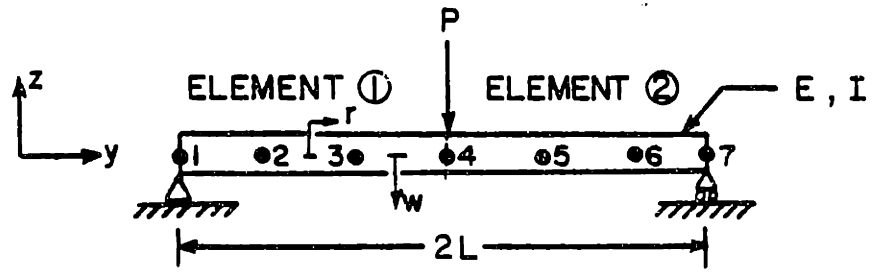
$$\left[ \underline{K} + \underline{K}_p^c(\alpha) \right] \underline{w} = \underline{F} \quad (4.7)$$

where  $\underline{K}$  and  $\underline{K}_p^c$  are, respectively, the linear stiffness matrix and the penalty matrix associated with the model displacements listed in  $\underline{w}$ , and  $\underline{F}$  is the load vector. Here we can notice the importance of the penalty parameter  $\alpha$ . The penalty contribution corresponds to the potential energy in a rotational spring with stiffness parameter  $\alpha$ , and the solution of Eq. (4.7) depends on the size of  $\alpha$ . In fact, the beam stiffness matrix  $\underline{K}$  is singular and the solution for  $\alpha=0$  corresponds to the unstable hinged beam. A large positive value of  $\alpha$ , or a large spring constant, enforces the compatibility between the elements and the solution converges to the usual beam results. A physical interpretation of the effects of the penalty parameter size on the solution is shown, pictorially, in Fig. 4.1(b), and Table 4.2.

Considering the elbow element we want to impose the constraints corresponding to two different conditions: firstly, the fixity condition when an element is clamped to a rigid flange and, secondly, the continuity condition when elements are joined.

#### 4.2.1 Fixity condition

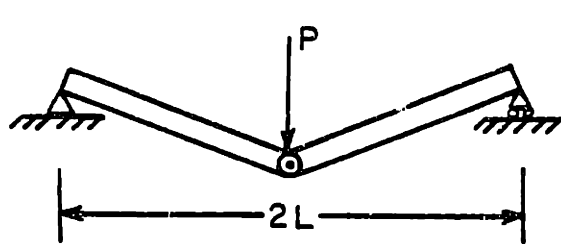
When an element is fixed or clamped to a rigid flange,



$$w(r) = \sum h_i w_i$$

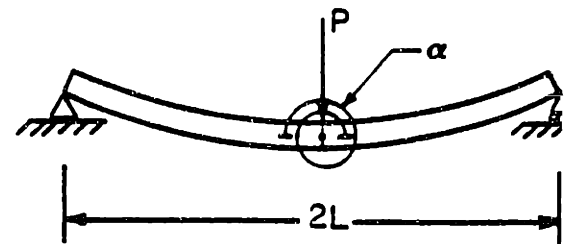
$$\text{CONSTRAINT} = \frac{2}{L} \left[ \left. \frac{dw}{dr} \right|_{r=+l}^{(1)} - \left. \frac{dw}{dr} \right|_{r=-l}^{(2)} \right] = 0$$

(a) The two equal beam element model.



UNSTABLE ( $\alpha = 0$ )

$$\underline{K} \underline{w} = \underline{F}$$



STABLE ( $\alpha \gg 0$ )

$$(\underline{K} + \underline{K}_p^c(\alpha)) \underline{w} = \underline{F}$$

(b) Solutions for different sizes of  $\alpha$ .

FIGURE 4.1 The Simply Supported Beam Considered.

TABLE 4.2 SOLUTIONS OF SIMPLY SUPPORTED BEAM FOR  
DIFFERENT SIZES OF  $\alpha$

E = Young's Modulus

I = Moment of Inertia

$$w_4^{th} = .166667 \frac{PL^5}{EI}$$

$$\beta_4^{th} = \frac{2}{L} \left( \frac{dw}{dr} \Big|_{r=+1}^{(1)} \right) = -\frac{2}{L} \left( \frac{dw}{dr} \Big|_{r=-1}^{(2)} \right) = 0.$$

$\alpha(L/EI)$	$w_4/w_4^{th}$	$\beta_4 (EI/PL^2)$
0.0	-	-
.1	16.0000	-2.499998
1.	2.5000	-.249999
10.	1.1500	-.025000
100.	1.0150	-.002500
1,000.	1.0015	-.000250
10,000.	1.0002	-.000025
100,000.	1.0000	-.000002

as shown schematically in Fig. 4.2(a), the boundary conditions are that at  $x=0$  there is no ovalization and  $\frac{dw_g}{dx} = 0$ . Hence, we have for the ovalization degrees-of-freedom, Eq. (3.10),

$$c_m^i = d_m^i = 0 \quad (\text{all } m) \quad (4.8)$$

and

$$\left[ \frac{2}{(R_n - a \cos \phi) \theta_n} \right] \frac{dw_g}{dr} \Big|_{r=-1} = 0 \quad (4.9)$$

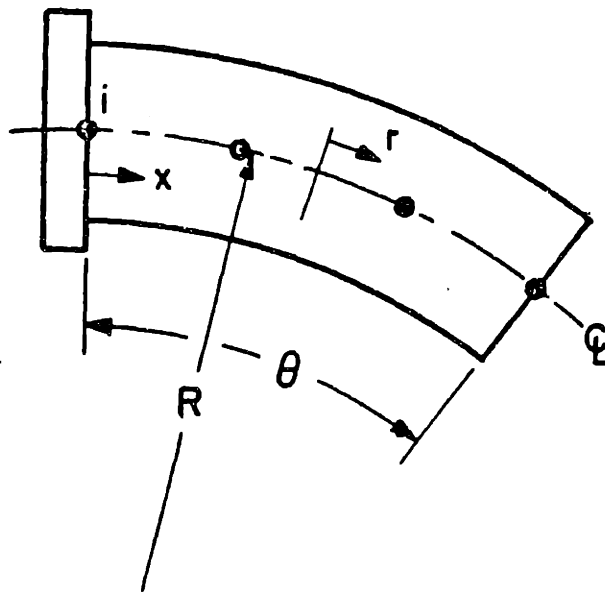
where

$$\frac{dw_g}{dr} \Big|_{r=-1} = - \sum_{k=1}^4 \left( \sum_{m=1}^{N_c} 2m c_m^k \frac{dh_k}{dr} \Big|_{r=-1} \cos 2m\phi \right.$$

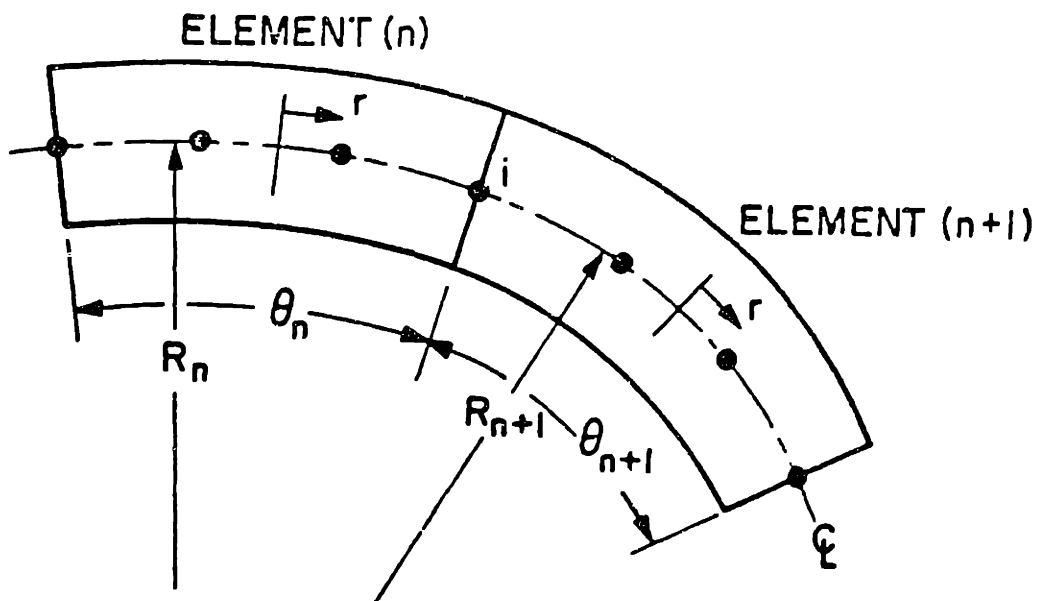
$$\left. - \sum_{m=1}^{N_d} 2m d_m^k \frac{dh_k}{dr} \Big|_{r=-1} \sin 2m\phi \right) \quad (4.10)$$

The constraint in Eq. (4.8) means that the ovalization degrees-of-freedom at node (i) must be set zero, whereas the constraint in Eq. (4.9) is imposed with a penalty parameter. Using in accordance with Eq. (4.2)

$$\text{CONSTRAINT} = \left[ \frac{2}{(R_n - a \cos \phi) \theta_n} \frac{dw_g}{dr} \Big|_{r=-1} - 0 \right] \quad (4.11)$$



(a) ELBOW WITH A RIGID FLANGE AT NODE  $i$



(b) ELBOWS OF DIFFERENT RADII JOINED AT NODE  $i$

FIGURE 4.2 - Interactions Considered in Analyses

then substituting into Eq. (4.3) and invoking the stationarity condition on  $\Pi$  results into the following penalty matrix

$$\underline{K}_p^F = \alpha \int_0^{2\pi} \underline{G}_F^T \left[ \frac{2}{(R_n - a \cos \phi) \theta_n} \right]^2 \underline{G}_F d\phi \quad (4.12)$$

where

$$\underline{G}_F = [\dots \bar{a}_1^k \bar{a}_2^k \bar{a}_3^k \bar{b}_1^k \bar{b}_2^k \bar{b}_3^k \dots] \quad (4.13)$$

$$\bar{a}_m^k = -2m \left. \frac{dh_k}{dr} \right|_{r=-1} \cos 2m\phi \quad (4.14)$$

$$\bar{b}_m^k = 2m \left. \frac{dh_k}{dr} \right|_{r=-1} \sin 2m\phi \quad (4.15)$$

and  $\underline{K}_p^F$  is defined corresponding to the degrees-of-freedom

$$\underline{u}^{FT} = [\dots \underbrace{c_1^k \ c_2^k \ c_3^k \ d_1^k \ d_2^k \ d_3^k}_{\text{node } k} \dots] \quad (4.16)$$

The matrix  $\underline{K}_p^F$  with a relatively large value of  $\alpha$  is added using the usual direct stiffness matrix procedure [19] to enforce the constraint in Eq. (4.11).

#### 4.2.2 Continuity condition

At the intersection of two elbow elements as shown in Fig. 4.2(b), the ovalization is automatically continuous because the same ovalization degrees-of-freedom pertain to both elements. In addition, we have the continuity condition

$$\text{CONSTRAINT} = \left[ \frac{2}{(R_n - a \cos \phi) \theta_n} \right] \left. \frac{dw_g}{dr} \right|_{r=+1} - \left[ \frac{2}{(R_{n+1} - a \cos \phi) \theta_{n+1}} \right] \left. \frac{dw_g}{dr} \right|_{r=-1}$$

This condition is imposed using the penalty-function method already used in Section 4.2. Substituting into Eq. (4.3) from Eq. (4.17) we now obtain the penalty matrix

$$\underline{K}_p^c = \alpha \int_0^{2\pi} \underline{G}_c^T \underline{G}_c d\phi \quad (4.18)$$

where

$$\underline{G}_c = \left[ \dots \bar{a}_1^{k(n)} \bar{a}_2^{k(n)} \bar{a}_3^{k(n)} \bar{b}_1^{k(n)} \bar{b}_2^{k(n)} \bar{b}_3^{k(n)} \dots \bar{a}_1 \bar{a}_2 \bar{a}_3 \bar{b}_1 \bar{b}_2 \bar{b}_3 \dots \right. \\ \left. \dots \bar{a}_1^{k(n+1)} \bar{a}_2^{k(n+1)} \bar{a}_3^{k(n+1)} \bar{b}_1^{k(n+1)} \bar{b}_2^{k(n+1)} \bar{b}_3^{k(n+1)} \dots \right] \quad (4.19)$$

$$\bar{a}_m^{k(n)} = - \left[ \frac{2}{(R_n - a \cos \phi) \theta_n} \right] \left. \begin{array}{l} 2m \frac{d h_k^{(n)}}{dr} \Big|_{r=+1} \cos 2m\phi \\ \end{array} \right\} k \neq 2 \quad (4)$$

$$\bar{b}_m^{k(n)} = \left[ \frac{2}{(R_n - a \cos \phi) \theta_n} \right] \left. \begin{array}{l} 2m \frac{d h_k^{(n)}}{dr} \Big|_{r=+1} \sin 2m\phi \\ \end{array} \right\} k \neq 2 \quad (4)$$

$$\bar{a}_m^{k(n+1)} = \left[ \frac{2}{(R_{n+1} - a \cos \phi) \theta_{n+1}} \right] \left. \begin{array}{l} 2m \frac{d h_k^{(n+1)}}{dr} \Big|_{r=-1} \cos 2m\phi \\ \end{array} \right\} k \neq 1 \quad (4)$$

$$\bar{b}_m^{k(n+1)} = - \left[ \frac{2}{(R_{n+1} - a \cos \phi) \theta_{n+1}} \right] \left. \begin{array}{l} 2m \frac{d h_k^{(n+1)}}{dr} \Big|_{r=-1} \sin 2m\phi \\ \end{array} \right\} k \neq 1 \quad (4)$$

and for the common node (i) of the two elements,

$$\bar{a}_m = \left[ - \left( \frac{2}{(R_n - a \cos \phi) \theta_n} \right) \frac{d h_2^{(n)}}{d r} \Big|_{r=+1} + \left( \frac{2}{(R_{n+1} - a \cos \phi) \theta_{n+1}} \right) \frac{d h_1^{(n+1)}}{d r} \Big|_{r=-1} \right] 2m \cos 2m\phi \quad (4.24)$$

$$\bar{b}_m = \left[ \left( \frac{2}{(R_n - a \cos \phi) \theta_n} \right) \frac{d h_2^{(n)}}{d r} \Big|_{r=+1} - \left( \frac{2}{(R_{n+1} - a \cos \phi) \theta_{n+1}} \right) \frac{d h_1^{(n+1)}}{d r} \Big|_{r=-1} \right] 2m \sin 2m\phi \quad (4.25)$$

This penalty matrix corresponds to the degrees-of-freedom

$$\underline{u}^{cT} = \left[ \begin{array}{cccccccc} \dots & c_1^{k(n)} & c_2^{k(n)} & c_3^{k(n)} & d_1^{k(n)} & d_2^{k(n)} & d_3^{k(n)} & \dots & c_1 & c_2 & c_3 & d_1 & d_2 & d_3 & \dots \\ & \underbrace{\hspace{10em}}_{\text{node } k \text{ of element } (n), k \neq 2} & & & & & & & \underbrace{\hspace{10em}}_{\text{node } i} & & & & & & \\ & & & & & & & & & & & & & & \\ & & & & & & & & & & & & & & \\ \dots & c_1^{k(n+1)} & c_2^{k(n+1)} & c_3^{k(n+1)} & d_1^{k(n+1)} & d_2^{k(n+1)} & d_3^{k(n+1)} & \dots & & & & & & & \\ & \underbrace{\hspace{10em}}_{\text{node } k \text{ of element } (n+1), k \neq 1} & & & & & & & & & & & & & \end{array} \right] \quad (4.26)$$

In the case of a straight pipe abutting a curved pipe, the



continuity condition in Eq. (4.17) needs be replaced by the approximate constraint expression

$$\text{CONSTRAINT} = \left[ \frac{2}{L} \right] \frac{dw_g}{dr} \Big|_{r=+1} - \left[ \frac{2}{R_n \theta_n} \right] \frac{dw_g}{dr} \Big|_{r=-1} \quad (4.27)$$

where  $L$  and  $R_n \theta_n$  are the centre lines' lengths of the straight and the curved adjoining elements. Accordingly, Eqs. (4.20) to (4.25) should also be modified by replacing the terms  $\left[ \frac{2}{(R_n - a \cos \phi) \theta_n} \right]$  and  $\left[ \frac{2}{(R_{n+1} - a \cos \phi) \theta_{n+1}} \right]$  by  $\left[ \frac{2}{L} \right]$  and  $\left[ \frac{2}{R_n \theta_n} \right]$ , respectively.

## 5. INTERNAL PRESSURE EFFECTS IN PIPES

The recent trend in piping design towards an increasing use of thin-walled bends subjected to high stresses has called for a closer attention to the effects of internal pressure on the pipe behavior. The fact that the internal pressure decreases the flexibility of the elbow was first considered by Thuloup [51], who assumed a deformation shape of the tube to obtain a solution using the method of minimum potential energy. Following the same method, other analytical solutions have also been obtained [52-54] where calculations of the work done by the internal pressure on the ovalized cross-section were employed to modify von Kármán's strain energy equation, see Eq. (2.4). This way some design formulae were derived for the flexibility and the stress intensification factors of pressurized curved pipes [51]. Thin elastic shell theories have also been employed in some analytical solutions including internal pressure effects [55-59]. For instance, Crandall and Dahl [56] followed the shell theory approach presented in Ref. [8] and recognized that for small displacements of the shell surface, a nonlinear coupling between pressure and change in pipe cross-sectional area could be identified as a negative loading term in the shell equilibrium equations. This nonlinear dependency of the pressure loading on the displacements in the plane of the elbow cross-section is regarded as a stiffening effect due to the pipe internal pressure.

In this chapter we discuss the additional work due to internal pressure, in order to include the internal pressure effects in the variational indicator of the elbow element. The presentation shows that by using the basic cross-sectional deformation modes of the elbow, the important stiffening mechanism in the bend acts towards the restoration of the circular shape of the pipe cross-section.

### 5.1 The Internal Pressure Work

As the cross-section of a pressurized bend deforms because of external loadings, an additional work represented by the internal pressure acting against the change in the cross-section of the elbow must be considered. The work to be added to the variational indicator of the elbow element is

$$W_{pr} = - \int_{r,\phi} p \, dA(r,\phi) \left[ \frac{(R-a \cos \phi)\theta}{2} \right] \frac{dr}{-1 \leq r \leq 1} \quad (5.1)$$

$$0 \leq \phi \leq 2\pi$$

where  $p$  is the internal pressure,  $[(R-a \cos \phi)\theta]$  is the longitudinal arc length of the bend midsurface and  $dA(r,\phi)$  is the differential of change in area due to the cross-sectional ovalization. As shown in Fig. 5.1, this differential area results from the deformation of an initially circular pipe section and is a function of the local displacements  $w_{\xi}$  and  $w_{\zeta}$ .

### 5.1.1 Calculation of area change in a deformed pipe section

Referring to Fig. 5.1 where points A and B on the initially underformed circular cross-section are displaced to points A' and B' on the ovalized cross-section, we approximate the differential area  $dA$  by the area of a quadrilateral polygon AA'B'B. The coordinates of the polygon vertices on the auxiliary coordinate axes  $\bar{x}$  and  $\bar{y}$  are

$$\begin{aligned} A(a, 0) ; B(a \cos d\phi, a \sin d\phi) ; A'(a + w_\zeta, w_\xi) \quad \text{and} \\ B'([a + w_\zeta + dw_\zeta] \cos d\phi - [w_\xi + dw_\xi] \sin d\phi, \\ [a + w_\zeta + dw_\zeta] \sin d\phi + [w_\xi + dw_\xi] \cos d\phi) \end{aligned} \quad (5.2)$$

and the area sought is given by the expression

$$dA = \frac{1}{2} \left[ (\bar{x}_A - \bar{x}_{B'}) (\bar{y}_{A'} - \bar{y}_B) - (\bar{y}_A - \bar{y}_{B'}) (\bar{x}_{A'} - \bar{x}_B) \right] \quad (5.3)$$

substituting the point coordinates from Eqs. (5.2) into Eq. (5.3), making the following two approximations

$$\sin d\phi \doteq d\phi \quad \text{and} \quad \cos d\phi \doteq 1, \quad (5.4)$$

we obtain

$$dA = \frac{1}{2} \left[ \underbrace{2aw_\zeta + w_\zeta \left( w_\zeta + \frac{dw_\zeta}{d\phi} \right)}_{\text{TERM 1}} + \underbrace{w_\xi^2 - w_\xi \frac{dw_\xi}{d\phi}}_{\text{TERM 2}} \right] d\phi \quad (5.5)$$

In Eq. (5.5) TERM 1 and TERM 2 are the changes in area due, respectively, to the stretching and the bending of a deformed cross-section. Using the inextensibility condition, assumption

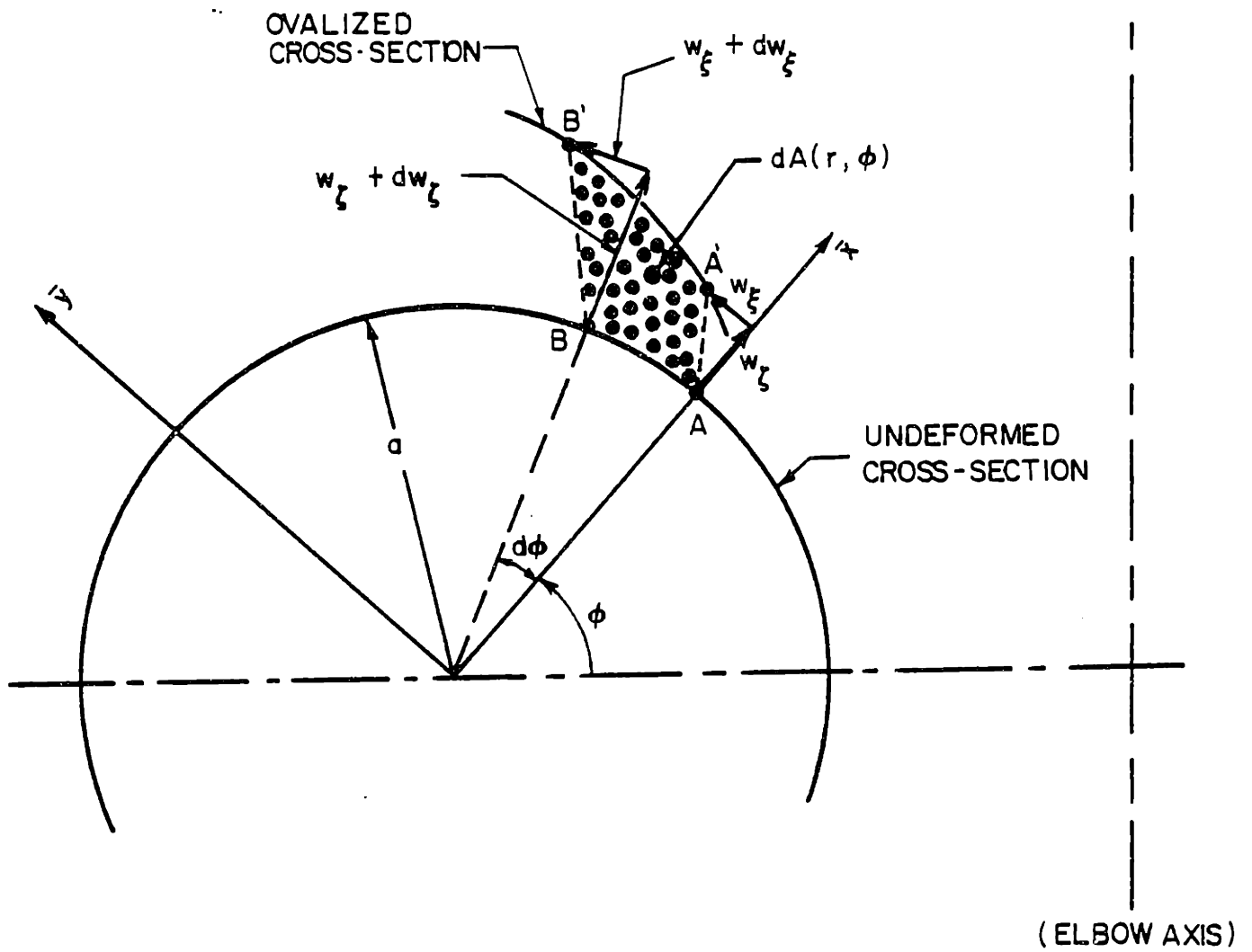


FIGURE 5.1 Area Change of an Ovalized Cross-section.

(c) in Section 2.1, it is required that  $AB = A'B'$  in Fig. 5.1. Hence, Eqs. (5.2) with the approximations in Eq. (5.4) yields

$$(a d\phi)^2 = [dw_\xi - (w_\xi + dw_\xi)d\phi]^2 + [(a + w_\xi + dw_\xi)d\phi + dw_\xi]^2, \quad (5.6)$$

and then we obtain the conditions,

$$w_\xi + \frac{dw_\xi}{d\phi} = 0 \quad (5.7)$$

$$w_\xi^2 + \left(\frac{dw_\xi}{d\phi}\right)^2 - 2w_\xi \frac{dw_\xi}{d\phi} + \left(\frac{dw_\xi}{d\phi}\right)^2 + 2w_\xi \frac{dw_\xi}{d\phi} + w_\xi^2 = 0 \quad (5.8)$$

In Eq. (5.7), which is the von Kármán's condition employed in the formulation of the elbow element -- Eq. (2.1) -- only first order approximations are considered for the deformations of the elbow cross-section. However, the area change in Eq. (5.5) depends upon second order displacement terms and, therefore, it is also necessary to include the second order relation in Eq. (5.8). Thus, combining the two equations above we obtain

$$-w_\xi \frac{dw_\xi}{d\phi} = -\frac{1}{2} \left[ w_\xi^2 + \left(\frac{d^2w_\xi}{d\phi^2}\right)^2 \right], \quad (5.9)$$

and inserting Eqs. (5.7) and (5.9) into Eq. (5.5) yields

$$dA = \left\{ -a \frac{dw_\xi}{d\phi} + \frac{1}{4} \left[ w_\xi^2 - \left(\frac{d^2w_\xi}{d\phi^2}\right)^2 \right] \right\} d\phi \quad (5.10)$$

Substituting the foregoing equation and the displacement patterns for  $w_\xi(r, \phi)$  given in Eq. (3.10) into Eq. (5.1), we note

that the non-squared term in Eq. (5.10) vanishes during the integration process. Hence, considering the bending deformations only, the expression for the area change reduces to

$$dA(r,\phi) = \frac{1}{4} \left[ w_{\xi}^2(r,\phi) - \left( \frac{d^2 w_{\xi}(r,\phi)}{d\phi^2} \right)^2 \right] d\phi \quad (5.11)$$

which, when substituted into Eq. (5.1) yields

$$\mathcal{W}_{pr} = \int_{-1}^{+1} \int_0^{2\pi} \left( \frac{p}{4} \right) \left[ \left( \frac{d^2 w_{\xi}(r,\phi)}{d\phi^2} \right)^2 - w_{\xi}^2(r,\phi) \right] \left( \frac{(R - a \cos \phi) \theta}{2} \right) d\phi dr \quad (5.12)$$

In the next section, the internal pressure effects are included in the formulation of the elbow element by adding the above equation to the variational indicator of the element.

## 5.2 The Elbow Element Formulation with Internal Pressure

In Eq. (5.12), the analytical expression of the work due to the internal pressure depends on the second power of the local circumferential displacement  $w_{\xi}$ . Physically, this dependence suggests that the additional work  $\mathcal{W}_{pr}$ , included in the total potential of the problem, adds directly to the pipe strain energy and gives an increasing bending stiffness to the pressurized elbow. In fact, substituting for the displacements  $w_{\xi}(r,\phi)$  from Eq. (3.10) into Eq. (5.12), the variation in the internal pressure work results in the following additional stiffness matrix

$$\underline{K}_{pr} = \frac{p}{2} \int_{-1}^{+1} \int_0^{2\pi} \left[ \underline{G}_{p1}^T \underline{G}_{p1} - \underline{G}_{p2}^T \underline{G}_{p2} \right] \left( \frac{(R - a \cos \phi) \theta}{2} \right) d\phi dr \quad (5.13)$$

where,

$$\underline{G}_{p1} = \left[ \dots \bar{a}_1^k \bar{a}_2^k \bar{a}_3^k \bar{b}_1^k \bar{b}_2^k \bar{b}_3^k \dots \right] \quad (5.14)$$

$$\bar{a}_m^k = -(2m)^2 h_k \sin 2m\phi \quad (5.15)$$

$$\bar{b}_m^k = -(2m)^2 h_k \cos 2m\phi \quad (5.16)$$

$$\underline{G}_{p2} = \left[ \dots \tilde{a}_1^k \tilde{a}_2^k \tilde{a}_3^k \tilde{b}_1^k \tilde{b}_2^k \tilde{b}_3^k \dots \right] \quad (5.17)$$

$$\tilde{a}_m^k = h_k \sin 2m\phi \quad (5.18)$$

$$\tilde{b}_m^k = h_k \cos 2m\phi \quad (5.19)$$



and  $\underline{K}_{pr}$  is defined corresponding to the ovalization degrees-of-freedom

$$\underline{u}^T = [\dots c_1^k \ c_2^k \ c_3^k \ d_1^k \ d_2^k \ d_3^k \ \dots] \quad (5.20)$$

At this point, it is important to note that the equilibrium equations that govern the linear response of a pressurized elbow element are given by

$$(\underline{K}_L + \underline{K}_p)\underline{u} = \underline{R} - \underline{F}_{pr} \quad (5.21)$$

where  $\underline{K}_L$  and  $\underline{K}_p$  are the element stiffness and penalty matrices defined in Chapters 3 and 4,  $\underline{R}$  is the element external load vector, and

$$\underline{F}_{pr} = \underline{K}_{pr} \underline{u} \quad (5.22)$$

which is the equivalent pressure loading vector. Because of its displacement dependence, the pressure load is transferred to the l.h.s. of Eqs. [5.21] for the solution of the element displacements  $\underline{u}$ .

## 6. ELBOW ELEMENT FORMULATION FOR NONLINEAR ANALYSES

The formulation of the elbow element presented in the preceding chapters has been developed for linear analysis of the pipe bends. In the formulation, the resulting equilibrium equations are derived with the assumption that during deformation the element undergoes infinitesimally small displacements without changes in geometry, material properties or boundary conditions. However, as the displacements become large or the material law does not follow Hooke's law, the effect of nonlinearities becomes prominent and the linear formulation presented above is inadequate in modeling the physical behavior of the pipe. In this chapter, we extend the elbow element formulation to an incremental formulation that incorporates geometric and material nonlinearities [60]. We present first the continuum mechanics equations and then develop the appropriate element matrices.

### 6.1 A Formulation for a Geometric-Nonlinear-Only Analysis

In a large displacement analysis of a piping system, the actual strains associated with the deformation may be small such that the elastic limit of the material is not exceeded. In this case, the nonlinearity of the problem is only embodied in the kinematics of the deformation. Such type of analysis can be considered as a geometric-nonlinear-only analysis which however is considerably more complex than the linear analysis [61].

Considering a large displacement motion of the bend in a stationary Cartesian coordinate system, we assume that the solutions for the static and kinematic variables for all time steps from time 0 (underformed configuration) to time  $t$  are known. The basic aim of the analysis is to establish an equation of virtual work from which the unknown static and kinematic variables in the configuration at time  $t+\Delta t$  ( $\Delta t$  is an increment in time) can be solved. Hence, in the analysis we follow all particles of the bend in their motion, from the original to the final configuration, meaning that we adopt a Lagrangian formulation of the problem [62-64].

Since a displacement-based finite element procedure is employed for numerical solution, the principle of virtual work is used to express the equilibrium of the body. Using tensor notation, this principle requires, at time  $t+\Delta t$ , that

$$\int_{t+\Delta t V} {}^{t+\Delta t} \tau_{ij} \delta {}_{t+\Delta t} e_{ij} {}^{t+\Delta t} dV = {}^{t+\Delta t} \mathcal{R} \quad (6.1)$$

where  ${}^{t+\Delta t} \tau_{ij}$  are the Cartesian components of the Cauchy stress tensor,  ${}_{t+\Delta t} e_{ij}$  are the Cartesian components of the infinitesimal strain tensor measured in the configuration at time  $t+\Delta t$ ,

$${}_{t+\Delta t} e_{ij} = \frac{1}{2} \left( \frac{\partial u_i}{\partial {}^{t+\Delta t} x_j} + \frac{\partial u_j}{\partial {}^{t+\Delta t} x_i} \right), \quad (6.2)$$

and the corresponding total external virtual work  ${}^{t+\Delta t}\mathcal{R}$  is due to the surface tractions with components  ${}_o f_i^S$  and body force components  ${}_o f_i^B$ ,

$${}^{t+\Delta t}\mathcal{R} = \int_{t+\Delta t_S} {}^{t+\Delta t}{}_o f_i^S \delta u_i {}^{t+\Delta t}dS + \int_{t+\Delta t_V} {}^{t+\Delta t}{}_o f_i^B \delta u_i {}^{t+\Delta t}dV \quad (6.3)$$

In Eqs. (6.1) and (6.3)  $u_i$  are the components of a displacement increment vector, and  $\delta$  means "variation in". Note that  $u_i = {}^{t+\Delta t}u_i - {}^t u_i$ , we also use

$${}^{t+\Delta t}x_i = {}^0 x_i + {}^{t+\Delta t}u_i \quad (6.4)$$

$${}^t x_i = {}^0 x_i + {}^t u_i \quad (6.5)$$

where  ${}^0 x_i$ ,  ${}^t x_i$  and  ${}^{t+\Delta t}x_i$  are components of the coordinates at times 0,  $t$  and  $t+\Delta t$  respectively.

Since the stress and strain measures used in Eq. (6.1) refer to the current unknown configuration at time  $t+\Delta t$ , this equation cannot be directly applied. However, an approximate solution can be obtained by referring all variables to previously calculated known configurations, and linearizing the resulting equation. This solution can then be improved upon by an iteration process. The desired transformation can be achieved using two equivalent transformations, namely, a total Lagrangian (T.L.) formulation or an updated Lagrangian (U.L.) formulation

[61, 65-67]. In the T.L. formulation, all static and kinematic variables are referred to the initial configuration at time 0 while in the U.L. formulation they are referred to the last known configuration, at time  $t$ . Both formulations are based on equivalent procedures and it has been shown that they are entirely equivalent [68]. The only advantage of using one formulation rather than the other lies in its better numerical efficiency.

In the present study we employ the T.L. formulation in the large displacement analysis of the pipe bend. Using the configuration at time 0 as a reference, the governing virtual work in Eq. (6.1) can be expressed as follows

$$\int_{0V}^{t+\Delta t} {}_0S_{ij} \delta {}_0^{t+\Delta t} E_{ij} {}^0 dV = {}^{t+\Delta t} \mathcal{R} \quad (6.6)$$

where the  ${}_0^{t+\Delta t} S_{ij}$  and  ${}_0^{t+\Delta t} E_{ij}$  are the components of the 2nd Piola-Kirchhoff stress tensor and Green-Lagrange strain tensor, both referred to the initial configuration, and  ${}^{t+\Delta t} \mathcal{R}$  is redefined considering the initial configuration of the body,

$${}^{t+\Delta t} \mathcal{R} = \int_{0S} {}^{t+\Delta t} f_i^s \delta u_i {}^0 dS + \int_{0V} {}^{t+\Delta t} f_i^B \delta u_i {}^0 dV \quad (6.7)$$

The actual equilibrium equation expressed in Eq. (6.6) is obtained from Eq. (6.1) through the following transformations:

$${}^{t+\Delta t}{}_0 S_{ij} = \frac{{}^0 \rho}{{}^{t+\Delta t} \rho} {}^{t+\Delta t} \chi_{i,p} {}^{t+\Delta t} \tau_{pq} {}^{t+\Delta t} \chi_{j,q} \quad (6.8)$$

$${}^{t+\Delta t}{}_0 E_{ij} = {}^{t+\Delta t} \chi_{i,p} {}^{t+\Delta t} e_{pq} {}^{t+\Delta t} \chi_{j,q} \quad (6.9)$$

where  ${}^{t+\Delta t} \chi_{i,p} \equiv \partial {}^{t+\Delta t} \chi_i / \partial {}^0 x_p$ , and  $\rho / {}^{t+\Delta t} \rho$  represents the ratio of mass densities that follows from mass conservation condition

$$\rho {}^0 dV = {}^{t+\Delta t} \rho {}^{t+\Delta t} dV \quad (6.10)$$

It should be noted that Eqs. (6.1) and (6.6) are entirely equivalent since the corresponding stress and strain measures used in these equations are energy-conjugate. The 2nd Piola-Kichhoff stress tensor is used in this study because it is a simple and symmetric tensor and its components are invariants when the material is subjected to a rigid body rotation [19].

To obtain an approximate solution of Eq. (6.6) we need to linearize the equation about the last calculated configuration at time  $t$ . Using incremental decompositions of the stress and strain tensors, we rewrite them as

$${}^{t+\Delta t}{}_0 S_{ij} = {}^t{}_0 S_{ij} + {}_0 S_{ij} \quad (6.11)$$

and

$${}^{t+\Delta t} \mathcal{E}_{ij} = {}^t \mathcal{E}_{ij} + {}_o \mathcal{E}_{ij} \quad (6.12)$$

where  ${}_o \mathcal{S}_{ij}$  and  ${}_o \mathcal{E}_{ij}$  are increments of the 2nd Piola-Kirchhoff stress tensor and of the Green-Lagrange strain tensor, respectively. Also,  ${}_o \mathcal{E}_{ij}$  can be decomposed into the following components,

$${}_o \mathcal{E}_{ij} = {}_o e_{ij} + {}_o \eta_{ij} \quad (6.13)$$

with

$${}_o e_{ij} = \frac{1}{2} \left( {}_o u_{i,j} + {}_o u_{j,i} + \underbrace{{}^t u_{k,i} \quad {}_o u_{k,j} + {}_o u_{k,i} \quad {}^t u_{k,j}} \right) \quad (6.14)$$

being the linear component, and

$${}_o \eta_{ij} = \frac{1}{2} \left( {}_o u_{k,i} \quad {}_o u_{k,j} \right) \quad (6.15)$$

being the nonlinear component. Both components are expressed in terms of unknown increments of displacement derivatives with  ${}_o u_{i,j} \equiv \partial u_i / \partial x_j$ . The underlined expression in Eq. (6.14), obtained in the T.L. formulation, is an initial displacement effect that contains the derivatives of the total displacements at time  $t$  with respect to the original configuration coordinates  ${}^o x_i$ ,  $i=1,2,3$ , i.e.,  ${}^t u_{i,j} \equiv \partial u_i / \partial x_j$ . Substituting Eqs. (6.11) and (6.12) into Eq. (6.6) and noting that

$$\delta^{t+\Delta t} \delta_0 \epsilon_{ij} = \delta_0 \epsilon_{ij} \quad (6.16)$$

and

$${}_0 S_{ij} = {}_0 C_{ijpq} \epsilon_{pq} \quad (6.17)$$

leads to the equation of motion to be solved in the T.L. formulation:

$$\int_{0V} {}_0 C_{ijpq} \epsilon_{pq} \delta_0 \epsilon_{ij} dV + \int_{0V} {}^t S_{ij} \delta_0 \eta_{ij} dV = {}^{t+\Delta t} R - \int_{0V} {}^t S_{ij} \delta_0 e_{ij} dV \quad (6.18)$$

where  ${}_0 C_{ijpq}$  is the incremental material property tensor referred to the initial configuration. To deal with the nonlinearity appearing in the first integral of Eq. (6.18) we introduce the following approximations

$${}_0 S_{ij} \doteq {}_0 C_{ijpq} \epsilon_{pq} \quad (6.19)$$

and

$$\delta_0 \epsilon_{ij} \doteq \delta_0 e_{ij} \quad (6.20)$$

to obtain the linearization. Therefore, the resulting approximate equations of motion referred to the original configuration



become

$$\int_{\circ V} \circ C_{ijpq} \circ e_{pq} \delta_{\circ} e_{ij} \circ dV + \int_{\circ V} \circ S_{ij}^t \delta_{\circ} \eta_{ij} \circ dV = \int_{\circ V} \circ S_{ij}^{t+\Delta t} \delta_{\circ} e_{ij} \circ dV \quad (6.21)$$

### 6.1.1 Finite element formulation (beam displacement modes only)

The general incremental continuum mechanics equations presented in the previous section are now used to develop the governing finite element equations.

In the derivation of the governing finite element equations we follow the same steps used in linear analysis: selected interpolation functions, employed in the interpolation of element coordinates and displacements, are used in the continuum mechanics equations. Also, in this derivation we only consider the beam deformation modes without ovalization and consider a single element, because the governing equilibrium equations of an assemblage of elements can be constructed using the direct stiffness procedure.

The aim is to solve the basic Eqs. (6.21), which express the equilibrium and compatibility requirements of a general body in the configuration at time  $t+\Delta t$ . Considering the components of the Green-Lagrange strain increments in Eqs. (6.14) and (6.15), two sets of terms, calculated at time  $t$ , are involved in the expressions: (a) displacement increment

derivatives, and (b) total displacement derivatives, both referred to the original configuration coordinates. The evaluation of these terms are obtained using the element kinematic relation in Eqs. (3.3) and (3.6). Hence, the displacement increment derivatives have already been obtained in Eq. (3.18) for the linear analysis formulation. The total displacement derivatives, which account for the initial displacement effects, are now calculated considering the element known configurations at time 0 and time  $t$ . Thus, because  ${}^t u_i = {}^t x_i - {}^0 x_i$ , we have for the beam deformations,

$${}^t u_i = \sum_{k=1}^N h_k {}^t u_i + t \sum_{k=1}^N \bar{a}_k h_k [{}^t V_{ti}^k - {}^0 V_{ti}^k] + s \sum_{k=1}^N \bar{a}_k h_k [{}^t V_{si}^k - {}^0 V_{si}^k] \quad (6.22)$$

Using Eq. (6.22), the displacement derivatives referred to the local  $r, s, t$  coordinates follow

$$\begin{aligned} {}^t u_{i,r} &= \sum_{k=1}^N h_{k,r} \left\{ {}^t u_i^k + \bar{a}_k \left[ t ({}^t V_{ti}^k - {}^0 V_{ti}^k) + s ({}^t V_{si}^k - {}^0 V_{si}^k) \right] \right\} \\ {}^t u_{i,s} &= \sum_{k=1}^N h_k \bar{a}_k ({}^t V_{si}^k - {}^0 V_{si}^k) \\ {}^t u_{i,t} &= \sum_{k=1}^N h_k \bar{a}_k ({}^t V_{ti}^k - {}^0 V_{ti}^k) \end{aligned} \quad (6.23)$$

Substituting Eqs. (6.23) with the Jacobian transformation of Eq. (3.17) we finally obtain

$$\begin{aligned}
 {}^t u_{i,j} = & \sum_{k=1}^N {}^0 J_{j1}^{-1} h_{k,r} \left\{ {}^t u_i^k + \bar{a}_k \left[ t \left( {}^t V_{ti}^k - {}^0 V_{ti}^k \right) + s \left( {}^t V_{sl}^k - {}^0 V_{sl}^k \right) \right] \right\} \\
 & + \sum_{k=1}^N {}^0 J_{j2}^{-1} h_k \bar{a}_k \left( {}^t V_{si}^k - {}^0 V_{si}^k \right) + \sum_{k=1}^N {}^0 J_{j3}^{-1} h_k \bar{a}_k \left( {}^t V_{ti}^k - {}^0 V_{ti}^k \right) \quad (6.24)
 \end{aligned}$$

### 6.1.2 Finite element discretization

At this point, we have the necessary ingredients to perform the integrations in Eq. (6.21). In addition, assuming the material density remains constant during the element deformation, i.e.,

$${}^{t+\Delta t} \rho = {}^t \rho = {}^0 \rho \quad (6.25)$$

the resulting equations of motion can be written in the following form

$$\left[ \int_{{}^0 V} {}^t \bar{\mathbf{B}}_L^T \bar{\mathbf{C}} {}^t \bar{\mathbf{B}}_L {}^0 dV + \int_{{}^0 V} {}^t \bar{\mathbf{B}}_{NL}^T {}^t \bar{\mathbf{S}} {}^t \bar{\mathbf{B}}_{NL} {}^0 dV \right] \underline{u} = {}^{t+\Delta t} \underline{R} - \int_{{}^0 V} {}^t \bar{\mathbf{B}}_L^T {}^t \bar{\mathbf{S}} {}^0 dV \quad (6.26)$$

where,

${}^t \bar{\mathbf{B}}_L, {}^t \bar{\mathbf{B}}_{NL}$  = linear and nonlinear local strain-displacement transformation matrices, as

summarized in Table 6.1

$\underline{\underline{\bar{C}}}$  = incremental stress-strain material property matrix, given in Eq. (3.32)

$\underline{\underline{\bar{S}}}, \underline{\underline{\bar{S}}}$  = matrix and vector of 2nd Piola-Kirchhoff local beam stresses, see Table 6.1

${}^{t+\Delta t} \underline{\underline{R}}$  = external nodal point load vector at time  $t+\Delta t$

$\underline{\underline{u}}$  = global beam displacement increment vector (does not include ovalization degrees-of-freedom)

In the derivation of Eq. (6.26), the global strain tensor is employed to calculate, using a second order tensor transformation, the local strain components  ${}^t \epsilon_{\eta\eta}$ ,  ${}^t \delta_{\eta\xi}$  and  ${}^t \delta_{\eta\zeta}$  referred to the convected coordinates, see Fig. 2.1.(a).

Following the approach used in linear analysis, the linear strain-displacement transformation matrix can now be modified to include the ovalization deformations of the pipe cross-section in Eq. (3.11). However, it is not clear how the geometric nonlinearities corresponding to the ovalization need be included and further studies are necessary (see Section 8.). If the geometric nonlinearities corresponding to the ovalization displacements are neglected, the entries in the total element nonlinear strain matrix  ${}^t \underline{\underline{\bar{B}}}_{NL}$  corresponding to the



TABLE 6.1 - (CONTINUED)

$${}^t \underline{I} = \begin{bmatrix} {}^t V_{r_1}^2 & {}^t V_{r_2}^2 & {}^t V_{r_3}^2 & {}^t V_{r_1}^t V_{r_2} & {}^t V_{r_1}^t V_{r_3} & {}^t V_{r_2}^t V_{r_3} \\ 2 {}^t V_{r_1}^t V_{s_1} & 2 {}^t V_{r_2}^t V_{s_2} & 2 {}^t V_{r_3}^t V_{s_3} & {}^t V_{r_2}^t V_{s_1} + {}^t V_{r_1}^t V_{s_2} & {}^t V_{r_3}^t V_{s_1} + {}^t V_{r_1}^t V_{s_3} & {}^t V_{r_3}^t V_{s_2} + {}^t V_{r_2}^t V_{s_3} \\ 2 {}^t V_{r_1}^t V_{t_1} & 2 {}^t V_{r_2}^t V_{t_2} & 2 {}^t V_{r_3}^t V_{t_3} & {}^t V_{r_2}^t V_{t_1} + {}^t V_{r_1}^t V_{t_2} & {}^t V_{r_3}^t V_{t_1} + {}^t V_{r_1}^t V_{t_3} & {}^t V_{r_3}^t V_{t_2} + {}^t V_{r_2}^t V_{t_3} \end{bmatrix}$$

$${}^t \underline{V}_r = \underline{V}_s \times \underline{V}_t$$

$${}^t \underline{B}_{L_1} = \begin{bmatrix} l_{11} h_{k,1} & l_{21} h_{k,1} & l_{31} h_{k,1} & l_{31} h_{k,1} & (\Phi 1)_{11}^k & (\Phi 2)_{11}^k & (\Phi 3)_{11}^k \\ l_{12} h_{k,2} & l_{22} h_{k,2} & l_{32} h_{k,2} & l_{32} h_{k,2} & (\Phi 1)_{22}^k & (\Phi 2)_{22}^k & (\Phi 3)_{22}^k \\ l_{13} h_{k,3} & l_{23} h_{k,3} & l_{33} h_{k,3} & l_{33} h_{k,3} & (\Phi 1)_{33}^k & (\Phi 2)_{33}^k & (\Phi 3)_{33}^k \\ (l_{11} h_{k,2} + l_{12} h_{k,1}) & (l_{21} h_{k,2} + l_{22} h_{k,1}) & (l_{31} h_{k,2} + l_{32} h_{k,1}) & (l_{31} h_{k,2} + l_{32} h_{k,1}) & (\Phi 1)_{12}^k + (\Phi 1)_{21}^k & (\Phi 2)_{12}^k + (\Phi 2)_{21}^k & (\Phi 3)_{12}^k + (\Phi 3)_{21}^k \\ (l_{12} h_{k,3} + l_{13} h_{k,2}) & (l_{22} h_{k,3} + l_{23} h_{k,2}) & (l_{32} h_{k,3} + l_{33} h_{k,2}) & (l_{32} h_{k,3} + l_{33} h_{k,2}) & (\Phi 1)_{23}^k + (\Phi 1)_{32}^k & (\Phi 2)_{23}^k + (\Phi 2)_{32}^k & (\Phi 3)_{23}^k + (\Phi 3)_{32}^k \\ (l_{13} h_{k,3} + l_{13} h_{k,1}) & (l_{23} h_{k,3} + l_{23} h_{k,1}) & (l_{33} h_{k,3} + l_{33} h_{k,1}) & (l_{33} h_{k,3} + l_{33} h_{k,1}) & (\Phi 1)_{13}^k + (\Phi 1)_{31}^k & (\Phi 2)_{13}^k + (\Phi 2)_{31}^k & (\Phi 3)_{13}^k + (\Phi 3)_{31}^k \end{bmatrix}$$

for nodal point k

$$l_{ij} = \partial^t u_i / \partial^0 x_j \quad ; \quad (\Phi m)_{ij}^k = \sum_{i=1}^3 l_{ij} (Gm)_{in}^k$$

TABLE 6.1 - (CONTINUED)

B. Nonlinear strain-displacement transformation matrix

$${}^t_0 \underline{B}_{NL} = {}^t \bar{I}^T {}^t_0 \underline{B}_{NL}$$

$${}^t_0 \underline{B}_{NL} = \begin{bmatrix} h_{k,1} & 0 & 0 & (G1)_{11}^k & (G2)_{11}^k & (G3)_{11}^k \\ h_{k,2} & 0 & 0 & (G1)_{12}^k & (G2)_{12}^k & (G3)_{12}^k \\ h_{k,3} & 0 & 0 & (G1)_{13}^k & (G2)_{13}^k & (G3)_{13}^k \\ 0 & h_{k,1} & 0 & (G1)_{21}^k & (G2)_{21}^k & (G3)_{21}^k \\ 0 & h_{k,2} & 0 & (G1)_{22}^k & (G2)_{22}^k & (G3)_{22}^k \\ 0 & h_{k,3} & 0 & (G1)_{23}^k & (G2)_{23}^k & (G3)_{23}^k \\ 0 & 0 & h_{k,1} & (G1)_{31}^k & (G2)_{31}^k & (G3)_{31}^k \\ 0 & 0 & h_{k,2} & (G1)_{32}^k & (G2)_{32}^k & (G3)_{32}^k \\ 0 & 0 & h_{k,3} & (G1)_{33}^k & (G2)_{33}^k & (G3)_{33}^k \end{bmatrix}$$

for nodal point k

$${}^t \bar{I} = \begin{bmatrix} {}^t \bar{I}^* & & \\ & {}^t \bar{I}^* & \\ & & {}^t \bar{I}^* \end{bmatrix}, \text{ where } {}^t \bar{I}^* = \begin{bmatrix} {}^t V_{r1} & {}^t V_{s1} & {}^t V_{t1} \\ {}^t V_{r2} & {}^t V_{s2} & {}^t V_{t2} \\ {}^t V_{r3} & {}^t V_{s3} & {}^t V_{t3} \end{bmatrix}$$

TABLE 6.1 - (CONTINUED)

C. 2nd Piola-Kirchhoff local stress matrix

$$\underline{\underline{tS}}_0 = \begin{bmatrix} \underline{\underline{tS}}_0 & & \\ & \underline{\underline{tS}}_0 & \\ & & \underline{\underline{tS}}_0 \end{bmatrix}, \text{ where } \underline{\underline{tS}}_0 = \begin{bmatrix} {}^tS_{0\eta\eta} & \text{Sym.} \\ {}^tS_{0\eta\epsilon} & 0 \\ {}^tS_{0\eta\zeta} & 0 & 0 \end{bmatrix}$$

D. 2nd Piola-Kirchhoff local stress vector

$$\underline{\underline{tS}}_0 = \begin{bmatrix} {}^tS_{0\eta\eta} \\ {}^tS_{0\eta\epsilon} \\ {}^tS_{0\eta\zeta} \end{bmatrix}$$



ovalization degrees-of-freedom would simply be set equal to zero. The finite element equilibrium equations in the global coordinate system can then be finally written in the following compact form

$$\left( {}^t_0\underline{K}_L + {}^t_0\underline{K}_{NL} \right) \underline{u} = {}^{t+\Delta t}\underline{R} - {}^t\underline{F} \quad (6.27)$$

where  ${}^t_0\underline{K}_L$  and  ${}^t_0\underline{K}_{NL}$  are the global linear and nonlinear stiffness matrices,  ${}^{t+\Delta t}\underline{R}$  is the external loading vector, and  ${}^t\underline{F}$  is the nodal point forcing vector equivalent to the stresses at time  $t$ .

## 6.2 Formulation for Elastic-Plastic Analysis

A derivation of the isothermal elastic-plastic incremental constitutive relations, employed in the material nonlinear analysis of the elbow element, is presented in this section. The approach used in the presentation follows the procedures for infinitesimal displacements presented in Ref. [69]. However, the model can also be employed for large displacement analysis in a T.L. formulation, by using the incremental 2nd Piola-Kirchhoff stress and Green-Lagrange strain measures defined in the previous sections of this chapter.

In addition to the linear elastic constitutive relation of a continuum, three basic conditions are required to establish

establish the stress-strain matrix in elasto-plasticity. These conditions are:

- (a) a yield condition, which specifies the state of multiaxial stress corresponding to start of plastic flow;
- (b) a flow rule, that relates the plastic strain increments to the current stresses and the increment of stresses beyond yielding; and
- (c) a hardening rule, which determines how the yield condition is modified during plastic flow.

Under isothermal conditions and isotropic hardening, the initial and subsequent yield criterion is written in the general form

$${}^tF({}^t\bar{\sigma}_{ij}, {}^t\bar{\epsilon}_{ij}^p) = 0 \quad (6.28)$$

where  ${}^t\bar{\sigma}_{ij}$  and  ${}^t\bar{\epsilon}_{ij}^p$  are the components of the effective stress tensor and the components of the total plastic strain tensor measured in the local coordinate system  $\eta$ ,  $\xi$  and  $\zeta$ , for example,

$${}^t\bar{\underline{\underline{\sigma}}} = \begin{bmatrix} \sigma_{\eta\eta} & \sigma_{\eta\xi} & \sigma_{\eta\zeta} \\ & \sigma_{\xi\xi} & 0 \\ \text{sym.} & & 0 \end{bmatrix} \quad (6.29)$$

The von Mises yield condition employed in the elbow element

formulation gives,

$${}^tF({}^t\bar{G}_{ij}, {}^t\bar{e}_{ij}^p) = \frac{1}{2} {}^t\bar{D}_{ij} {}^t\bar{D}_{ij} - \frac{1}{3} {}^t\bar{G}_y^2 \quad (6.30)$$

where  ${}^t\bar{D}_{ij}$  are the components of the deviatoric stress tensor at a time  $t$ , defined as

$${}^t\bar{D}_{ij} = {}^t\bar{G}_{ij} - \frac{1}{3} {}^t\bar{G}_{mm} \delta_{ij} \quad (6.31)$$

with  $\delta_{ij}$  being the Kronecker delta and  ${}^t\bar{G}_y$  is the current yield stress at time  $t$  which is a function of the plastic work per unit of volume  ${}^tW^p$ ,

$${}^tW^p = \int_0^{e_{ij}^p} {}^t\bar{G}_{ij} de_{ij}^p \quad (6.32)$$

A simple tension test performed in a material with elastic modulus  $E$  and constant strain hardening modulus  $E_T$  gives an explicit expression for  ${}^tW^p$ . From Fig. 6.1, we obtain the expression

$${}^tW^p = \frac{1}{2} \left( \frac{E - E_T}{E E_T} \right) ({}^t\bar{G}_y^2 - {}^0\bar{G}_y^2) . \quad (6.33)$$

Since during plastic deformation  ${}^tF=0$ , we have

$$d{}^tF = \frac{\partial {}^tF}{\partial {}^t\bar{G}_{ij}} \bar{G}_{ij} + \frac{\partial {}^tF}{\partial {}^t\bar{e}_{ij}^p} \bar{e}_{ij}^p = 0 \quad (6.34)$$

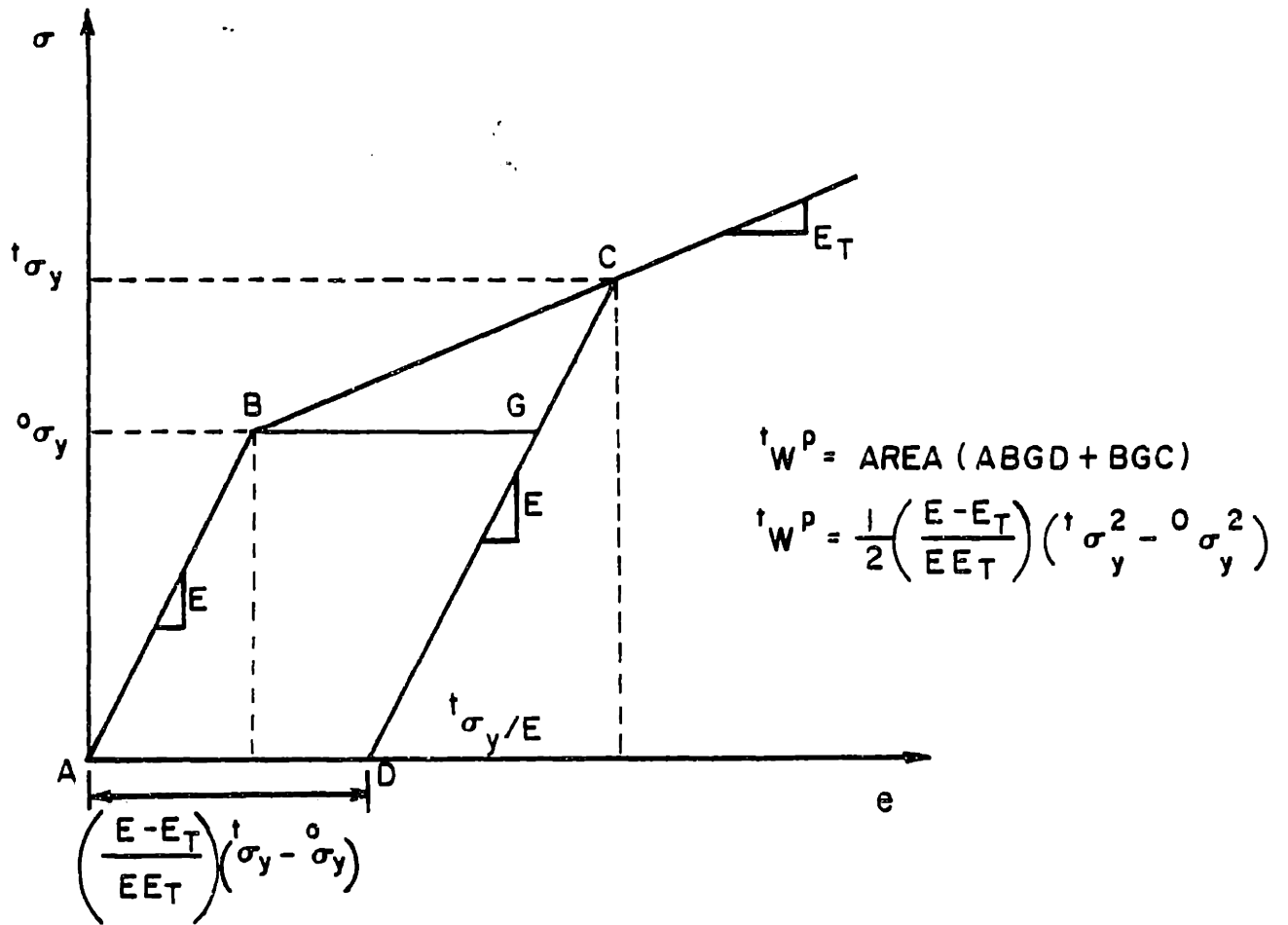


FIGURE 6.1 Stress-strain Relation in a Simple Tension Test.

where the  $\bar{G}_{ij}$  and  $\bar{e}_{ij}^P$  are components of differential increments in local stresses and local plastic strains. The coefficients of these increments in Eq. (6.34) can now be evaluated using Eqs. (6.30) to (6.33) resulting [70],

$$\frac{\partial {}^t F}{\partial {}^t \bar{G}_{ij}} = {}^t \bar{D}_{ij} \quad (6.35)$$

$$\frac{\partial {}^t F}{\partial {}^t \bar{e}_{ij}^P} = -\frac{2}{3} {}^t G_\gamma \frac{\partial {}^t G_\gamma}{\partial {}^t W^P} \frac{\partial {}^t W^P}{\partial {}^t \bar{e}_{ij}^P} = -\frac{2}{3} \left( {}^t G_\gamma \frac{\partial {}^t G_\gamma}{\partial {}^t W^P} \right) {}^t \bar{G}_{ij} \quad (6.36)$$

but, from Eq. (6.33) we have

$${}^t G_\gamma \frac{\partial {}^t G_\gamma}{\partial {}^t W^P} = \frac{E E_T}{E - E_T} \quad (6.37)$$

that gives

$$\frac{\partial {}^t F}{\partial {}^t \bar{e}_{ij}^P} = -\frac{2}{3} \left( \frac{E E_T}{E - E_T} \right) {}^t \bar{G}_{ij} \quad (6.38)$$

Applying the normality rule to the plastic potential function  ${}^t F$ , the strain increments reduces to

$$\bar{e}_{ij}^P = {}^t \lambda \frac{\partial {}^t F}{\partial {}^t \bar{G}_{ij}} = {}^t \lambda {}^t \bar{D}_{ij} \quad (6.39)$$

and the stress increments are evaluated from the equation

$$\bar{G}_{ij} = {}^t \bar{C}_{ijpq}^E (\bar{e}_{pq} - \bar{e}_{pq}^P) \quad (6.40)$$

where  ${}^t\bar{C}_{ij}^E$  are the components of the linear stress-strain tensor for isotropic materials in a three-dimensional analysis given in Ref. [19], Sec. 4.2.3. Finally, substituting from Eq. (6.35) and (6.38) to (6.40) into the incremental Eq. (6.34), the elastic-plastic material law at time  $t$  becomes

$$\bar{G}_{ij} = {}^t C_{ijpq}^{EP} \bar{e}_{pq} \quad (6.41)$$

with,

$${}^t\bar{C}_{ik}^{EP} = {}^t\bar{C}_{ik}^E - \frac{{}^t\bar{P}_{ij} {}^t\bar{P}_{jk}}{{}^tD_{ij} {}^tP_{ij} - \frac{2}{3} \left( \frac{EE_T}{E-E_T} \right) {}^t\bar{G}_{ij} {}^t\bar{D}_{ij}} \quad (6.42)$$

where we employ the notation

$${}^t\bar{P}_{ij} = {}^t\bar{C}_{ijpq}^E {}^t\bar{D}_{pq} \quad (6.43)$$

The elbow element elastic-plastic incremental constitutive relation  ${}^t\bar{C}^{EP}$  is then formed by imposing the element zero stress conditions:  $\bar{G}_{\xi\xi} = \bar{G}_{\zeta\zeta} = 0$ . This is done by performing static condensation on the appropriate rows and columns of the matrix  ${}^t\bar{C}^{EP}$ .

### 6.3 Numerical Integration

To evaluate the linear stiffness matrix in Eq. (3.2) and the stiffness matrices and force vectors in Eq. (6.26) we are using numerical integration. In linear analysis it may be possible and more effective to evaluate some of the integrations

required in closed form, but in general nonlinear analysis numerical integration must be employed. As a general procedure, we choose to employ in all analysis numerical integration [19].

In recent years, much emphasis has been given to reduced numerical integration in the use of low order elements such as beam or plate elements [32, 71]. The use of reduced integration is necessary in those cases, because if the stiffness matrices of very thin low-order elements are evaluated exactly, the elements display much too stiff a behavior. Using reduced integration in the evaluation of low-order elements can drastically improve some analysis results, but may also introduce spurious zero energy modes that result in solution difficulties, and make it difficult to access the reliability of the solution results in general analysis. Using the higher-order elbow element presented here, reduced numerical integration is not needed for an accurate response prediction, and a reliable and effective solution is obtained using high-order integration [33, 35].

Considering the assumed displacement distributions for the elbow element, the Newton-Cotes formulas can be employed for the numerical integration with the following integration orders: 3 point integration through the wall thickness, 5 point integration along the elbow, and, using the composite trapezoidal rule around the circumference, 12 point integration for in-plane

loading and 24 point integration for out-of-plane loading [19]. This integration order around the circumference assumes that all 3 ovalization patterns are included in the analysis: less integration stations can be employed if a smaller number of ovalization degrees-of-freedom are used. Also, instead of the Newton-Cotes formulae, Gauss numerical integration could be employed.



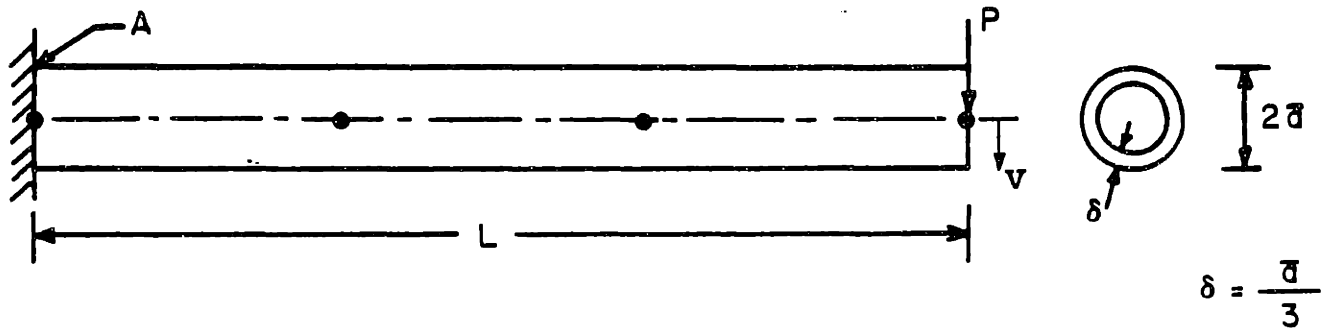
## 7 - SAMPLE ANALYSES

In this chapter, the analysis of a number of linear and nonlinear piping problems are presented to indicated the applicability and the effectiveness of the elbow element. First, corresponding to the von Kármán's model, we present the solutions to some in-plane and out-of-plane bending analyses that do not include interaction effects. Next, solutions including flanged pipes and straight-curved pipe assemblages with interaction effects are presented.

The element formulation has been implemented in a version of the computer program ADINA [67] (called ADINAP) and in this section the response predicted using the elbow element is compared to available numerical and experimental results. In all analyses the Newton-Cotes integration scheme described in Section 6.3 was employed, and the pipe geometric parameter used was  $\lambda = R\delta/[a^2\sqrt{1-\nu^2}]$  [27].

### 7.1 Linear Analysis of Two Cantilvered Pipe Cross-Section Beams

The objective in analyzing the two cantilevered beams is to demonstrate: (a) the effectiveness of the element in the analyses of slender structural members, and (b) the accuracy obtained with the element when the ovalization effects are neglected. The beam formulation includes transverse shear deformations at a pipe cross-section and it is instructive to



E = YOUNG'S MODULUS  
 I = MOMENT OF INERTIA

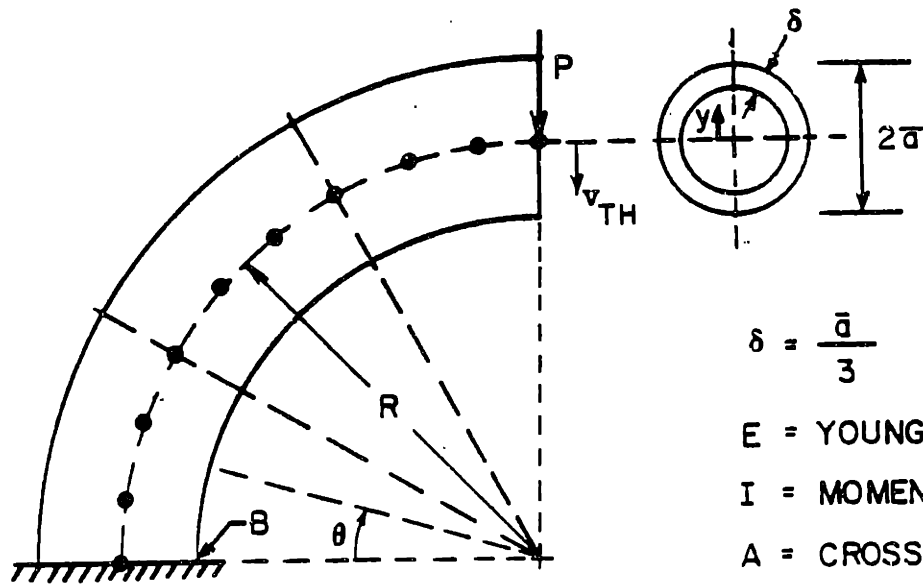
$$v_{TH} = \frac{PL^3}{3EI}$$

$$\gamma_{TH} = \frac{PL^2}{2EI}$$

$$\sigma_{\eta\eta} = \frac{PL\bar{a}}{I}, \text{ AT POINT A}$$

$L/2\bar{a}$	$\frac{v - v_{TH}}{v_{TH}}$	$\frac{\gamma - \gamma_{TH}}{\gamma_{TH}}$	$\frac{\sigma_{\eta\eta} - \sigma_{\eta\eta_{TH}}}{\sigma_{\eta\eta_{TH}}}$
10	.007042	.0000	.0000
100	.000071	.0000	.0000
1,000	.000001	.0000	.0000
10,000	.000000	.0000	.0000

(a) Analysis of cantilever straight pipe using a one element model.



$$\delta = \frac{\bar{a}}{3}$$

E = YOUNG'S MODULUS

I = MOMENT OF INERTIA

A = CROSS-SECTIONAL AREA

$$v_{TH} = \frac{\pi}{4} \frac{PR^3}{EI}$$

$$y_{TH} = \frac{PR^2}{EI}$$

$$(\sigma_{\eta\eta})_{TH}^{\dagger} = \frac{M}{AR} \left[ 1 + \frac{1}{Z} \frac{y}{R+y} \right] - \frac{P \cos \theta}{A}$$

WHERE,

$$Z = - \frac{1}{A} \int_A \frac{y}{R+y} dA$$

$$\text{AT POINT B: } (\sigma_{\eta\eta})_{TH}^B = - \frac{P\bar{a}}{Z^*(R-\bar{a})}, \quad Z^* = \frac{1}{\sqrt{1-(\bar{a}/R)^2}} - 1$$

R/2	$(v - v_{TH})/v_{TH}$	$(y - y_{TH})/y_{TH}$	$[\sigma_{\eta\eta}^B - (\sigma_{\eta\eta})_{TH}^B] / (\sigma_{\eta\eta})_{TH}^B$
.8	.07600	.23316	.00042
1.0	.06483	.14663	.04033
2.0	.01982	.03646	.07780
5.0	.00182	.00634	.08517

† Winkler-Bach formula for curved beams (Ref. [72], pp. 336-341)

(b) Analysis of 90 deg. cantilever bend using a three elbow element model.

Figure 7.1 Linear Analysis of Two Cantilevered Pipe Beams.

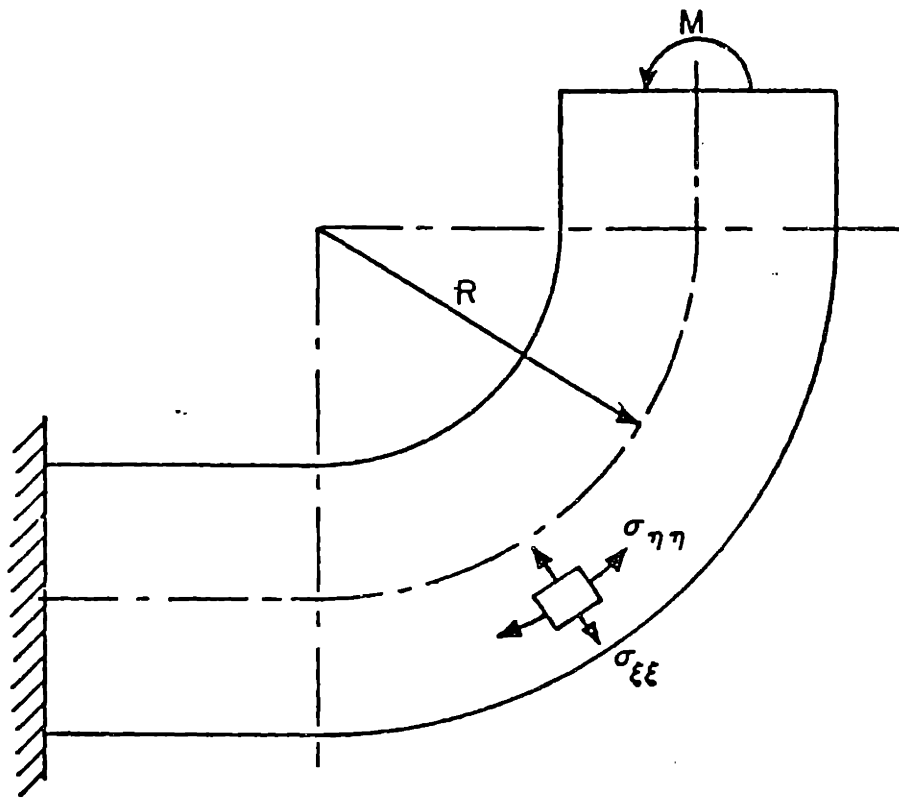
evaluate this assumption in the solution of these problems. In the analyses one element was used to model the straight pipe and three equal elements were used to model the 90° bend.

Figs. 7.1 compare the analysis results obtained with elementary beam theory solutions for different geometric aspect ratios. As expected, the displacements and stresses predicted using ADINAP are very close to those obtained using elementary beam theory when neglecting shear deformations for large aspect ratios, because in those cases the shear deformations contribute negligibly to the tip displacement of the pipe. Hence, it can be concluded that the element is effective when transverse shear deformation effects can be neglected, which is the case in the analyses of thin-walled pipes.

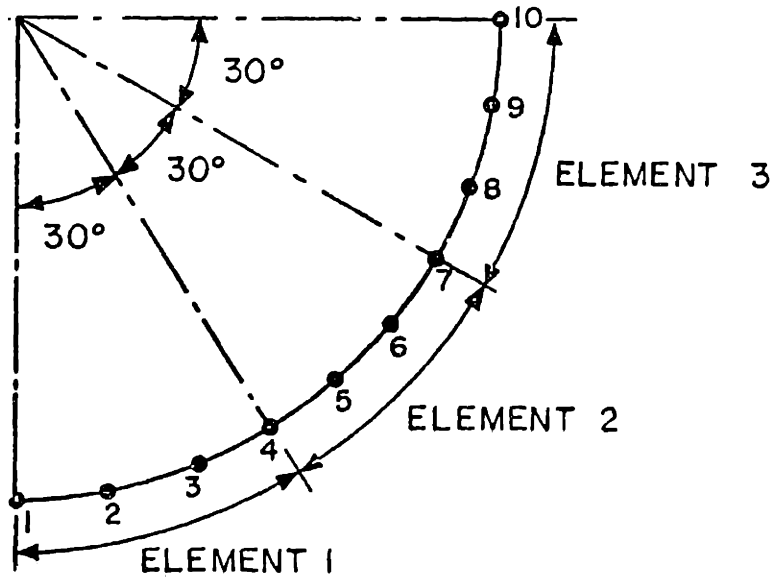
## 7.2 Analysis of a Pipe Bend

The pipe structure shown in Fig. 7.2 was analyzed using ADINAP, assuming no variation on the ovalization along the length of the pipe because the analysis results could be compared with the results presented by Sobel in Ref. [27]. Using ADINAP the pipe bend was modeled using three equal elbow elements as shown in Fig. 7.2.

In his work Sobel used the state-of-the-art tools provided in the MARC computer program [73] to analyze the bend. Based on an extensive convergence study, Sobel concluded that 32 or 64 of the MARC pipe-bend segment elements must be used to model the bend.



a) PIPE STRUCTURE;  $R/a = 3.07$ ,  $a/\delta = 20.8$ ,  $\nu = .3$



b) THREE ELEMENT MODEL (CENTRE LINE OF ELEMENTS AND NODAL POINTS ARE SHOWN)

FIGURE 7.2 - Pipe Bend and Finite Element Model Used





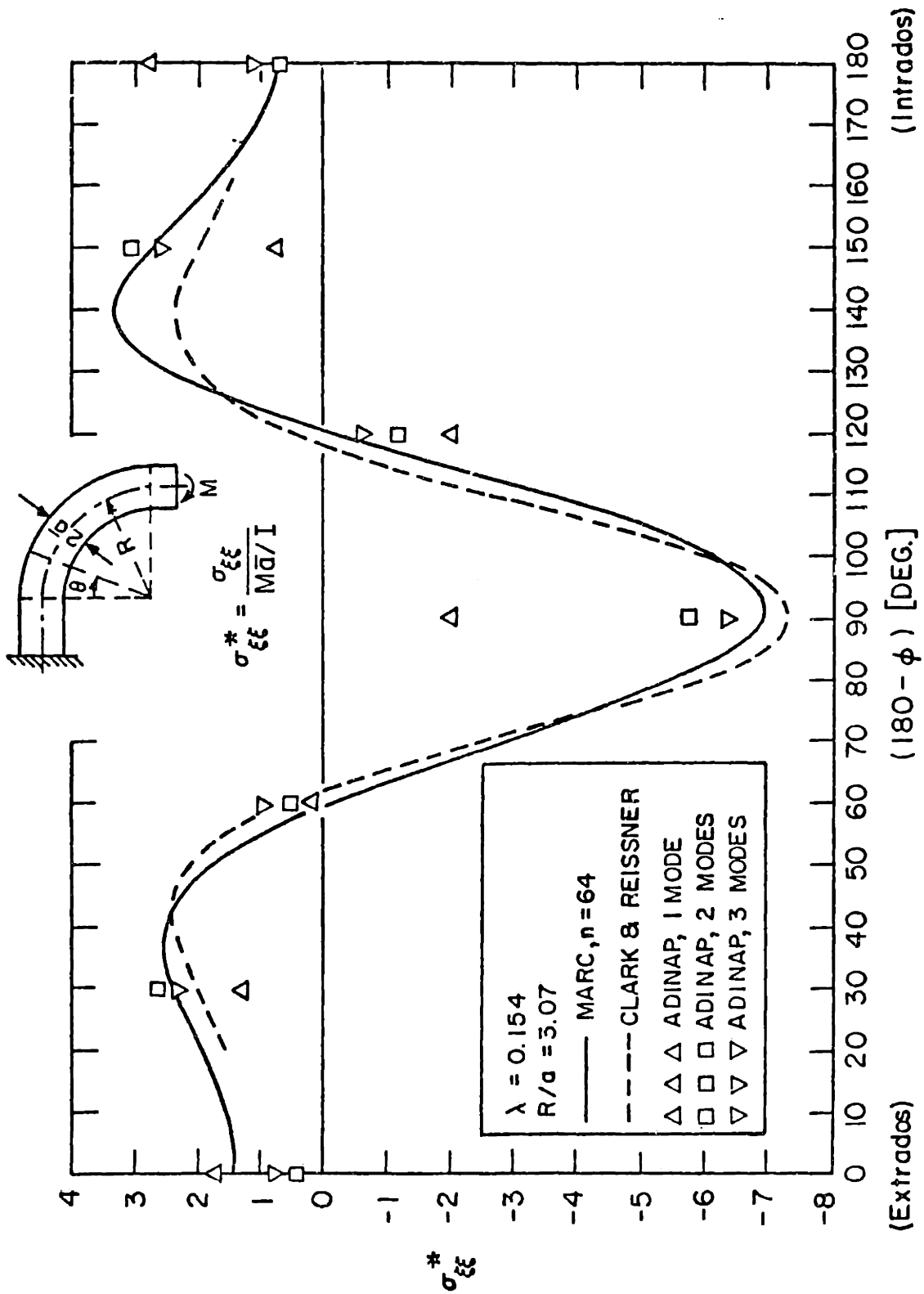


FIGURE 7.5 - Hoop Stresses at Inside Surface of Bend in  
 Fig. 7.2 (No End Constraints)



To simulate the conditions that were assumed in the analysis by Sobel, the ovalization degrees-of-freedom at nodes 1 and 10 (and 2 to 9, see Fig. 7.2) were left free. Figures 7.3 to 7.5 show some stress components calculated using ADINAP and the corresponding results obtained by Sobel using the MARC program and the Clark and Reissner Shell Theory [8]. The ADINAP analysis was performed using the 1, 2 and 3 in-plane bending ovalization terms of Eq. (3.10). Good correspondence between ADINAP, MARC and Clark and Reissner shell theory results is observed. It is also noted that in the ADINAP analysis all three terms of ovalization had to be included for an accurate response prediction, which corresponds to the recommendation given in Table 2.1 for the bend geometry considered. In the subsequent analyses of this bend in Section 7.7, we therefore included also all these ovalization terms.

### 7.3 In-Plane and Out-of-Plane Bending Analysis of a Second Pipe Bend

A second 90° pipe bend was analyzed for in-plane and out-of-plane bending using the same finite element mesh as was employed in the previous analysis (see Fig. 7.2(b)). Some longitudinal and hoop stress results calculated with ADINAP are shown for the in-plane bending in Figs. 7.6 and 7.7, and for out-of-plane bending in Figs. 7.8 and 7.9. The computed results are compared in the figures with the experimental values obtained by Smith and Ford in Ref. [74], and good correspondence

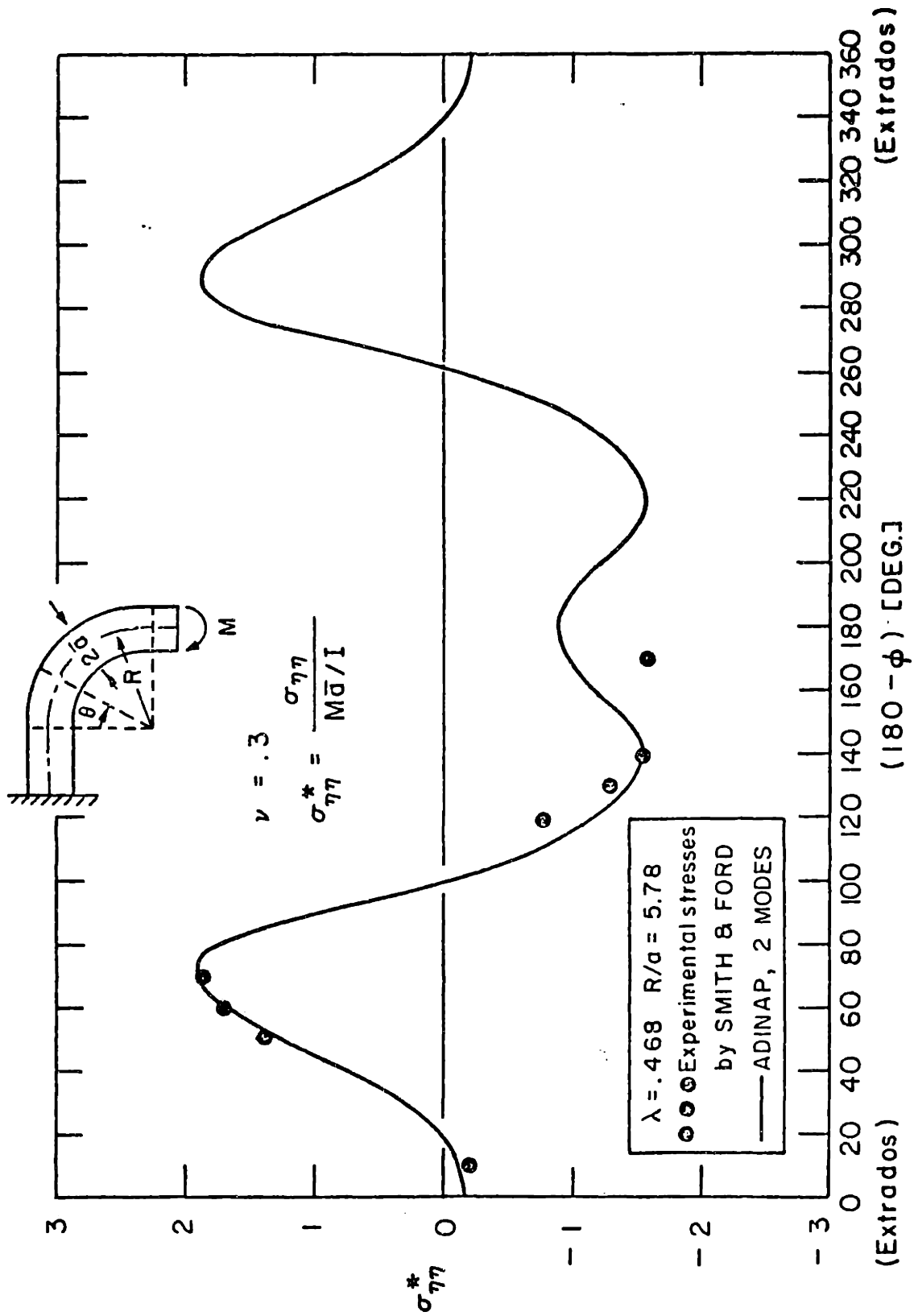


FIGURE 7.6 - Longitudinal Stresses at Outside Surface and at  $\theta=45^\circ$  of Smith & Ford Bend Subjected to an In-plane Bending Moment

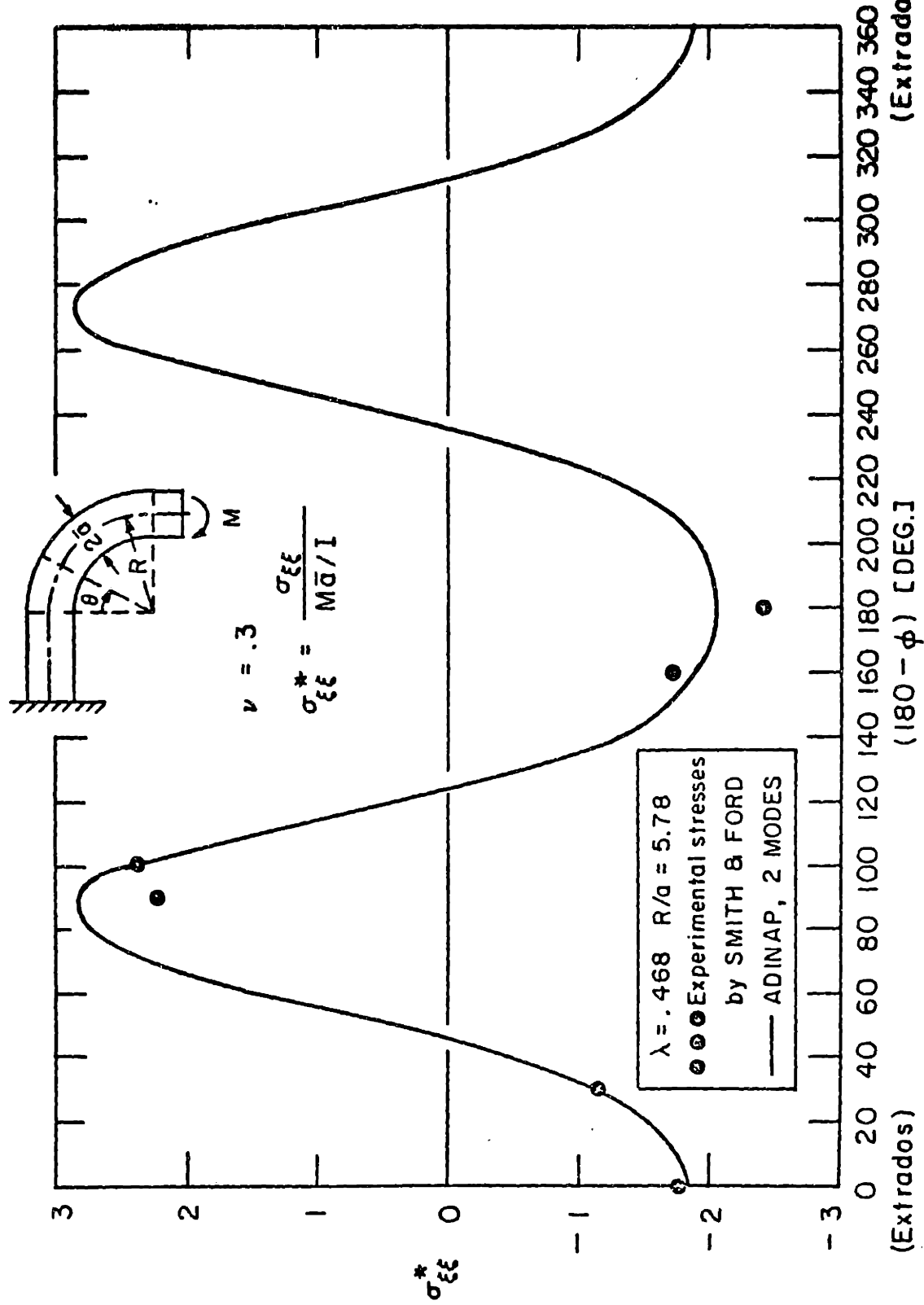


FIGURE 7.7 - Hoop Stresses at Outside Surface and at  $\theta=45^\circ$  of Smith & Ford Bend Subjected to an In-plane Bending Moment

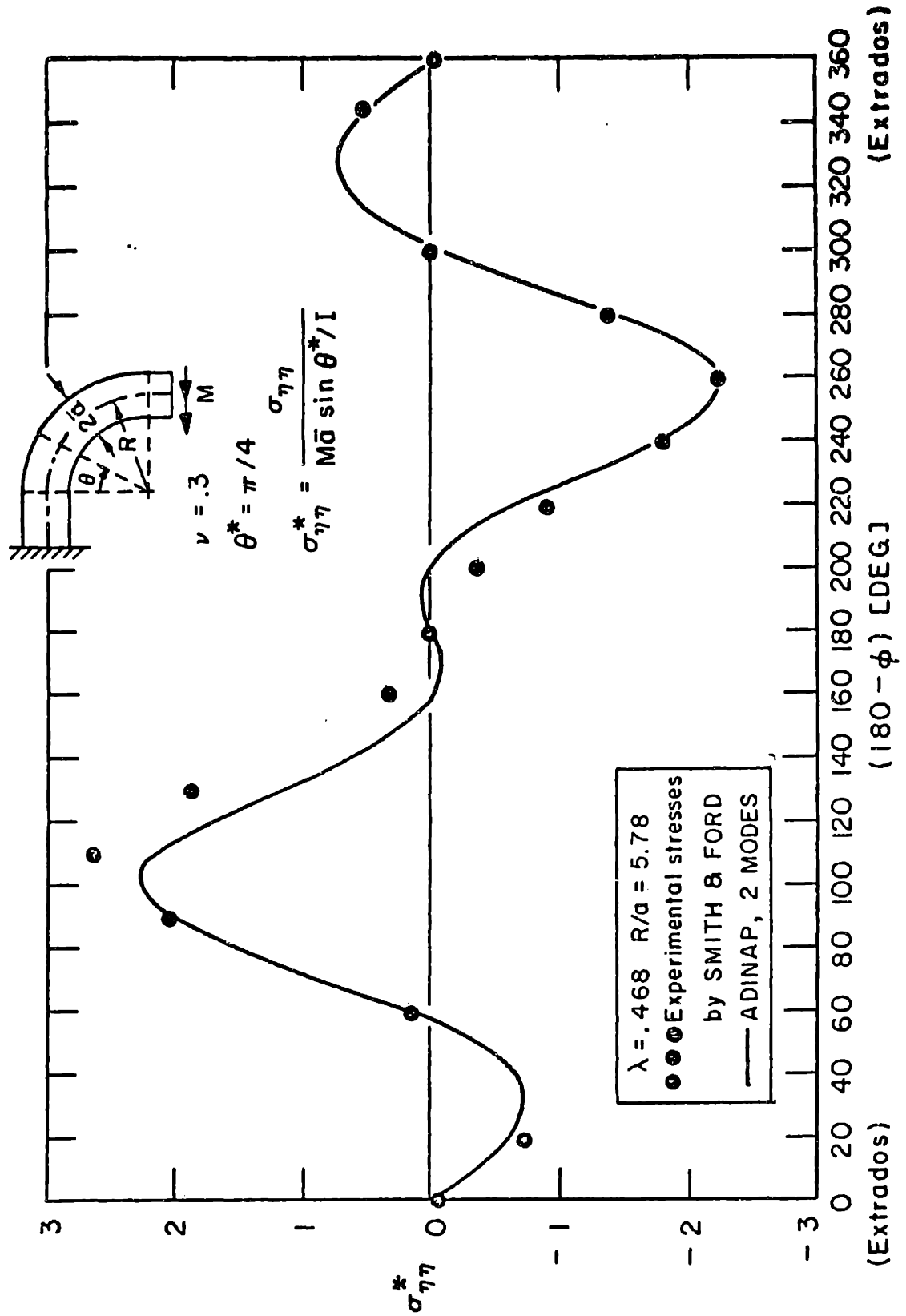


FIGURE 7.8 - Longitudinal Stresses at Outside Surface and at  $\theta=45^\circ$  of Smith & Ford Bend Subjected to an Out-of-Plane Bending Moment

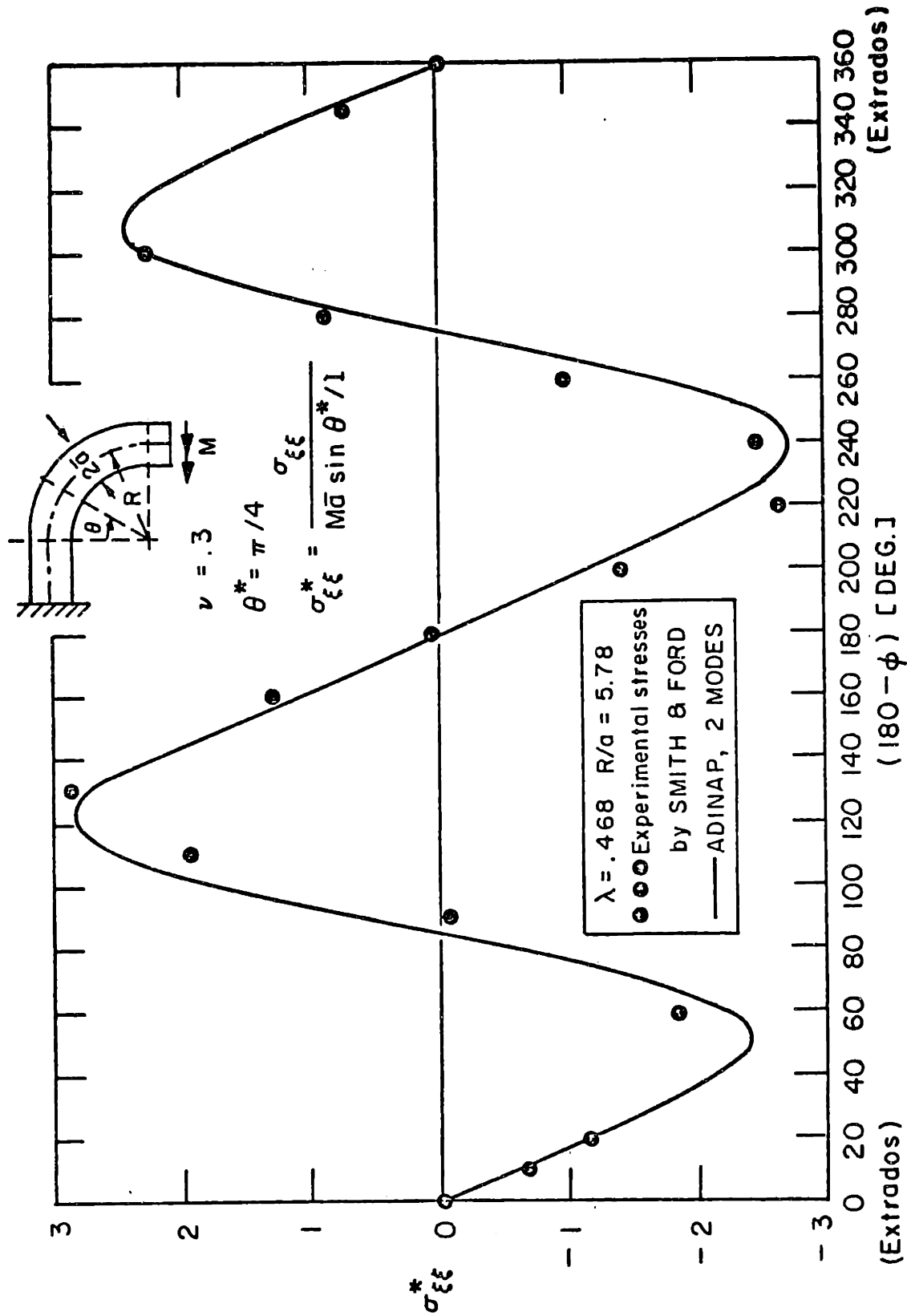


FIGURE 7.9 - Hoop Stresses at Outside Surface and at  $\theta=45^\circ$  of Smith & Ford Bend Subjected to an Out-of-Plane Bending Moment

is noted.

#### 7.4 Analysis of Pressurized Bends

The effect of internal pressure on the flexibility of curved pipes is assessed in the present analyses. Experimental results for the in-plane bending of a short bend radius and three long bend radius 90° bends were reported in Refs. [53, 54]. The geometric properties of these bends are shown in Fig. 7.10, together with the finite element model employed in the ADINAP analyses. Due to symmetry, only half of the test structure is used in the model that was subjected to a concentrated load  $P$  and internal pressure  $p$  varying from 0 to 1100 psi.

Figure 7.11 shows the predicted flexibilities for the elbow element models, and compares the finite element responses with the experimental results. As expected, the elbow element flexibilities, for increasing values of internal pressures, are larger than given in the test results because the stretching of the pipe midsurface in the circumferential direction is neglected in the formulation. It is interesting to notice, however, that moderate thin pipes (Bend 1) and very thin pipes (Bend 2) with similar geometric parameter  $\lambda$ , present quite different stiffening behaviors under internal pressure. This way, the flexibility of the bends depend not only on the pipe factor  $\lambda$  but also on the amount of ovalization in the pipe cross-section. Hence, the flexibility of the pipe is also a

PARAMETER	BEND 1	BEND 2	BEND 3	BEND 4
R	45.	14.25	12.4	10
$\delta$	.5	.016	.020	.016
$\bar{a}$	15.	1.5	1.75	1.5
$\lambda$	.10483	.10623	.08489	.074545

(a) Bend Geometric Parameters (all dimensions in inches)

Bound. Conditions:

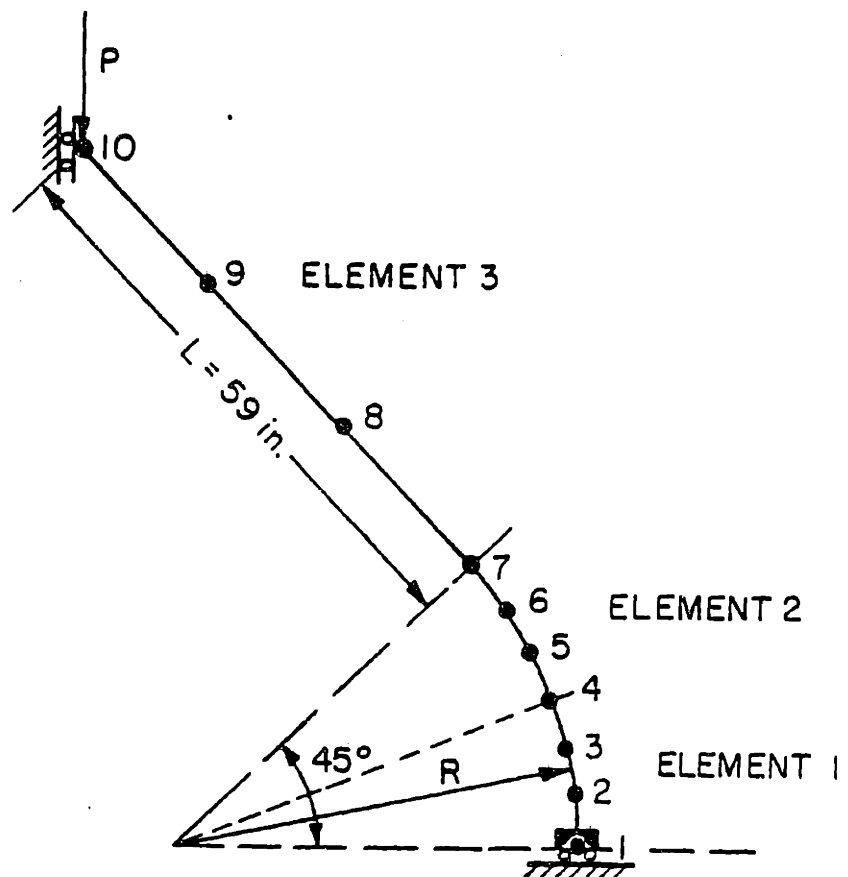
At node 1:

- no cross-sectional rotation,  $\gamma_1=0$ .

$$-\frac{dw}{dx} = 0$$

At nodes 4 and 7:

- ovalization and derivative of ovalization continuous



(b) Finite Element Model Used

FIGURE 7-10 - Analysis of Pressurized Bends

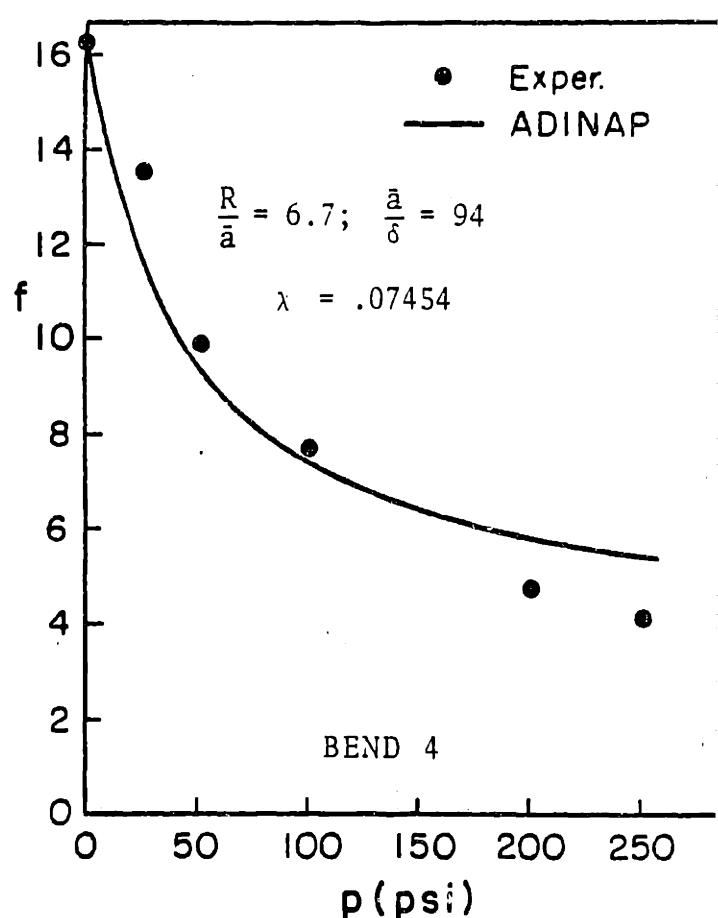
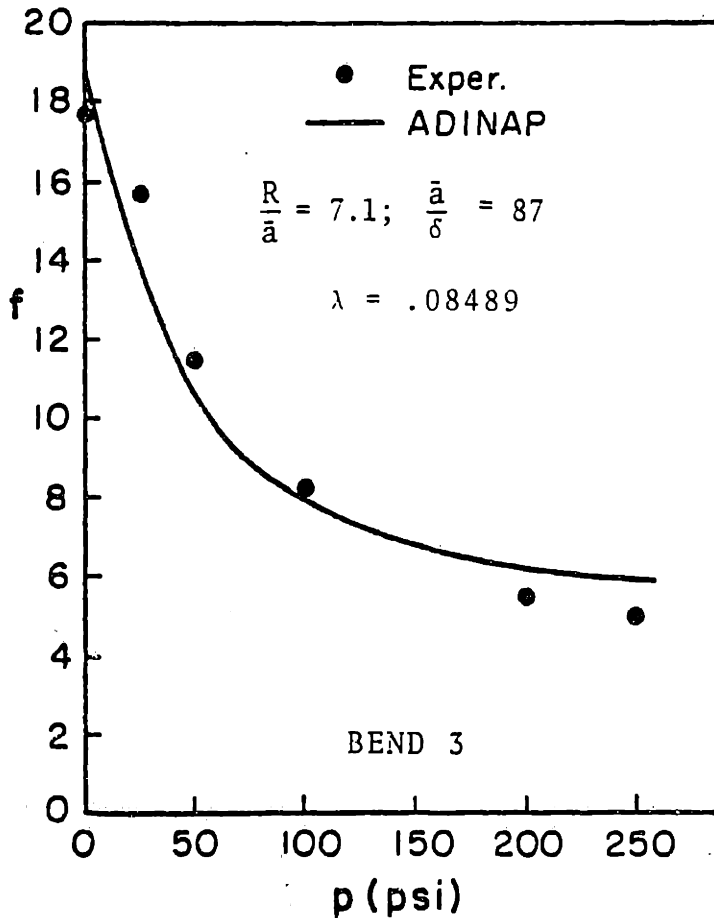
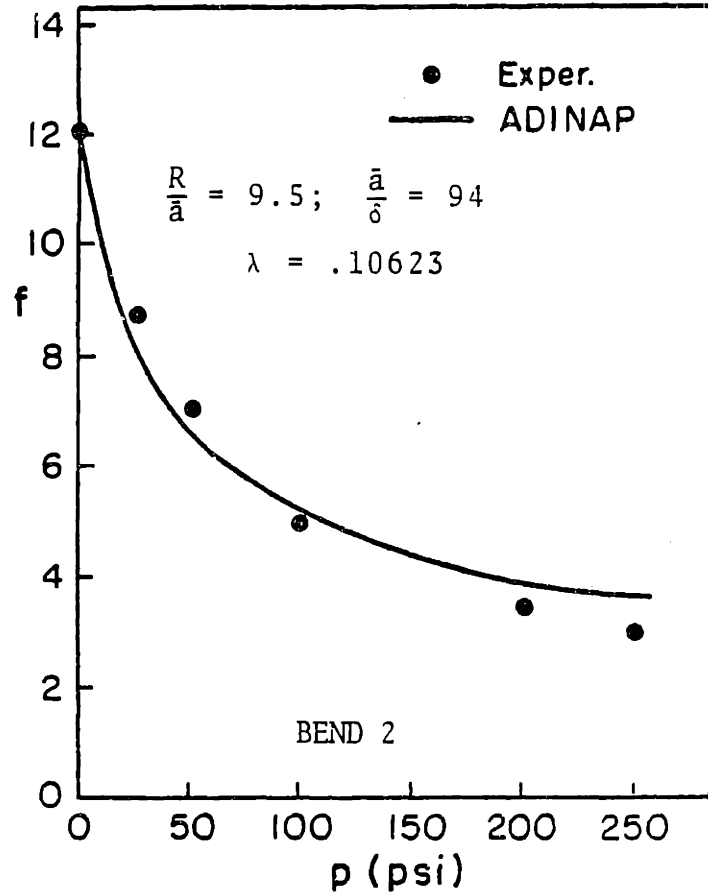
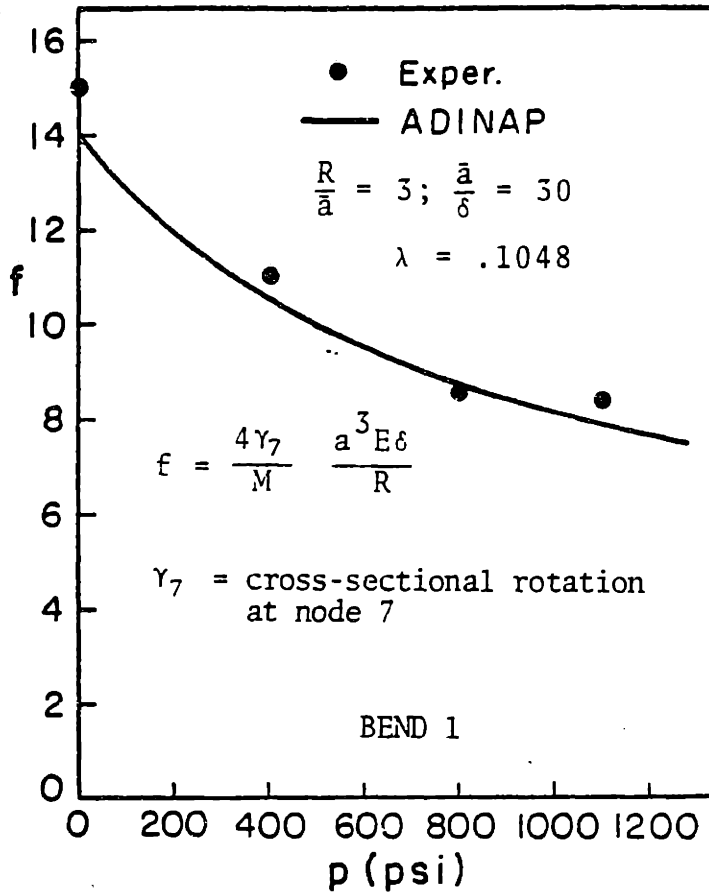


FIGURE 7.11 Stiffening Effects on Pipes due to Internal Pressure.



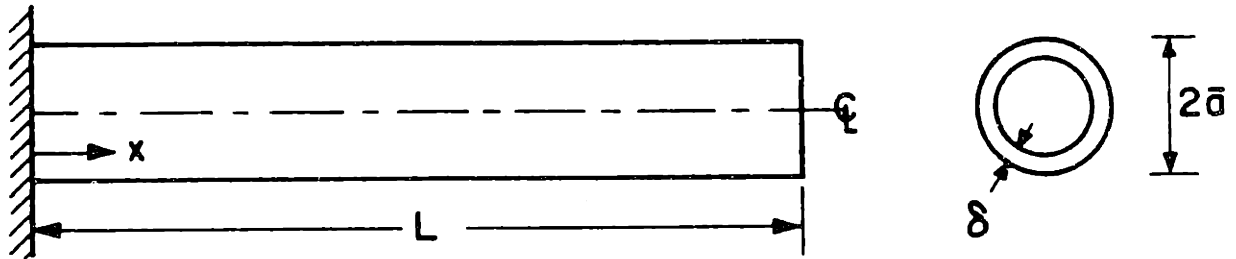
function of the geometric factor  $a/\delta$  [54].

#### 7.5 Convergence of Stress Continuity, and Effect of Penalty Parameter Size - Some Studies with the Elbow Element

The straight cantilever pipe shown in Fig. 7.12 was analyzed for a prescribed ovalization. The purpose of this analysis was to investigate the effects of the element size and penalty parameter size on the response predicted, and thus arrive at some guidelines for the use of the element in modeling more complex piping systems.

Figure 7.13 shows the response predicted in the analysis when using four equal size elements. It is seen that although  $dw_g/dx$  is continuous, the second derivative of  $w_g$  with respect to  $x$  is strongly discontinuous at the junction of the first and second elements. Hence, the pipe skin bending strain due to deformation of the cross section (in Eq. (2.39a)) displays a large jump at this point and a finer finite element mesh is required at the fixed end if the stress distribution is to be predicted accurately.

The appropriate element size for stress continuity between elements is evaluated by recognizing that in the straight pipe stiffness matrix (its closed form expression is presented in Table 7.1), the pipe skin bending strain contribution should be at least as large as the shearing strain contribution in Eq. (2.39c). This condition gives that for an element in which these two strain contributions are important we want that, from



### OVALIZATION BOUNDARY CONDITIONS

$$\text{AT } x = 0 \quad : \quad w_{\zeta} = 0., \quad \frac{dw_{\zeta}}{dx} = 0.$$

$$\text{AT } x = L \quad : \quad C_1 = 0.5 \text{ in. (CORRESPONDING TO UNIT OVALIZATION IN FIRST VON KÁRMÁN MODE)}$$

### ANALYSIS PARAMETERS

$L = 4.8 \text{ in.}$	$E = 2.8 \times 10^7 \text{ psi}$
$\bar{a} = 8.0 \text{ in.}$	$\alpha = 5.6 \times 10^{11} \text{ lb-in}$
$\delta = 0.37 \text{ in.}$	

FIGURE 7.12 - Straight Cantilever Pipe Test Problem

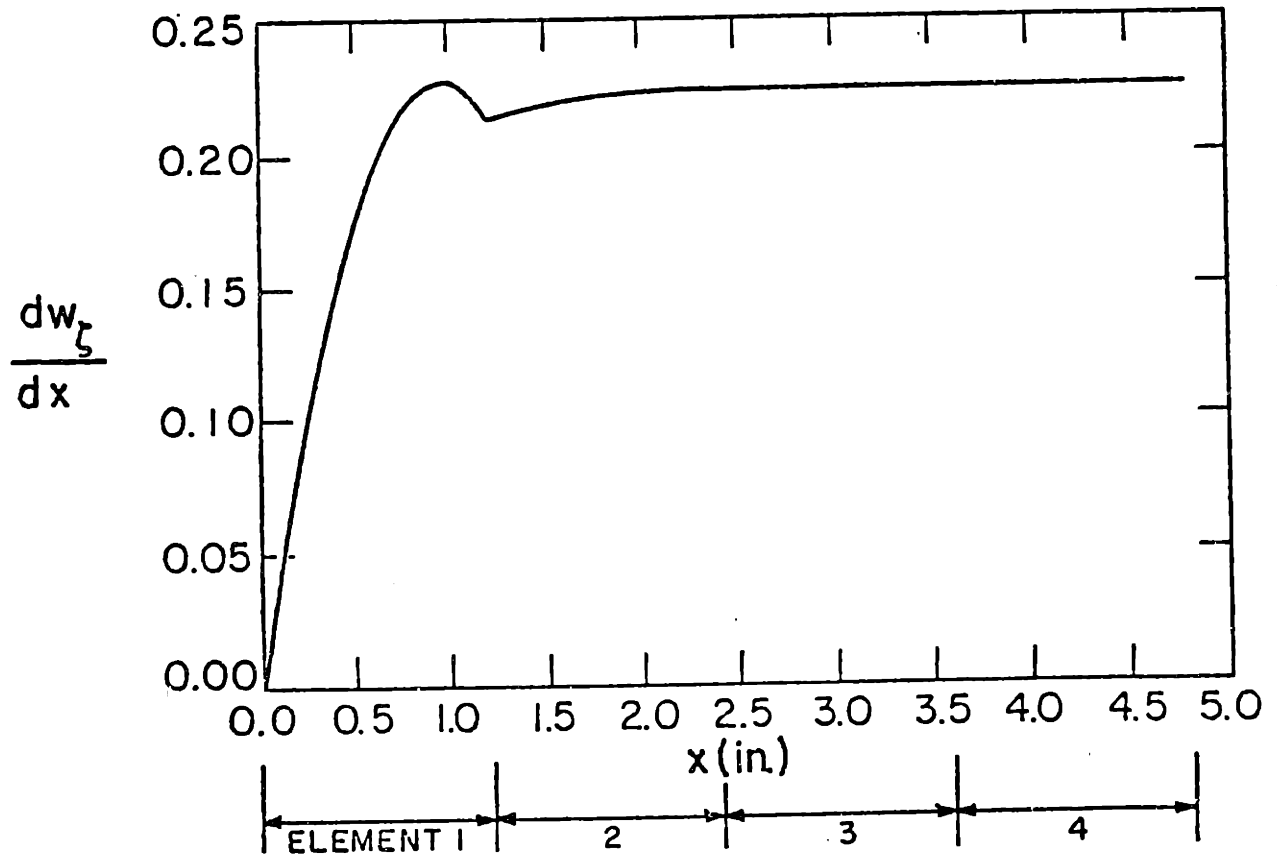
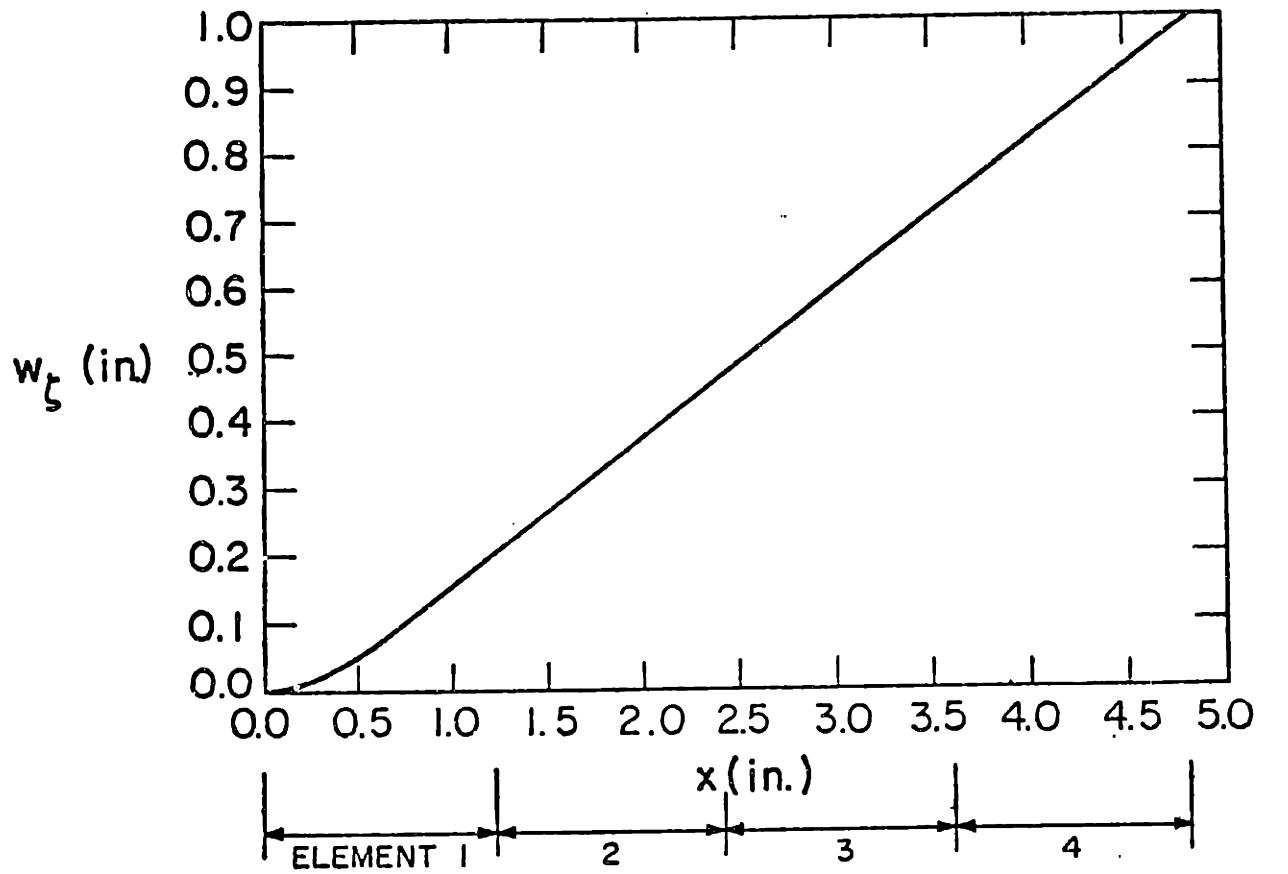


FIGURE 7.13 - Predicted Response of Cantilevered Pipe Using Four Equal Elements

TABLE 7.1 - STRAIGHT PIPE ELEMENT STIFFNESS MATRIX ASSOCIATED WITH OVALIZATION DEGREES-OF-FREEDOM (1st VON KÁRMÁN MODE)

$27 \bar{a} (s/L)^3$	+	$-(135/2) \bar{a} (s/L)^3$	-	$54 \bar{a} (s/L)^3$	+	$-(27/2) \bar{a} (s/L)^3$	-	first term
$(37/20) \bar{a} (s/L)$	+	$(109/80) \bar{a} (s/L)$	+	$(27/40) \bar{a} (s/L)$	-	$(13/80) \bar{a} (s/L)$	+	second term
$(8/35) L (s/\bar{a})^3$		$(99/560) L (s/\bar{a})^3$		$(9/140) L (s/\bar{a})^3$		$(19/560) L (s/\bar{a})^3$		third term
		$189 \bar{a} (s/L)^3$	+	$-(351/2) \bar{a} (s/L)^3$	-	$54 \bar{a} (s/L)^3$	+	
		$(27/5) \bar{a} (s/L)$	+	$(297/80) \bar{a} (s/L)$	-	$(27/40) \bar{a} (s/L)$	-	
		$(81/70) L (s/\bar{a})^3$		$(61/560) L (s/\bar{a})^3$		$(9/140) L (s/\bar{a})^3$		
				$189 \bar{a} (s/L)^3$	+	$-(135/2) \bar{a} (s/L)^3$	-	
				$(27/5) \bar{a} (s/L)$	+	$(109/80) \bar{a} (s/L)$	+	
				$(81/70) L (s/\bar{a})^3$		$(99/560) L (s/\bar{a})^3$		
						$27 \bar{a} (s/L)^3$	+	
						$(37/20) \bar{a} (s/L)$	+	
						$(8/35) L (s/\bar{a})^3$		

Sym.

$$\bar{K} = (\pi E)$$

NOTE: In every sum the first term is the pipe skin bending strain contribution, the second term is the shear strain contribution and the third term is the circumferential bending contribution.

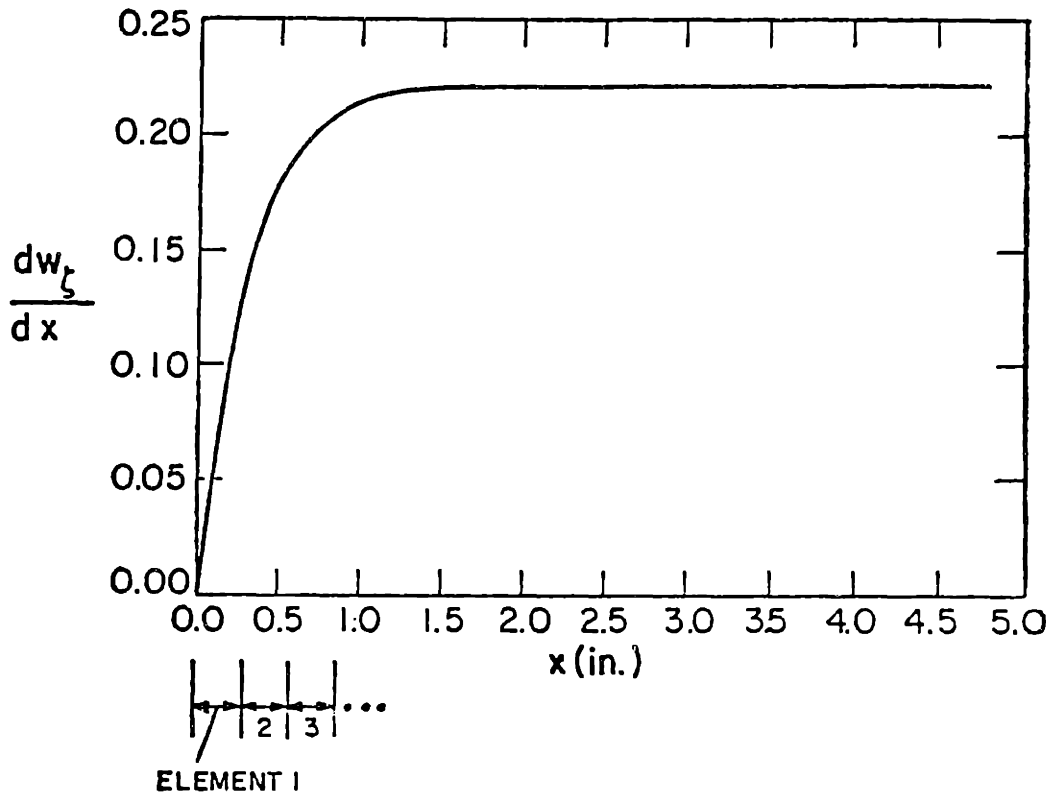
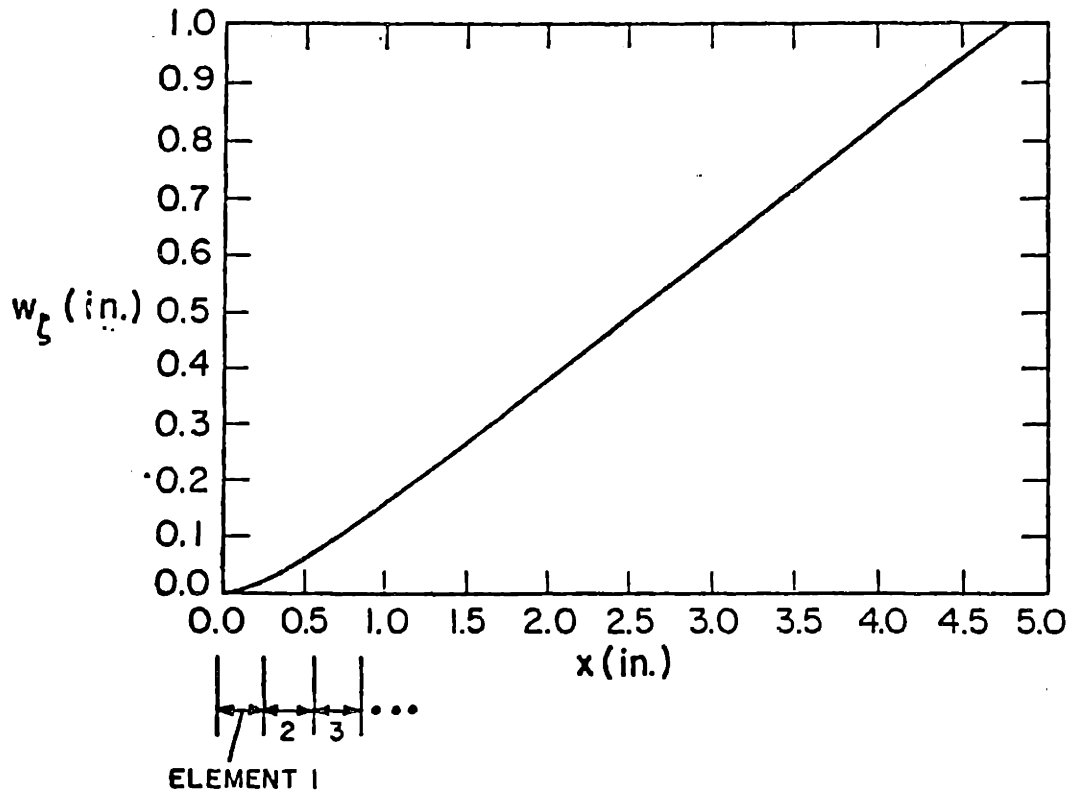


FIGURE 7.14 - Predicted Response of Cantilevered Pipe Using Fine Finite Element Idealization (same response obtained using 16 elements of length 0.3 in., or 6 elements of 0.3 in. and 1 element of 3.0 in.)

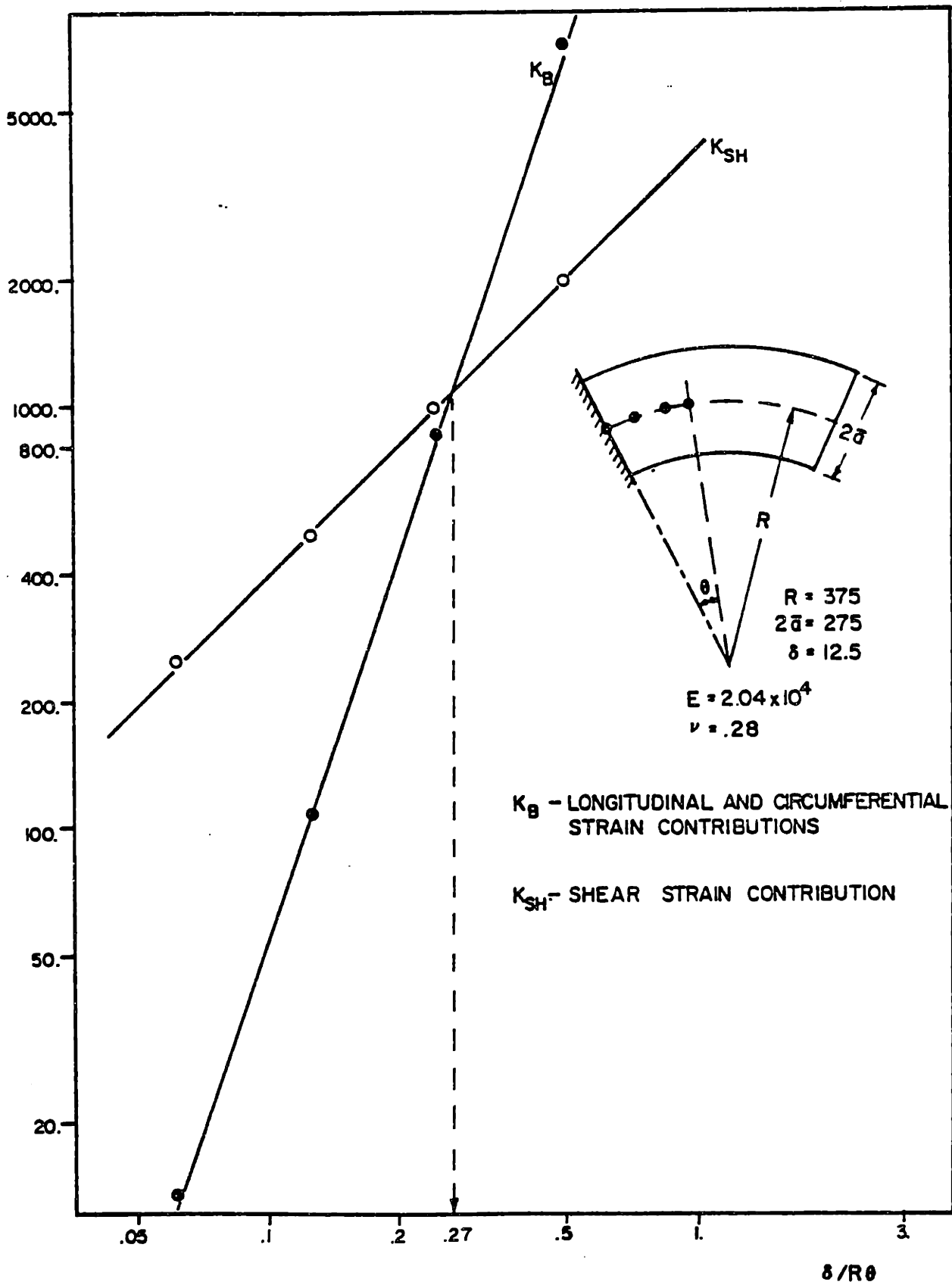


FIGURE 7.15 Element Size Study for the Analysis of Bends.

Table 7.1,  $\frac{\delta}{L} > .26$ . Figure 7.14 shows the response predicted using a fine finite element idealization for which this criterion is satisfied. It is seen that in the predicted response the second derivative of  $w_g$  is now continuous. It is also important to note that the ovalization displacement  $w_g$  has changed very little from the response given in Fig. 7.13.

In the study of the appropriate element size for the analyses of curved pipes, we follow the above procedure with the stiffness matrix being obtained numerically. Figure 7.15 shows a comparison between the bending and shearing strain contributions to the stiffness matrix, for various bend element sizes. It is interesting to note that the condition for the bending strain contribution to be larger than shearing strain contribution results in  $\frac{\delta}{R\theta} > .27$ , which is practically the condition obtained for straight pipes.

To investigate the effect of the size of the penalty parameter  $\alpha$ , the 16 element model of the cantilevered straight pipe was analyzed using the values of  $\alpha$  listed in Fig. 7.16. As expected, when  $\alpha$  is very small, the fixity condition at  $x=0$  is not properly imposed and when  $\alpha$  is very large, the complete element stiffness matrix is singular. However, for a large range of  $\alpha$  (see cases 2 and 3) an identical response is predicted. In practice, it is effective to choose  $\alpha$  equal to the largest value in the stiffness matrix corresponding to the ovalization degrees-of-freedom, and this is how  $\alpha$  was chosen in the following analyses.

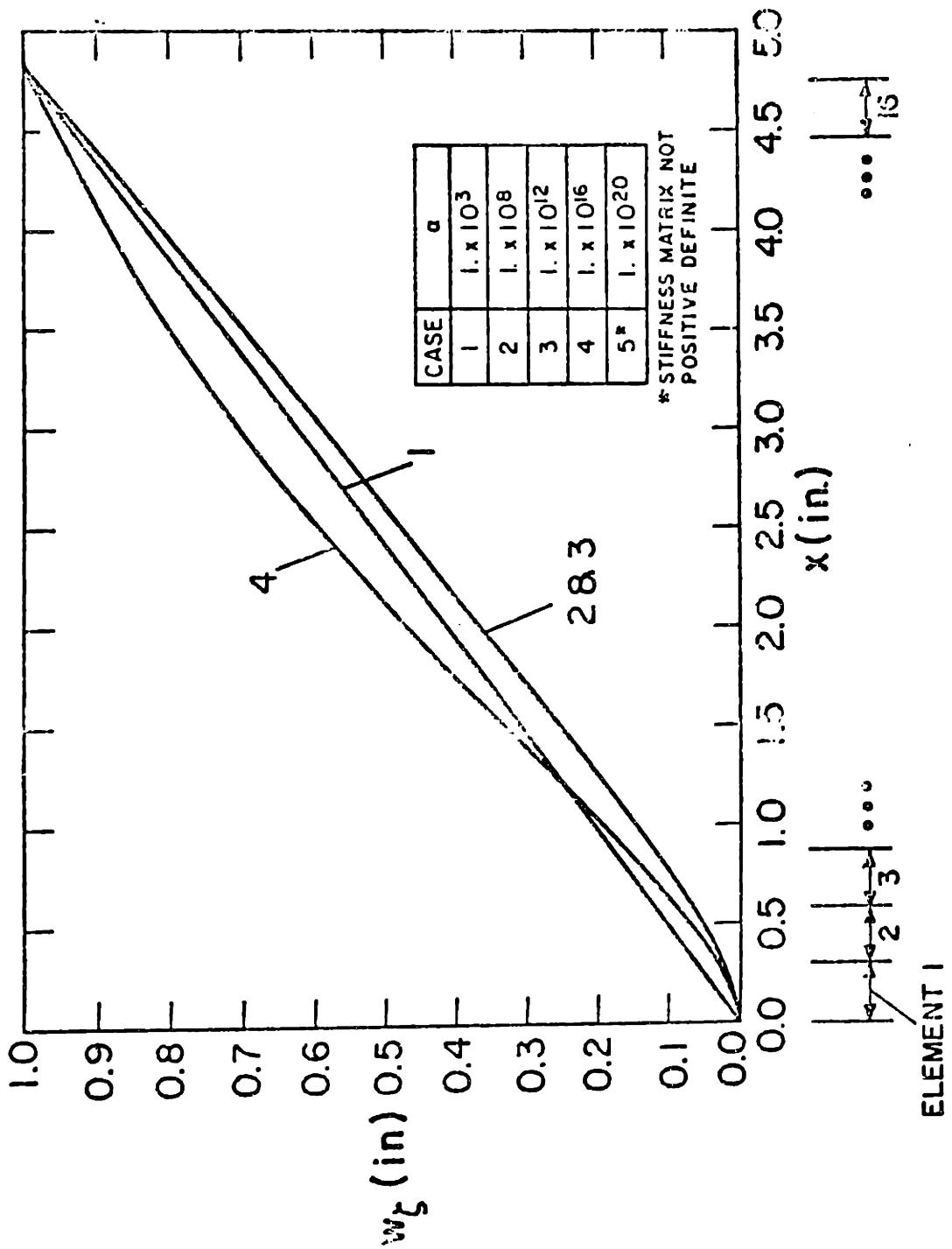


FIGURE 7.16 - Effect of Size of Penalty Parameter on Predicted Response of Straight Cantilevered Pipe



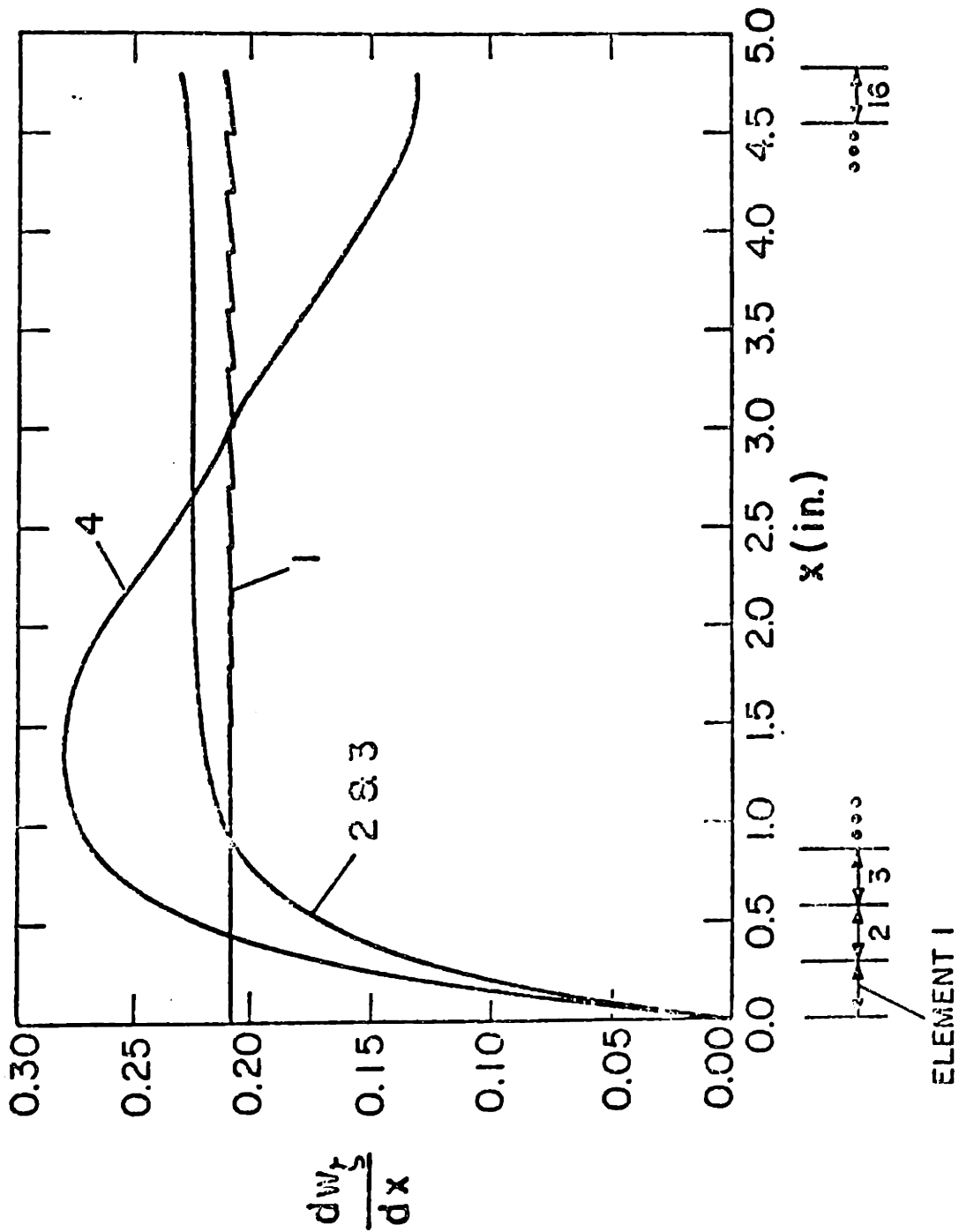


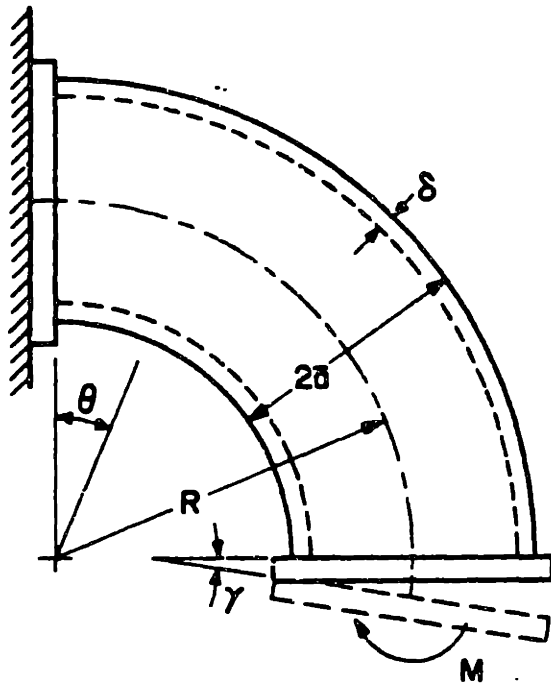
FIGURE 7.16 - (Continued)

## 7.6 Analysis of a Flanged Pipe Bend

The flanged bend shown in Fig. 7.17 was analyzed using the finite element model given. Figures 7.18 to 7.22 show the computed response for two different bend radii and give also the experimental results presented by Whatham in Ref. [37]. It is seen that the correspondence between the computed and experimental flexibility factors and longitudinal stresses is good, but there is less good correspondence between the measured and computed circumferential stresses.

## 7.7 Analyses of a Pipe Bend for Different End Constraints

The pipe bend shown in Fig. 7.23 was analyzed in Section 7.2 and in previous studies [8, 27]. In these analyses interaction effects were not considered. Figure 7.24 shows the response predicted when now including interaction effects using the idealizations described in Fig. 7.25. For comparison, also the responses predicted using two finite element shell idealizations of the piping system with flanges at A and B are shown. First, we used in these analyses a triangular flat 18 degrees-of-freedom plate/shell element described in Ref. [75]. The following element mesh was used: 12 layers of elements around half the circumference (one layer being two triangles), 9 layers for the 90 degrees bend and 3 layers for the straight pipe, see Fig. 7.25. Thus, a total of 216 and 288 elements were used to model Case I/flanges at A and B and case II/flanges at A and B, respectively. Second, the isoparametric 16-node



$$R = \begin{cases} 250 \text{ mm} \\ 375 \text{ mm} \end{cases}$$

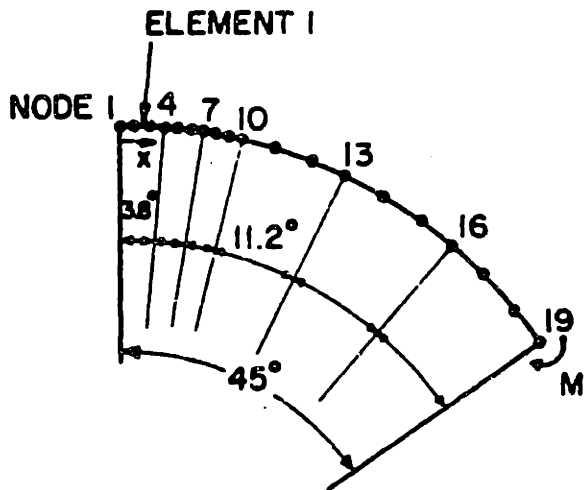
$$\delta = 12.5 \text{ mm}$$

$$2\bar{a} = 275 \text{ mm}$$

$$E = 200 \text{ GPa}$$

$$\nu = 0.28$$

(a) PIPE BEND CONSIDERED



OVAL. BOUND. CONDITIONS

AT NODE 1:  $w_{\zeta} = 0, \frac{dw_{\zeta}}{dx} = 0$

AT NODE 19  $\frac{dw_{\zeta}}{dx} = 0$

CONTINUITY AT NODES 4, 7, 10, 13 & 16

(b) FINITE ELEMENT MODEL USED (SIX 4-NODE ELEMENTS)

FIGURE 7.17 - Whatham Pipe Bend, E=Young's Modulus,  $\nu$ =Poisson's Ratio

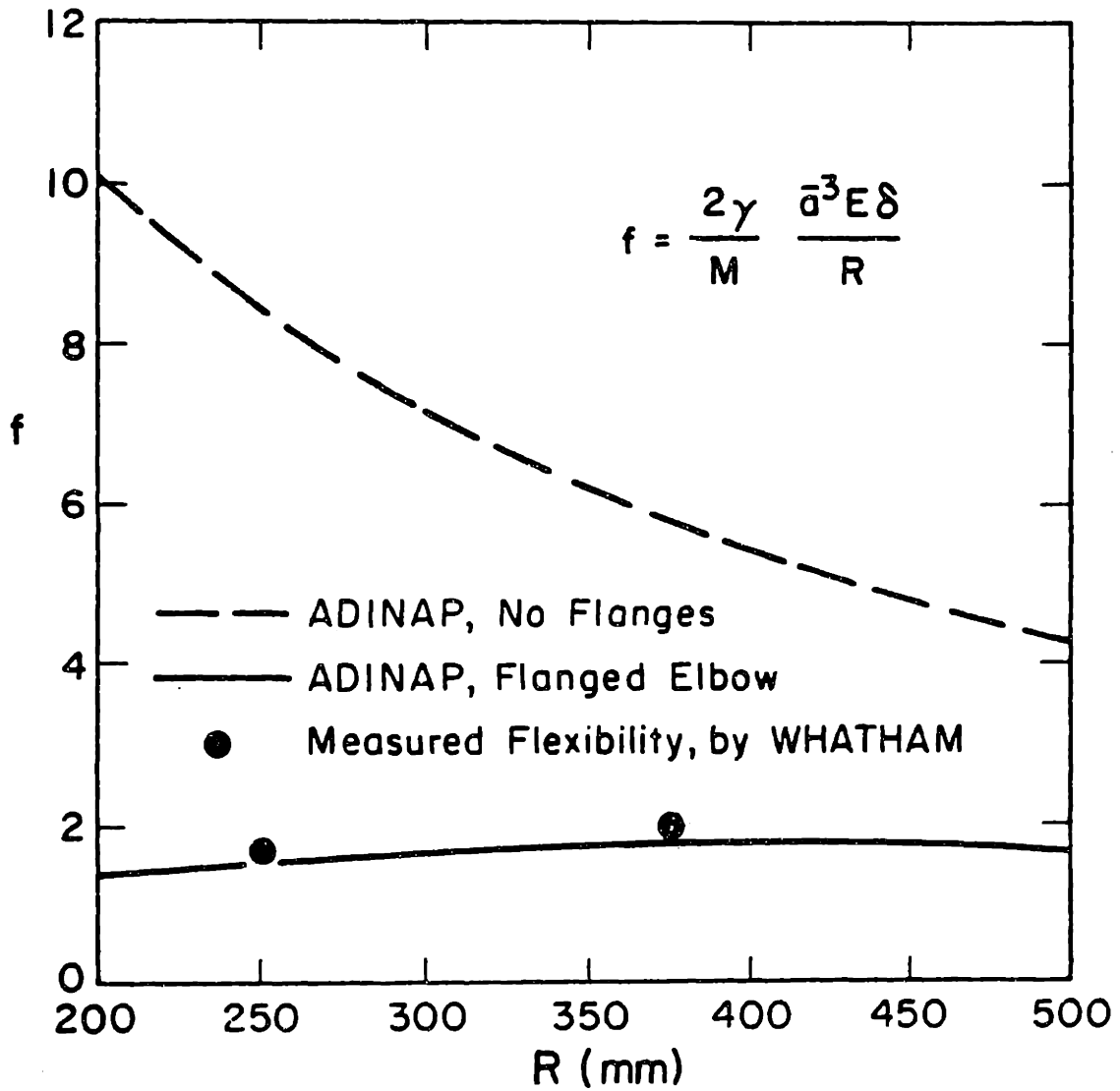


FIGURE 7.18 - Predicted Flexibility Factors for Whatham Pipe Bend

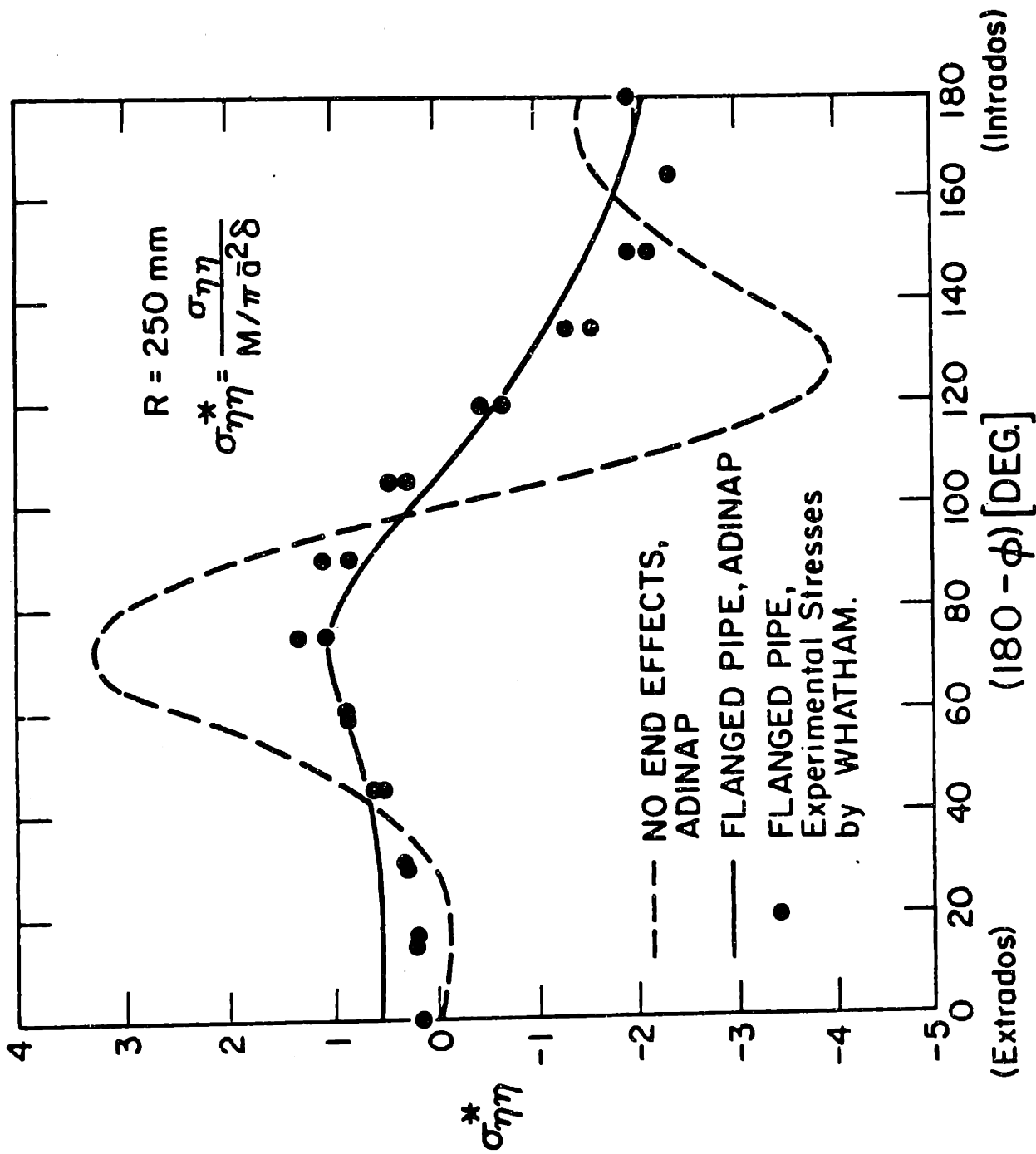


FIGURE 7.19 - Predicted Longitudinal Stresses at  $\theta=45^\circ$  and at Outside Surface in Analysis of Whatham Pipe Bend,  $R=250 \text{ mm}$

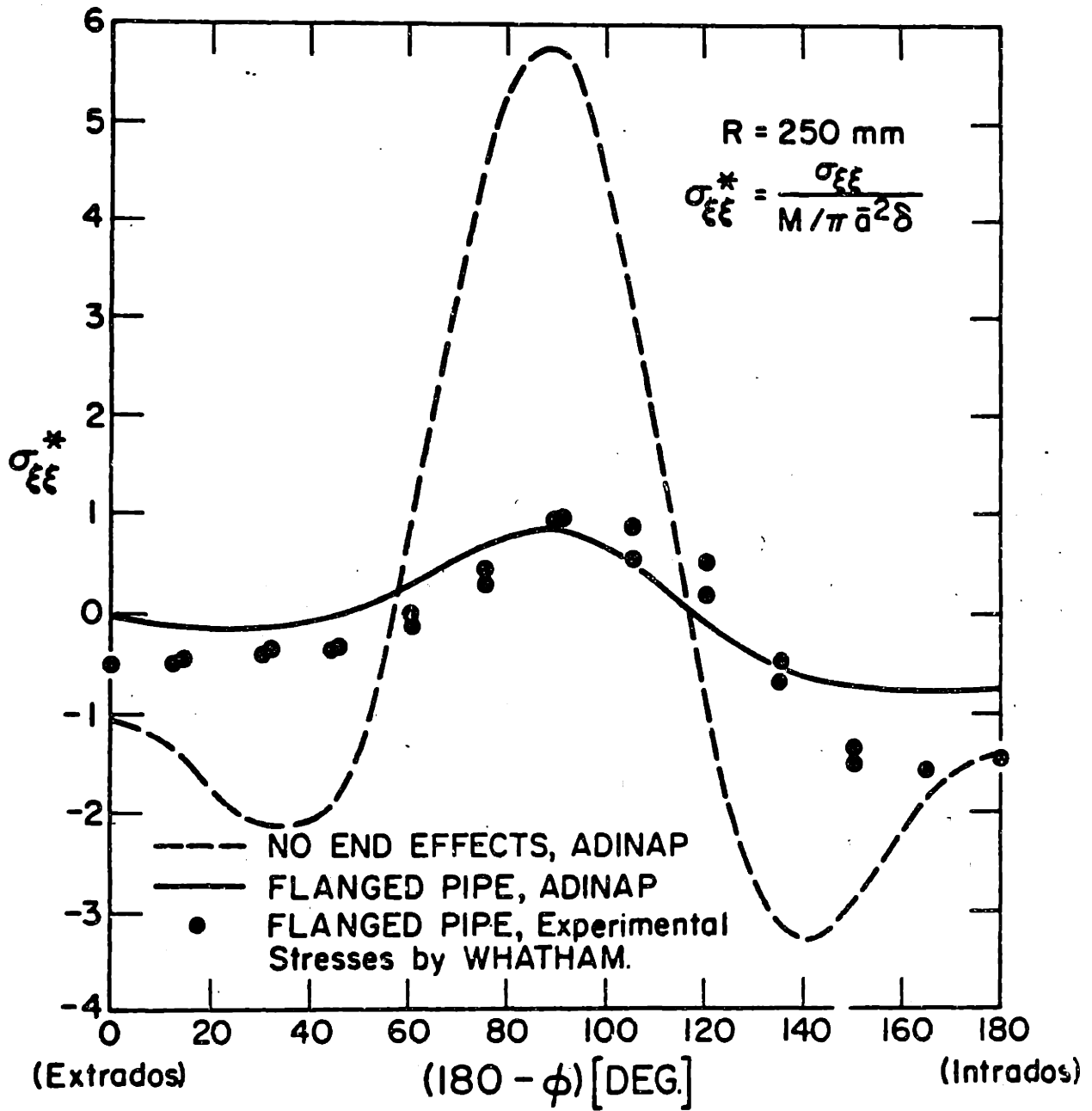


FIGURE 7.20 - Predicted Circumferential Stresses at  $\theta=45^\circ$  and at Outside Surface in Analysis of Whatham Pipe Bend,  $R=250 \text{ mm}$

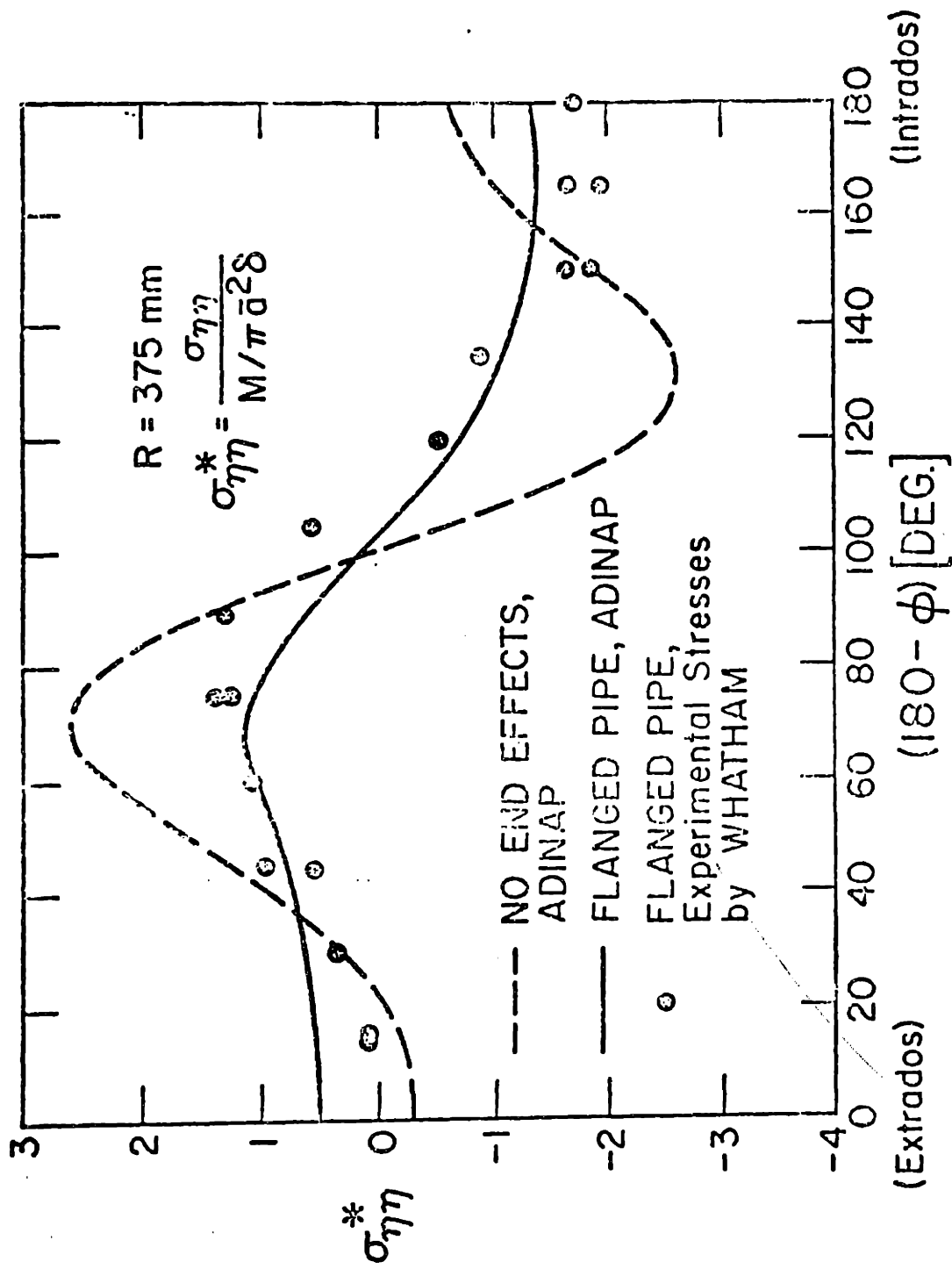


FIGURE 7.21 - Predicted Longitudinal Stresses at  $\theta=45^\circ$  and at Outside Surface in Analysis of Whatham Pipe Bend,  $R=375 \text{ mm}$

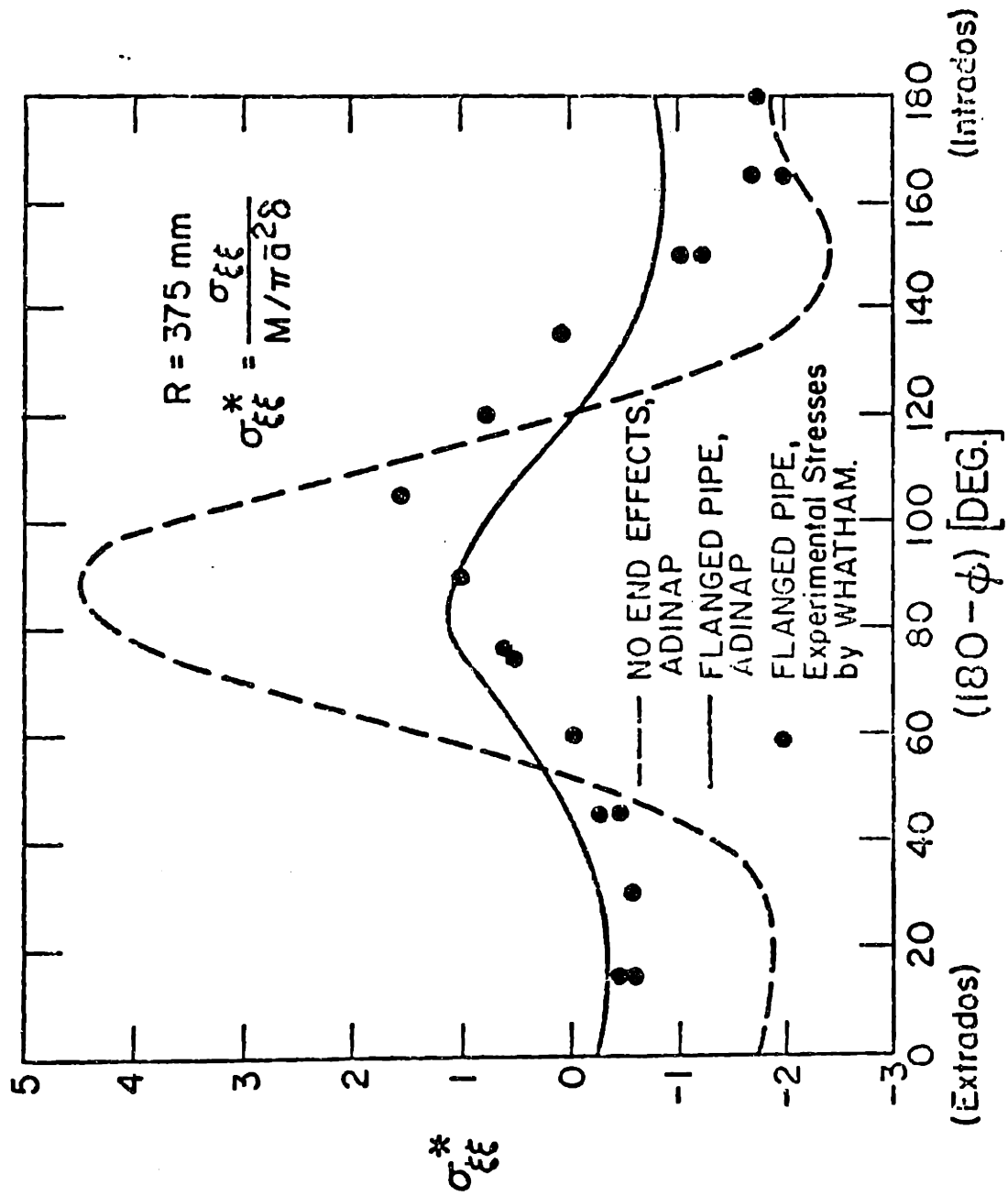


FIGURE 7.22 - Predicted Circumferential Stresses at  $\theta = 45^\circ$  and at Outside Surface in Analysis of Whatham Pipe Bend,  $R = 375 \text{ mm}$



curved shell element described in Ref, [35] was employed to analyze the problem. The following shell element models were used: 4 layers of elements around half circumference, 3 layers for the 90 degrees bend portion, see Fig. 7.26, and 1 layer for the straight pipe portion. Hence, 12 and 16 shell elements were employed in the analysis of cases I and II, respectively. Figure 7.24 shows that the ovalizations predicted using the elbow element are close to the ovalizations calculated with the shell element idealizations. The differences between the finite element solutions represent only 3% of the reduction in cross sectional ovalization if the interaction effects are included. Considering the response of the piping structure, we note that the ovalizations of the piping systems are reduced very significantly when the interaction effects are included. In Table 7.2, the required solution times for Case I/flanged at A and B analysis using three different element models, are presented. The analyses were performed on a CDC Cyber 175, and the required solution time was substantially less when the elbow element was employed.

#### 7.8 Elastic-Plastic Analysis of Whatham Pipe Bend

The 90 deg. flanged elbow shown in Fig. 7.17 was analyzed for its elastic-plastic response. Two different finite element idealizations were employed in this study. Namely, the elbow element model shown in Fig. 7.17 with 5 Newton-Cotes integration points through the thickness, and the isoparametric shell element

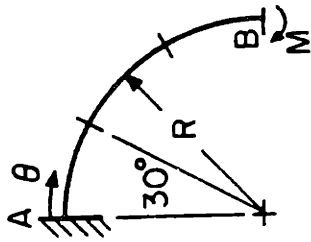
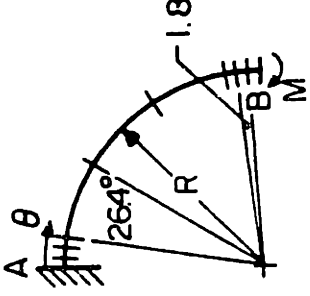
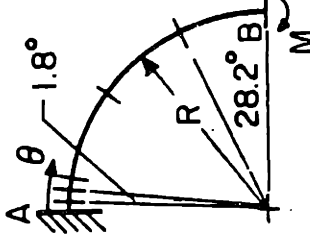
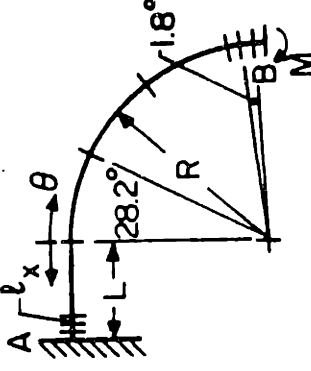
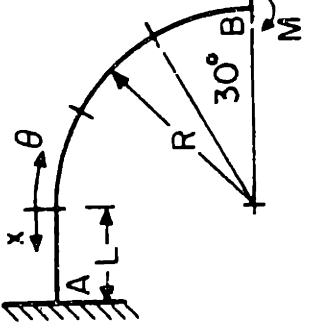
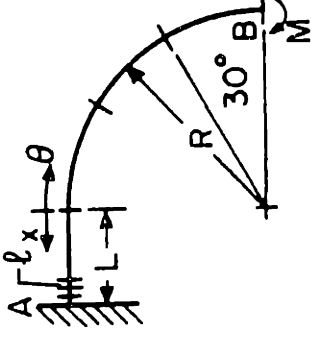
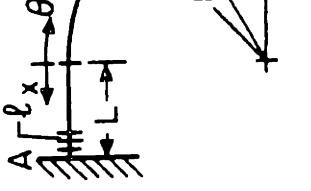
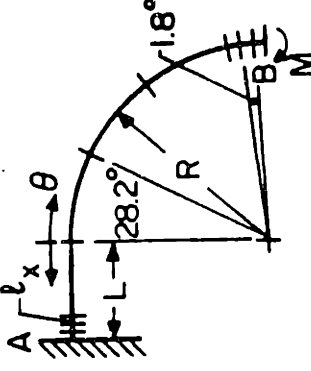
		WITH FLANGES	
		AT END A	AT ENDS A & B
CASE I	NO FLANGES	 <p>3 ELEMENTS</p>	 <p>9 ELEMENTS</p>
	WITH FLANGES	 <p>6 ELEMENTS</p>	 <p>10 ELEMENTS</p>
CASE II	NO FLANGES	 <p>4 ELEMENTS</p>	 <p>7 ELEMENTS</p>
	WITH FLANGES	 <p>7 ELEMENTS</p>	 <p>10 ELEMENTS</p>
<b>GEOMETRIC PARAMETERS</b> $R/\alpha = 3.07$ , $\alpha/\delta = 20.8$ , $R/L = 2.0$ , $L/l = 9.0$ , $\nu = 0.3$			

FIGURE 7.23 - Pipe Bends and Finite Element Models Used

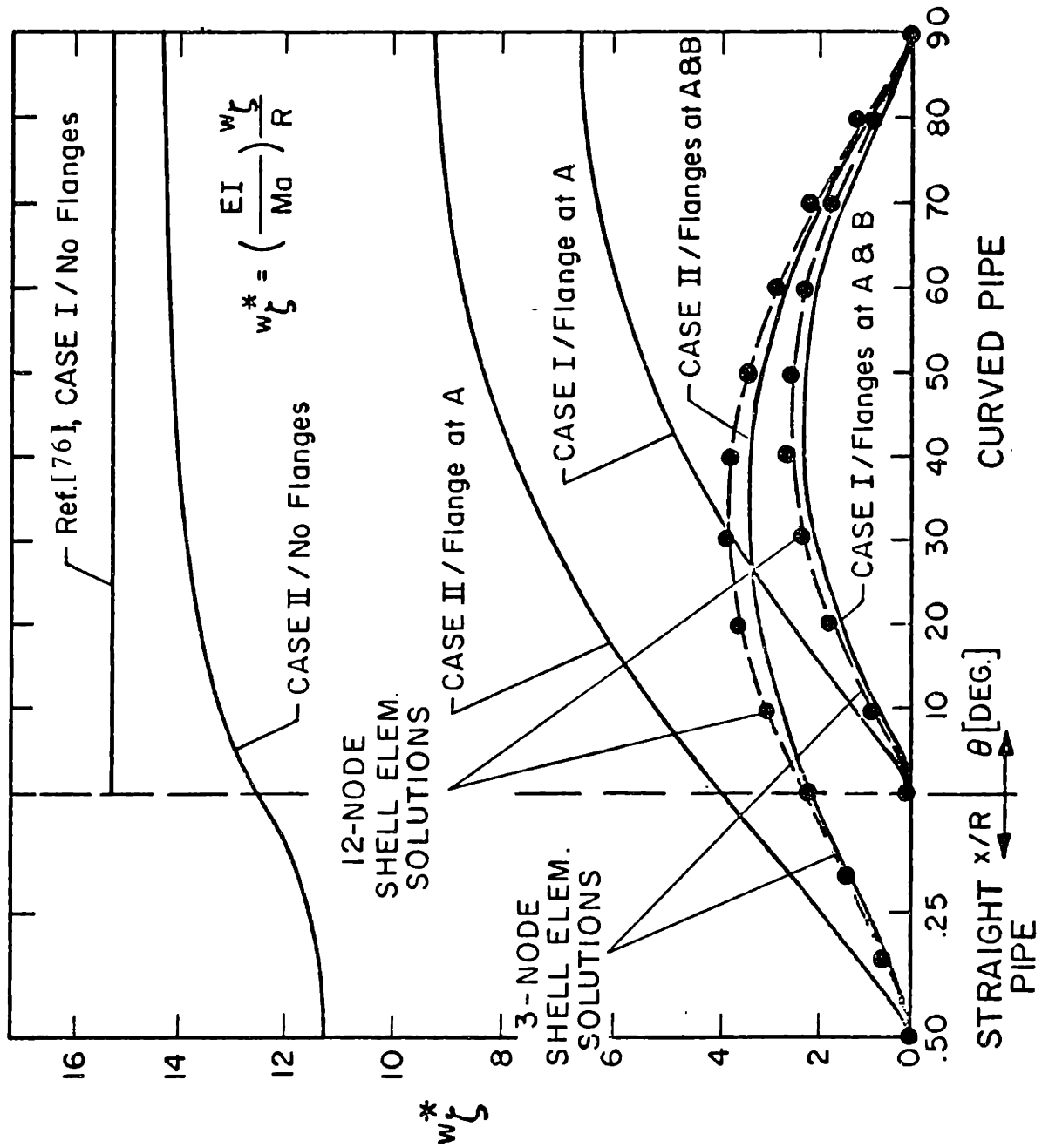


FIGURE 7.24 - Predicted Ovalization Response of Bends Defined in Fig. 7.23. Ovalization Measured at  $\phi=90^\circ$ .

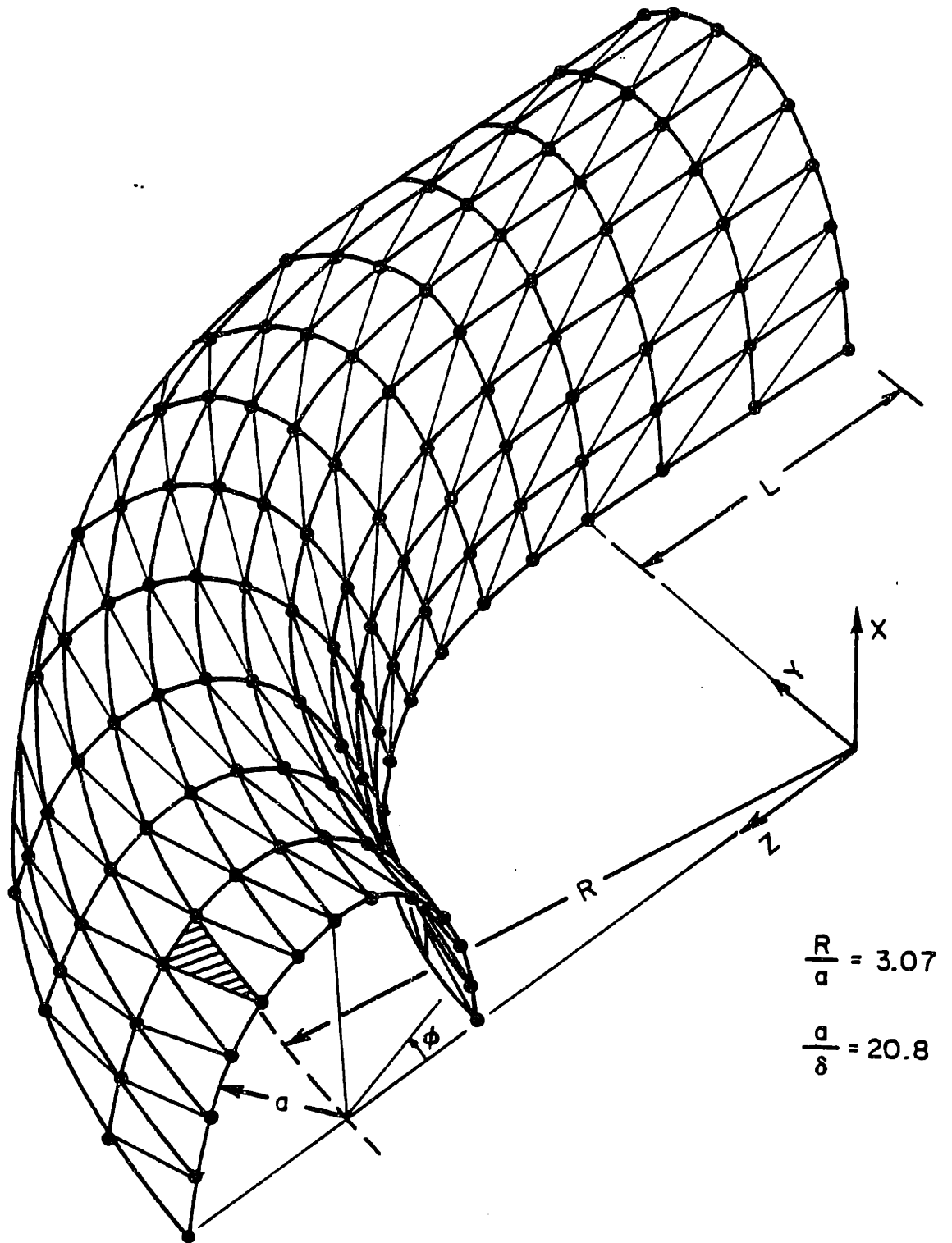


FIGURE 7.25 Plate Element Model Used in Case II/Flanges at A and B Analysis.

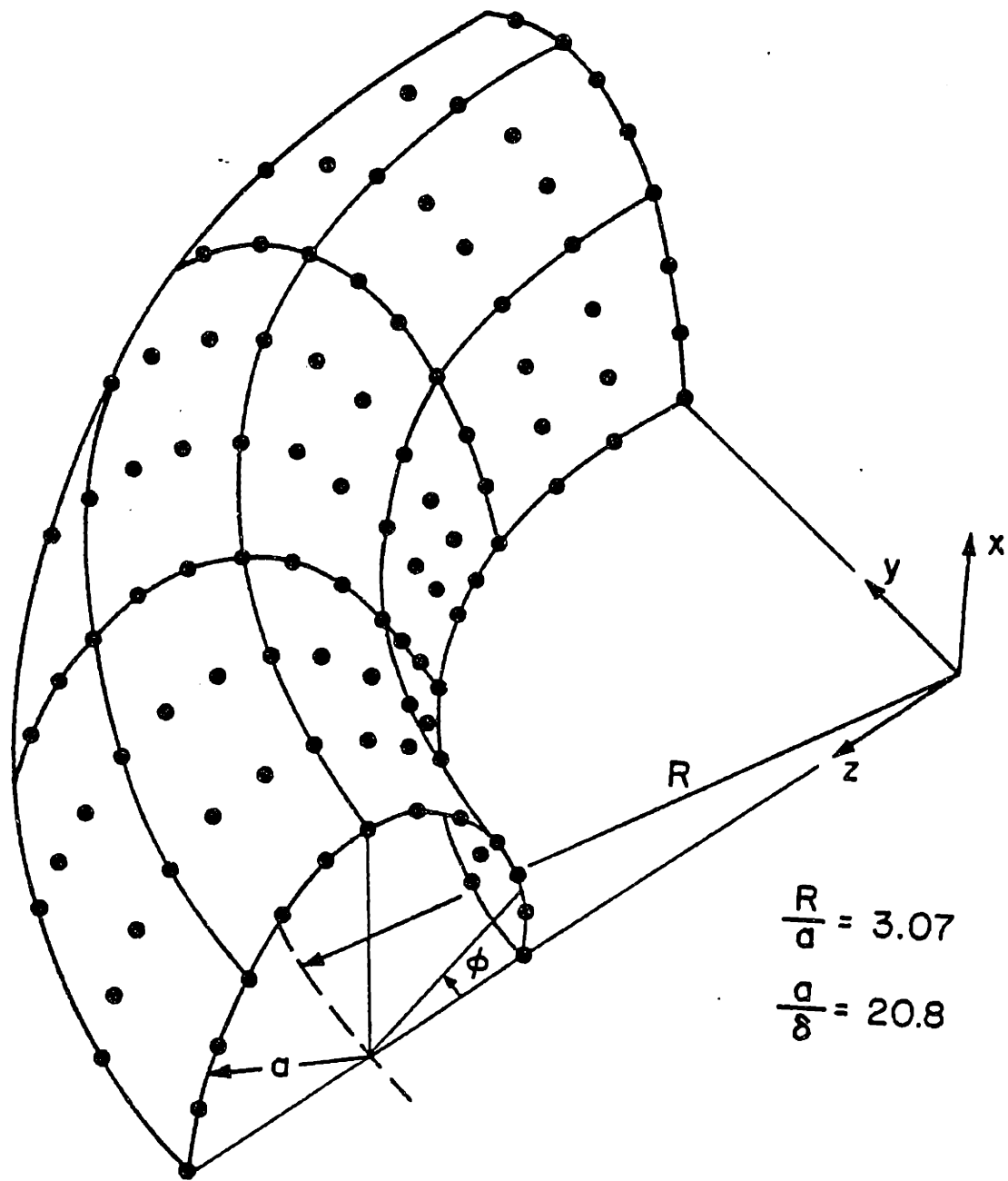


FIGURE 7.26 Shell Element Model Used in Case I/Flanges at A and B Analysis.

TABLE 7.2 REQUIRED SOLUTION TIMES<sup>†</sup> IN CASE 1/FLANGED AT A AND B, ANALYSIS  
 USING THE ELBOW, PLATE AND SHELL ELEMENT IDEALIZATIONS (SOLUTION  
 TIME LOG IN SECONDS)

	ELBOW	PLATE	SHELL
INPUT PHASE	.15	1.02	.76
ASS. LINEAR STIFF. MATRIX	2.20	2.05	12.25
TRIANG. OF EFF. STIFF. MATRIX	.03	1.04	2.33
SOLUTION OF EQUATIONS	.01	.11	.17
PRINT DISPLACEMENTS	.03	.10	.09
# OF ELEMENTS	3(4-node elem.)	216(3-node elem.)	12(16-node elem.)
INTEGRATION ORDER	3 x 3 x 12	3 mid-side points	3x3x2

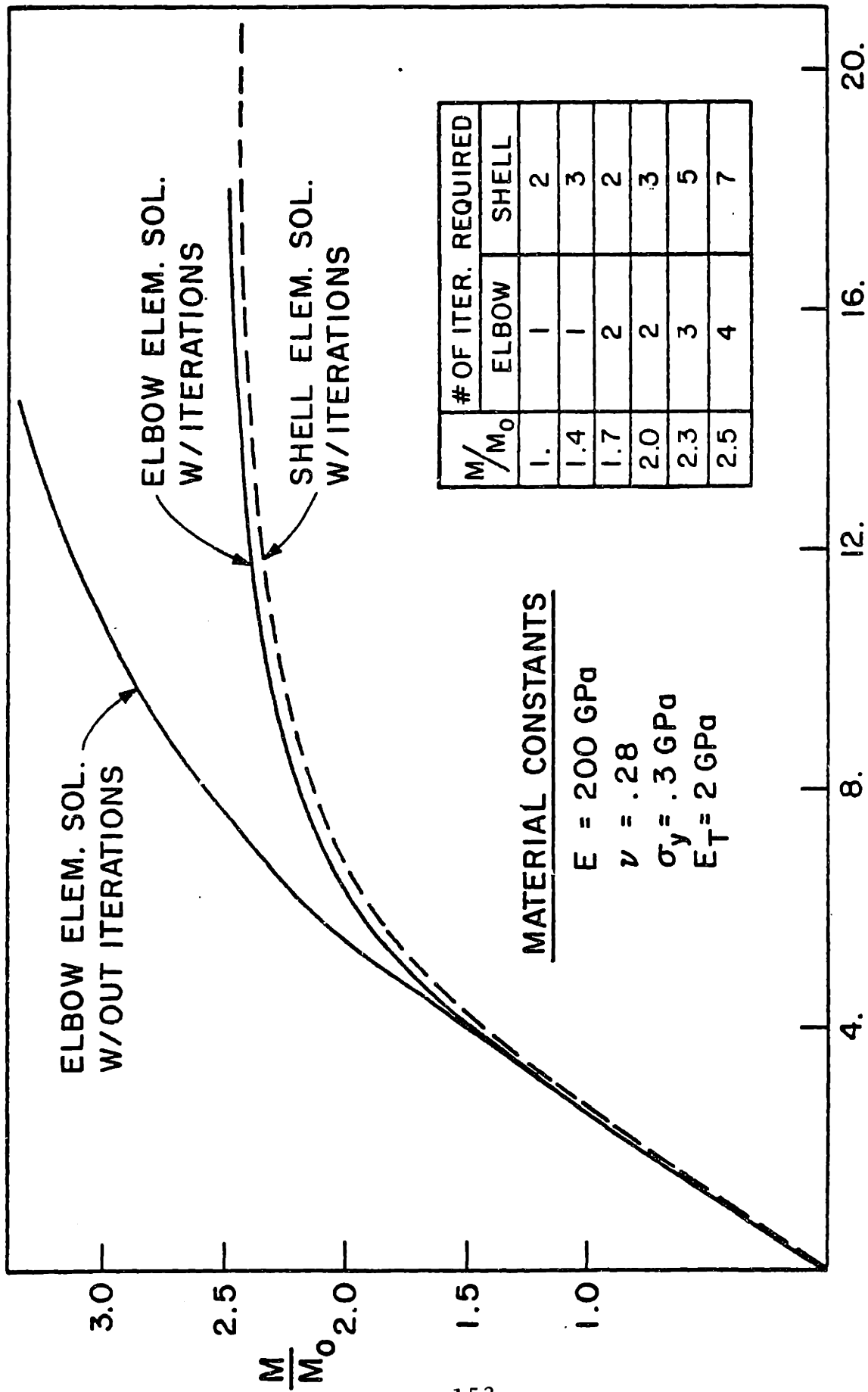
<sup>†</sup> On a CDC Cyber 175

model using 4 Gauss integration points through the thickness, see Fig. 7.26. The bilinear elastic-plastic material model with isotropic hardening was used in the analysis.

Figure 7.27 shows the calculated response of the bend using two finite element models. Good agreement between the two solutions is noted. The predicted stiffness of the bend is slightly higher using the elbow element model because of the assumptions that the cross-sections of the bend remain plane and in-plane cross-sectional displacements are confined to a number of deformation patterns. The stress results for different loading sizes are presented in Figs. 7.28 to 7.30. It is noted that the longitudinal stress predictions are in good agreement, while the correspondence between the circumferential stresses is not so good.

#### 7.9 Large Displacement Analysis of a Cantilever Pipe Section Beam

One four-node element, that does not include ovalization of the cross-section, was employed in the analysis of a cantilever pipe section beam subjected to a concentrate bending moment. The load deflection responses for different displacement/rotation quantities are shown in Fig. 7.31. The predicted results are in very good agreement with the analytical solution given in Ref. [33].



**ROTATION AT BEND TIP CROSS-SECTION -  $\gamma \times 10^{-3}$  [RAD.]**

FIGURE 7.27 - Responses of Elbow and Shell Element Models in Analysis of Whatham Pipe Bend.  $M_0$  is the Limit Load for Yield Initiation.



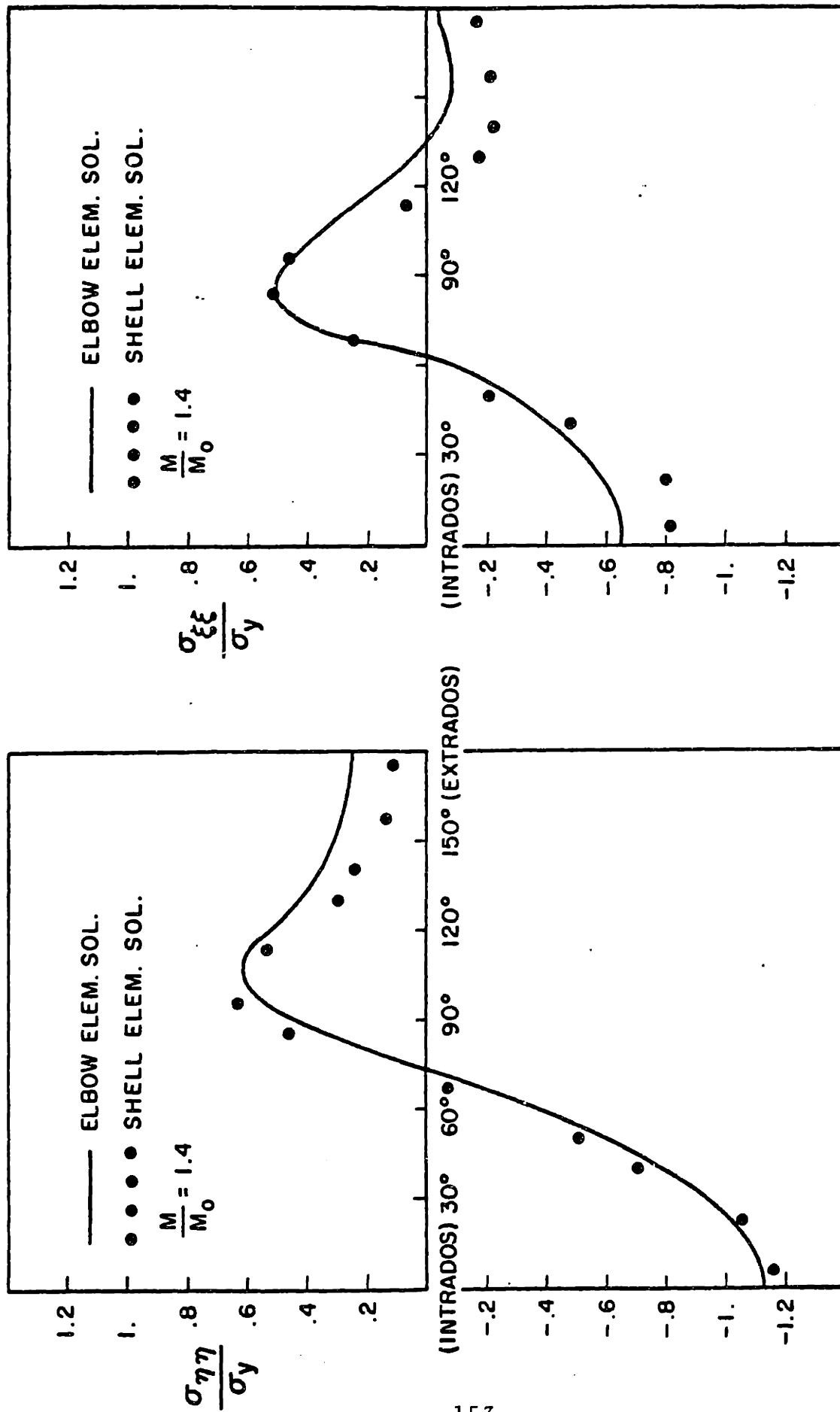


FIGURE 7.28 - Predicted Longitudinal and Circumferential Stresses at  $\theta = 45^\circ$  and at Outside Surface ( $M/M_0 = 1.4$ ).

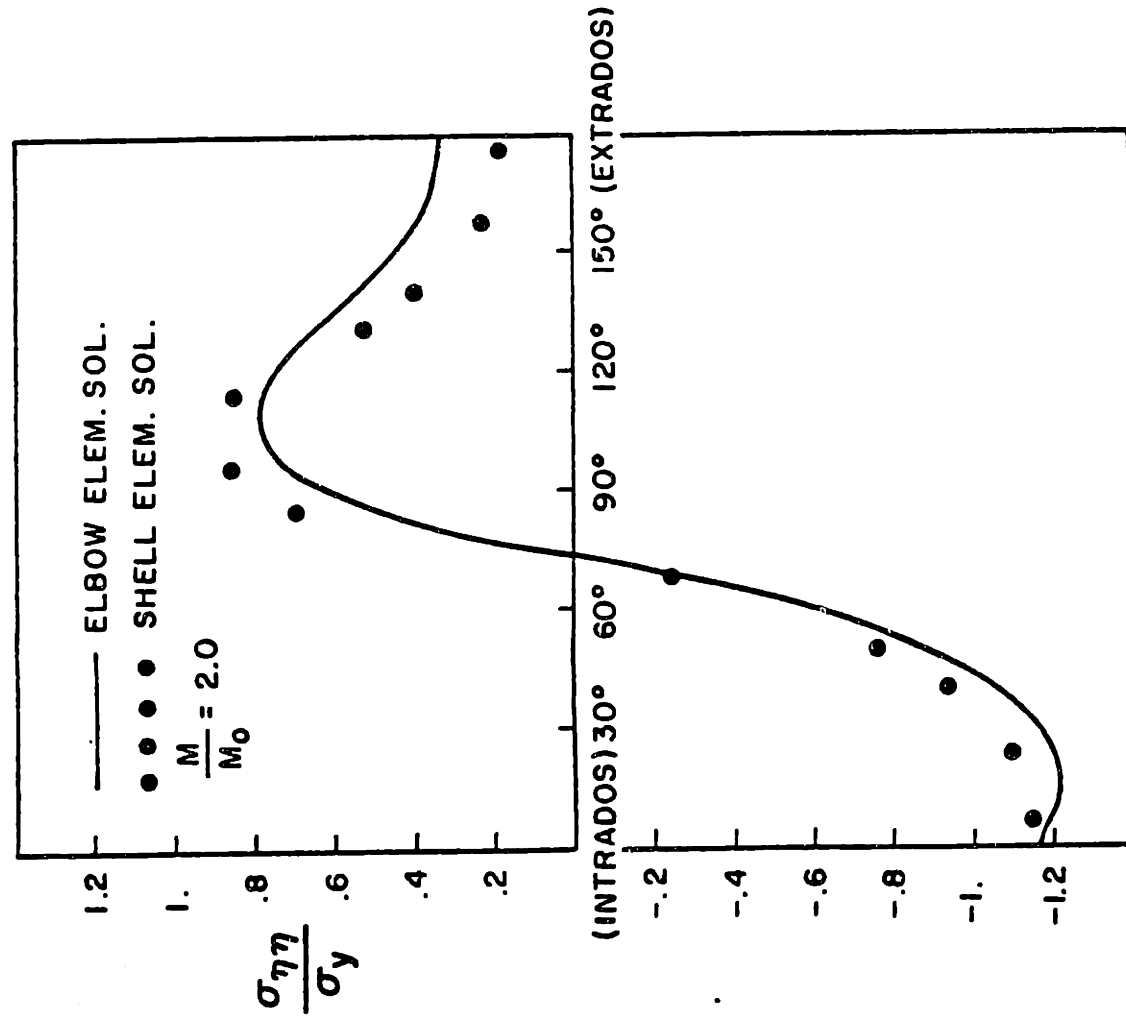
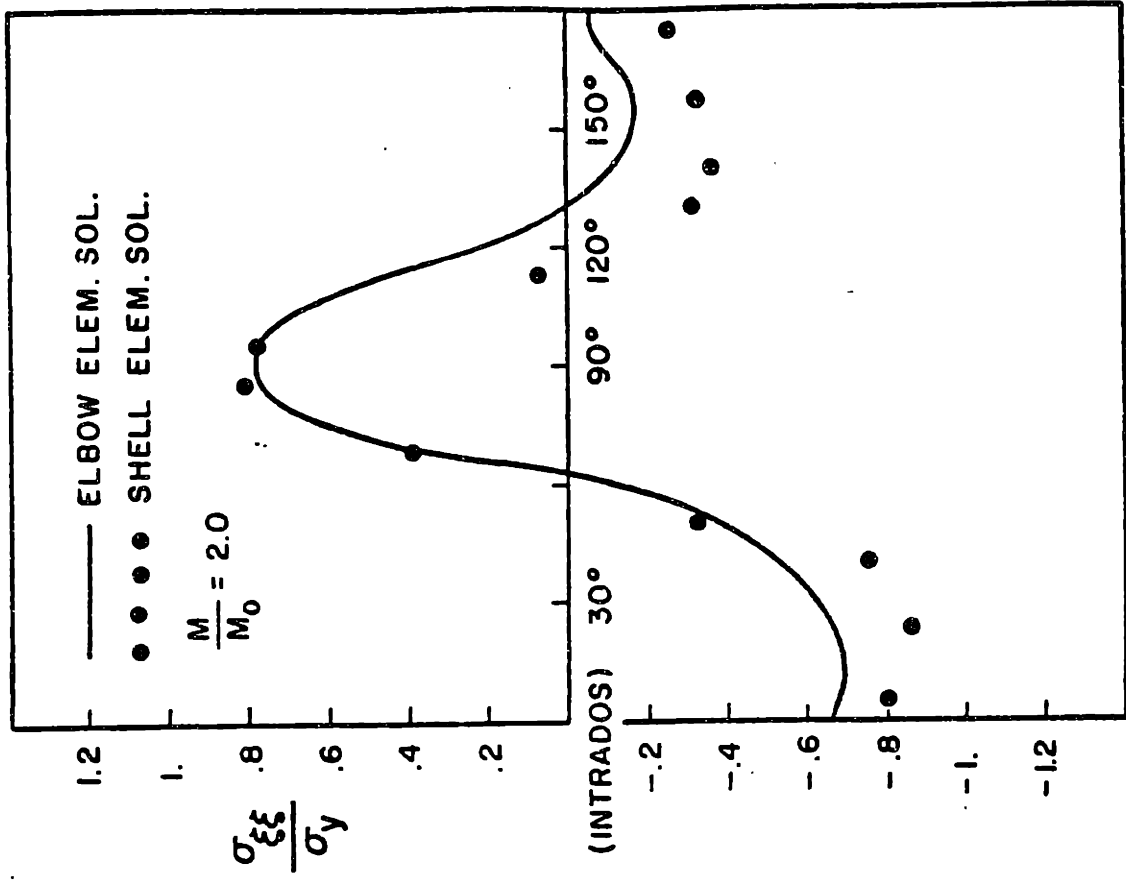


FIGURE 7.29 - Predicted Longitudinal and Circumferential Stresses at  $\theta = 45^\circ$  and at Outside Surface ( $M/M_0 = 2.0$ ).

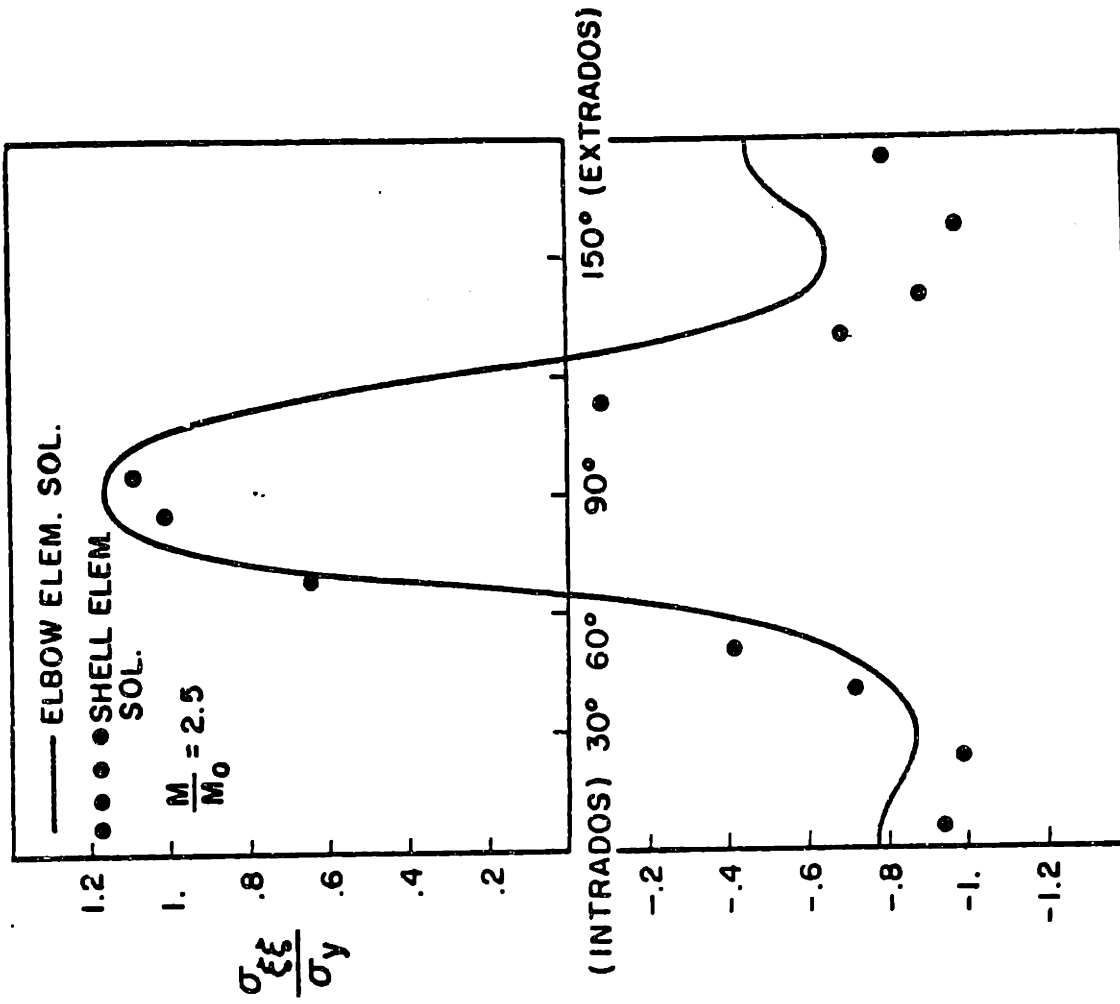
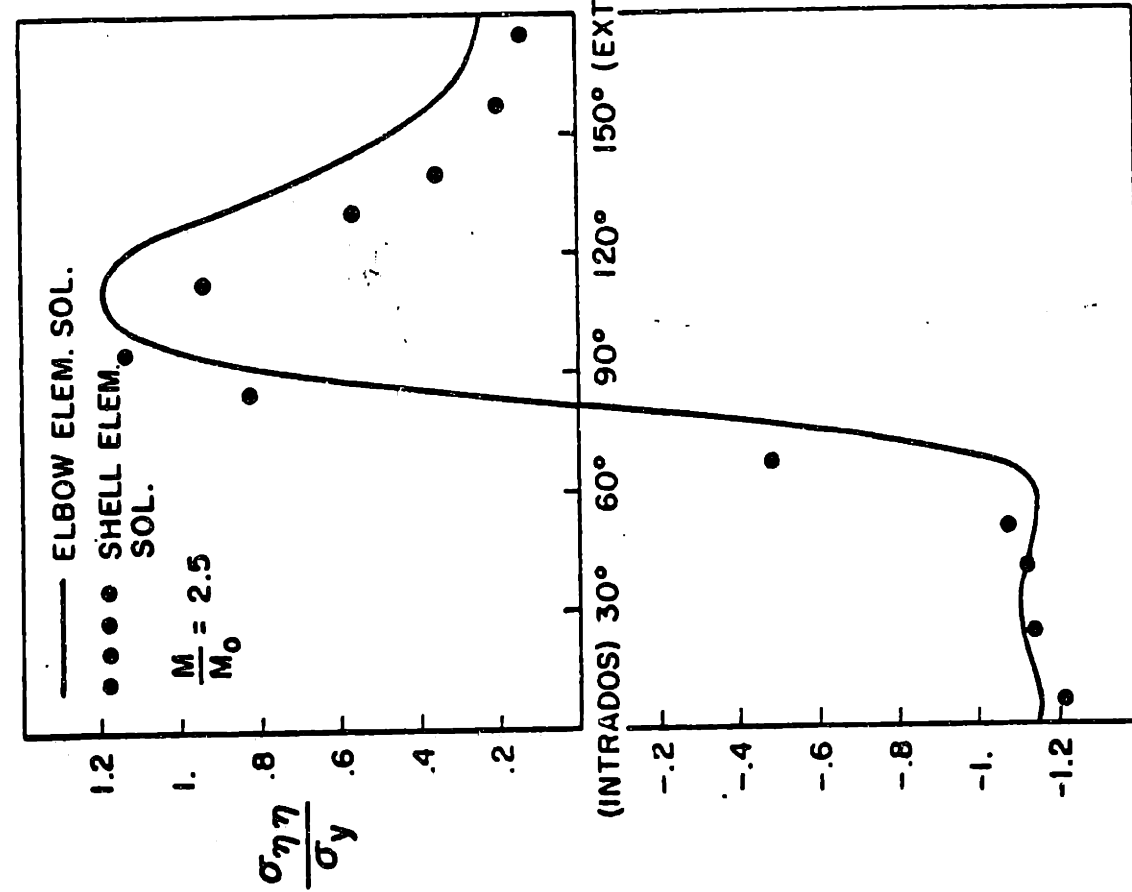
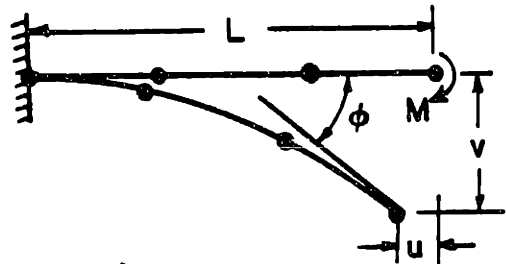


FIGURE 7.30 - Predicted Longitudinal and Circumferential Stresses at  $\theta = 45^\circ$  and at Outside Surface ( $M/M_0 = 2.5$ ).



$L = 12 \text{ in.}$   
 $a = .408 \text{ in.}$   
 $\delta = .389 \text{ in.}$   
 $E = 3.0 \times 10^7 \text{ psi.}$

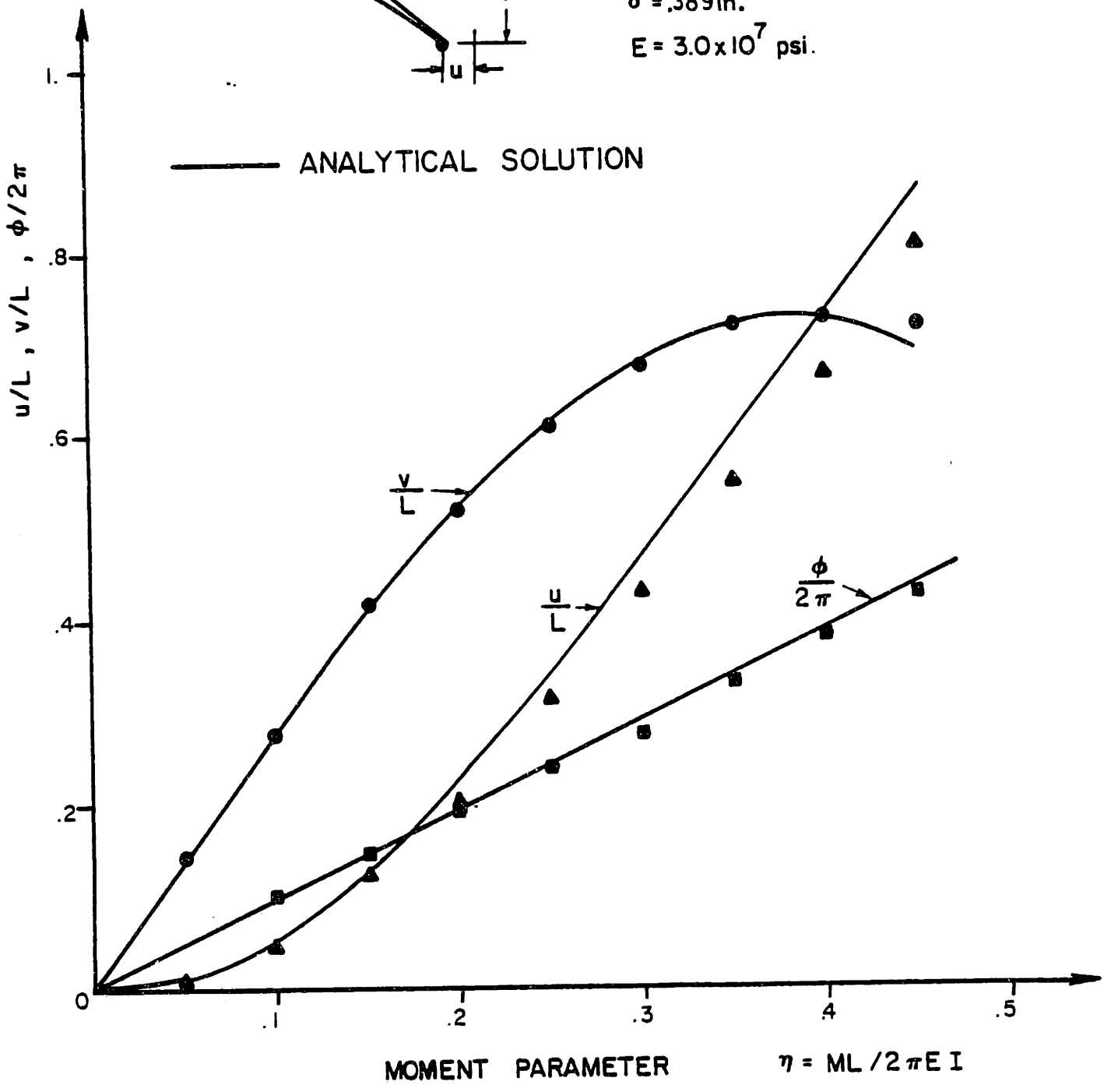


FIGURE 7.31 Large Displacement Response of a Cantilever Using One 4-node Element.

## 8. CONCLUSIONS

A simple and effective pipe elbow element has been formulated for linear and nonlinear analysis. The element exhibits various important features that make it a state-of-the-art tool for piping analysis:

- the ovalization varies cubically along the length of the element,
- the element can be employed to model elbows of different curvatures, elbow-straight pipe intersections, and elbows clamped to rigid flanges,
- pressure stiffening effects are included, and
- the element can be used in elastic-plastic nonlinear analysis.

With these features the element is significantly more effective than other previously published analysis tools for various piping analyses.

Although a geometric nonlinear formulation is also presented, this formulation does not include the geometric nonlinearities in the ovalization displacements and is therefore still of limited value.

Considering future work for further developments of the element, the following important research areas should be considered:

1. The element formulation for linear analysis has been derived in detail but a further study would be valuable in which the limits of applicability of the element are identified.

Various sample solutions are presented in this thesis, but a more detailed investigation considering the element sizes required for certain problems and the element applicability to pipe geometries, boundary conditions and loading conditions would be valuable.

2. The geometric nonlinear formulation should be refined to include the nonlinearities in the ovalization model. In this thesis, only the geometric nonlinearities of the beam deformation modes have been considered and tested. The appropriate nonlinear ovalization terms to be included in the formulation may be identified using shell theory. Once these nonlinear terms are included in the formulation, the geometric buckling behavior of elbows can be analyzed.

3. Piping structures are frequently subjected to high temperatures and creep effects. The analysis of displacements and stresses including these effects could be achieved by extending the element formulation, but an investigation would be required to identify whether the appropriate kinematic assumptions are made for such analysis.

4. Dynamic analysis using the element was not considered in this thesis. The construction of appropriate mass matrices requires further research. In particular, if the element is to be used in explicit time integration. In this case the ovalization modes may govern the time step that can be employed for stability of the integration.

5. In the nonlinear analysis, numerical integration is employed. The cost of calculating the element matrices is

directly proportional to the number of integration stations used. An investigation in the use of numerical integration would be valuable with the objective to identify an optimum scheme.

## REFERENCES

- [1] Rodabaugh, E.C. and Pickett, A.G., "Survey Report on Structural Design of Piping Systems and Components," USAEC Report TID-25553. Division of Technical Information, Dec. 1970.
- [2] Von Kármán, T., "Über die Formänderung Dünnwandliger Röhre, Insbesondere Federnder Ausgleichröhre," Zeitschrift des Vereines deutscher Ingenieure," vol. 55, pp. 1889-1895, 1911.
- [3] Hovgaard, W., "The Elastic Deformation of Pipe Bends," Journal of Mathematics and Physics, M.I.T., vol. 6, n. 2, pp. 69-118, 1926.
- [4] Vigness, I. "Elastic Properties of Curved Tubes," Trans. ASME, vol. 65, pp. 105-120, 1943.
- [5] Beskin, L., "Bending of Curved Thin Tubes," J. Appl. Mech., pp. A1-7, March 1945.
- [6] Pardue, T.W. and Vigness, I., "Properties of Thin-Walled Curved Tubes of Short-Bend Radius," Trans. ASME, vol. 73, pp. 77-84, 1951.
- [7] Reissner, E., "On Bending of Curved Thin-Walled Tubes", Proc. Natl. Acad. Sci. U.S., vol. 35, pp. 204-208, 1949.
- [8] Clark, R.A., and Reissner, E., "Bending of Curved Tubes," Advances in Applied Mechanics, vol. 2, pp. 93-122, 1951.
- [9] Tueda, M., "Mathematical Theories of Bourdon Pressure Tubes and Bending of Curved Pipes," 1st and 2nd Reports, College of Eng. Memoirs, Kyoto Imp. Univ., vol. 8, pp. 102-115, 1934-1935, and Vol. 9, pp. 132-152, 1936.
- [10] Gross, N. and Ford, H., "The Flexibility of Short-Radius Pipe Bends," Proc. Inst. Mech. Eng., vol. 166, pp. 480-491, 1952.
- [11] Turner, C.E. and Ford, H., "Examination of the Theories for Calculating the Stresses in Pipe Bends Subject to In-Plane Bending," Proc. Inst. Mech. Engrs., vol. 171, pp. 513-525, 1957.



- [12] Smith, R.T., "Theoretical Analysis of the Stresses in Pipe Bends Subjected to Out-of-Plane Bending," J. Mech. Eng. Sci., vol. 9, n. 2, p. 115-123, 1967.
- [13] Jones, N., "In-Plane Bending of a Short-Radius Curved Pipe Bend," J. Eng. for Ind., vol. 89, pp. 271-277, 1967.
- [14] Cheng, D.H., Thailer, H.J., "On Bending of Curved Circular Tubes," J. Eng. for Ind., vol. 92, pp. 62-66, 1970.
- [15] Dodge, W.G. and Moore, S.E., "Stress Indices and Flexibility Factors for Moment Loadings on Elbows and Curved Pipes," Welding Research Council Bulletin 179, Dec. 1972.
- [16] Robert, A., and DuFloret, C., "Analysis of the Flexibility and the Stresses in Curved Pipes Subjected to In-Plane or Out-of-Plane Bending", 2nd Int. Conference on Pressure Vessel Tech., Part I - Design and Analysis, San Antonio, Texas, Oct. 1973.
- [17] Iwata, K., Asai, S. and Takeda, H., "A New Finite Element for Structural Analysis of Piping Systems", 5th SMiRT Conf., paper M 5/5, 1979.
- [18] Hellen, T.K., "An Analysis of a Pipe Bend Subjected to In-Plane Loads", Compilation of Piping Benchmark Problems-- Cooperative International Effort, Report IWGFR/27, IAEA, June 1979.
- [19] Bathe, K.J., Finite Element Procedures in Engineering Analysis, Prentice-Hall, Inc., 1981
- [20] Whatham, J.F., "The Use of Finite Element Code SAP-4 to Analyze the Stresses Produced in Curved Pipes by Pure In-Plane Bending", 2nd SAP-Conference, U. of Southern Calif., Los Angeles, June 23-24, 1977.
- [21] Shimizu, T. et al., "Some Experiences on Elastic-Plastic Analysis of Shell Structure," in Applications Using ADINA, Proceedings of the ADINA Conference, Aug. 1977, Bathe, K.J. (ed.), Report AVL-82448-6, Department of Mechanical Engineering, M.I.T., Aug. 1977.
- [22] Hibbitt, H.D., "Special Structural Elements for Piping Analysis", Pressure Vessels and Piping Conference, Miami Beach, Florida, June 24-28, 1974.
- [23] MARC-CDC, Nonlinear Finite Element Analysis Program, MARC Analysis Corporation, Palo Alto, California, and Control Data Corporation, Minneapolis, Minnesota, 1974.

- [24] Ohtsubo, H. and Watanabe, O., "Stress Analysis of Pipe Bends by Ring Elements," J. of Press. Vessel Tech., vol. 100, pp. 112-122, Feb. 1978.
- [25] Thompson, J.J. "Shell Theory Analysis of Pure In-Plane Bending of a Pipe Bend," 3rd SMiRT Conf., paper F 6/1, Sept. 1975.
- [26] Kalnins, A., "Stress Analysis of Curved Tubes", 1st International Conf. on Pressure Vessel Technology, Delft, Netherlands, Sept-Oct. 1969.
- [27] Sobel, L.H., "In-Plane Bending of Elbows," J. Computers and Structures, vol. 7, pp. 701-715, 1977.
- [28] Bathe, K.J., "Finite Element Formulation, Modeling and Solution of Nonlinear Dynamic Response," Chapter in Numerical Methods for Partial Differential Equations, Academic Press, 1979.
- [29] Novozhilov, V.V., Thin Shell Theory, Translated by P.G. Lowe, P. Noordhoff Ltd., Groningen, Netherlands, 1964.
- [30] Kirchhoff, G., "Vorlesungen über Mathematische Physik, Vol. 1, Mechanik, 1876.
- [31] do Carmo, M.P., Differential Geometry of Curves and Surfaces, Prentice-Hall, 1976.
- [32] Zienkiewicz, O.C., The Finite Element Method, McGraw-Hill, 1977.
- [33] Ramm, E., "A Plate/Shell Element for Large Deflections and Rotations", in Formulations and Computational Algorithms in Finite Element Analysis, Bathe, K.J., Oden, J.T., and Wunderlich, W. (Eds.), M.I.T. Press, 1977.
- [34] Kråkeland, B., and Mo, O., "Nonlinear Analysis of Stiffened Shells," Proc. 7th Structural Analysis S.I.G. Meeting, Nice, France, Oct. 1978.
- [35] Bathe, K.J., and Bolourchi, S., "A Geometric and Material Nonlinear Plate and Shell Element", J. Comp. and Struct., vol. 11, pp. 961-985, 1980.
- [36] Vissat, P. L., and del Buono, A. J., "In-Plane Bending Properties of Welding Elbows", Trans. ASME, vol. 77, pp. 161-171, 1955.
- [37] Whatham, J. F., "In-Plane Bending of Flanged Elbows,"

Proceedings, Metal Structures Conference, the Institution of Engineers, Australia, Perth, Nov. 30-Dec. 1, 1978.

- [38] Imamasa, J., and Uragami, K., "Experimental Study of Flexibility Factors and Stresses of Welding Elbows with End Effects", 2nd. Int. Conf. on Press. Vessel Tech., San Antonio, Texas, Paper I-30, pp. 417-426, Oct. 1973.
- [39] Jacobs, R.L., and Surosky, H., "Experimental Investigation of the effects of end conditions and bend angle on the stress distribution of welded elbows", NSRDC, Annapolis Div., Reports 2835-Phase I (Nov. 1973) and 3044-Phase II (Sept. 1969).
- [40] Rodabaugh, E. C., Iskander, S.K., and Moore, S. E., "End Effects on Elbows Subjected to Moment Loadings", Report ORNL-2913/7, March 1978.
- [41] Thailer, H.J., and Cheng, D.H., "In-Plane Bending of a U-Shaped Circular Tube with End Constraints", J. of Eng. Ind., vol. 92, No. 4, pp. 792-796, 1970.
- [42] Findlay, G.E., and Spence, J., "The Effects of Flanges on Smooth Pipe Bends in Piping Systems", 2nd SMIRT Conf., Berlin, paper F3/5, Sept. 10-14, 1973.
- [43] Matarajan, R., and Blomfield, J.A., "Stress Analysis of Curved Pipes with end Restraints", J. Comp. Struc., vol. 5, pp. 187-196, 1975.
- [44] Courant, R., "Variational Methods for the Solution of Problems of Equilibrium and Vibrations", Am. Math. Soc. Bull., vol. 49, pp. 1-23, 1943.
- [45] Moe, J., "Penalty-function Methods", Chapter in Optimum Structural Design-Theory and Applications, Gallagher, R.H., and Zienkiewicz, O.C., Eds., John Wiley, 1973.
- [46] Zienkiewicz, O.C., and Heinrich, J.C., "A Unified Treatment of Steady-State Shallow Water and Two-Dimensional Navier-Stokes Equations -- Finite Element Penalty Function Approach", FENOMECH - Proceedings Int. Conf. on Finite Element in App. Mech., Stuttgart, German, pp. 673-698, Aug 30-Sept. 1, 1978.
- [47] Zienkiewicz, O.C., et al., "A Simple and Efficient Element for Axisymmetric Shells", Int. J. Num. Meth. Eng., vol. 11, pp. 1545-1558, 1977.
- [48] Felippa, C.A., "Iterative Procedures for Improving Penalty Function Solutions of Algebraic Systems", Int. J. Num.

- Meth. Eng., vol. 12. pp. 821-836, 1978.
- [49] Bathe, K.J., and Almeida, C.A., "A Simple and Effective Pipe Elbow Element - Interaction Effects", J. App. Mech., to appear.
- [50] Oden, J.T., "Exterior Penalty Methods for Contact Problems in Elasticity", Nonlinear Finite Element Analysis in Structural Mechanics, W. Wunderlich, et al., Eds., Springer-Verlag, Berlin, 1981.
- [51] Thuloup, M.A., "Essai sur la Fatigue des Tuyaux Minces à Fibre Moyenne Plane au Gauche", Bull. de l'Assoc. Tech. Aeron., vol. 32, pp. 643-680, 1928.
- [52] Bathélemy, J., "Étude de la Déformation et des Tensions Internas des Tuyaux a Ligne Moyenne Plane Soumis a des Efforts Extérieurs et a Une Pression Interne", Bull. de l'Assoc. Marit. Aeron., v. 46, pp. 411-458, 1947.
- [53] Kafka, P.G., and Dunn, M.B., "Stiffness of Curved Circular Tubes with Internal Pressure", J. Appl. Mech., v. 78, pp. 247-254, 1956.
- [54] Rodabaugh, E. C., and George, H. H., "Effect of Internal Pressure on Flexibility and Stress-Intensification Factors of Curved Pipe or Welding Elbows", J. Appl. Mech., v. 79, pp. 939-948, 1957.
- [55] Dean, W.R., "The Distortion of a Curved Tube due to Internal Pressure", Phil. Mag., Ser. 7, v. 28, pp. 452-464, 1939.
- [56] Crandall, S.H., and Dahl, N.C., "The Influence of Pressure on the Bending of Curved Tubes", Proc. of Ninth Int. Conf. Appl. Mech., v. 6, pp. 331-343, Brussels, 1957.
- [57] Reissner, E., "On Finite Bending of Pressurized Tube", J. Appl. Mech., v. 81, pp. 386-392, 1959.
- [58] Blomfield, J.A., and Turner, C.E., "Theory of Thin Elastic Shells Applied to Pipe Bends Subjected to Bending and Internal Pressure", J. Strain Anal., v. 7, N. 4, pp. 285-293, 1972.
- [59] Whatham, J.F., and Thompson, J.J. "The Bending and Pressurizing of Pipe Bends with Flanged Tangents", J. Nuclear Eng. and Dgn., vol. 54, pp. 17-28, 1979.
- [60] Biot, M.A., Mechanics of Incremental Deformations, J.

Wiley & Sons, 1965.

- [61] Bathe, K.J., Ramm, E. and Wilson, E.L., "Finite Element Formulations for Large Deformation Dynamic Analysis", *Int. J. Num. Meth. Eng.*, vol. 9, pp. 353-386, 1975.
- [62] Malvern, L.E., Introduction to the Mechanics of a Continuous Medium, Prentice-Hall, Inc., Englewood Cliffs, New Jersey, 1969.
- [63] Fung, Y.C., Foundations of Solid Mechanics, Prentice-Hall, Inc., 1965.
- [64] Prager, W., Introduction to the Mechanics of Continua, Dover, 1973.
- [65] Hibbitt, J.T., Marcal, P.V., and Rice, J.R., "Finite Element Formulations for Problems of Large Strain and Large Displacements", *Int. J. Solids Struct.*, vol. 6, pp. 1069-1086, 1970.
- [66] Key, S.W., "A Finite Element Procedure for the Large Deformation Dynamic Response of Axisymmetric Solids", *Comp. Meth. in Appl. Mech. and Eng.*, vol. 4, pp. 195-218, 1974.
- [67] Bathe, K.J., "ADINA - Finite Element Program for Automatic Dynamic Incremental Nonlinear Analysis", Report 82448-1, Acoustics and Vibration Lab., Mechanical Engineering Dept., M.I.T., September 1975 (rev. Dec. 1978).
- [68] Bathe, K.J. and Bolourchi, S., "Large Displacement Analysis of Three-Dimensional Beam Structures", *Int. J. Num. Eng.*, vol. 14, pp. 961-985, 1979.
- [69] Bathe, K.J., "Static and Dynamic Geometric and Material Nonlinear Analysis Using ADINA", Acoustics and Vibration Lab., Report 82448-2, Dept. of Mechanical Eng., M.I.T., May 1977.
- [70] Hill, R., The Mathematical Theory of Plasticity, Clarendon Press, Oxford, England, 1950.
- [71] Hughes, T.J.R., Taylor, R.L., and Kanoknukulchai, W., "A Simple and Efficient Finite Element for Plate Bending", *Int. J. Num. Meth. in Eng.*, vol. 11, pp. 1529-1543, 1977.
- [72] Seely, F.B., Resistence of Materials, John Wiley & Sons NY, 1935.

- [73] MARC-CDC, Nonlinear Finite Element Analysis Program, MARC Analysis Corporation, Palo Alto, Calif., and Control Data Corporation, Minneapolis, Minn., 1974.
- [74] Smith, R.T. and Ford, H., "Experiments on Pipelines and Pipe Bends Subjected to Three-Dimensional Loading", J. Mech. Eng. Sci., vol. 9, N.2, pp. 124-137, 1967.
- [75] Bathe, K.J., and Ho, L.W., "A Simple and Effective Element for Analysis of General Shell Structures", Journal Computer and Structures, vol. 13, pp.673-687, 1981.
- [76] Bathe, K.J., and Almeida, C.A., "A Simple and Effective Pipe Elbow Element - Linear Analysis", ASME J. of Appl. Mechanics, vol.47, N.1, pp.93-100, 1981.

## APPENDIX A

In this Appendix the rules for the differentiation of a set of orthogonal unit vectors  $\underline{e}_\eta$ ,  $\underline{e}_\xi$  and  $\underline{e}_\zeta$  are presented. First, consider two neighboring points  $P_1$  and  $P_2$  on the line of principal curvilinear coordinates  $s_1$  of the pipe midsurface, see Fig. A.1(a). The vector change of the normal  $\underline{e}_\zeta$  along  $s_1$  leads to

$$\partial \underline{e}_\zeta = \partial \Psi \underline{e}_\eta \quad (\text{A.1})$$

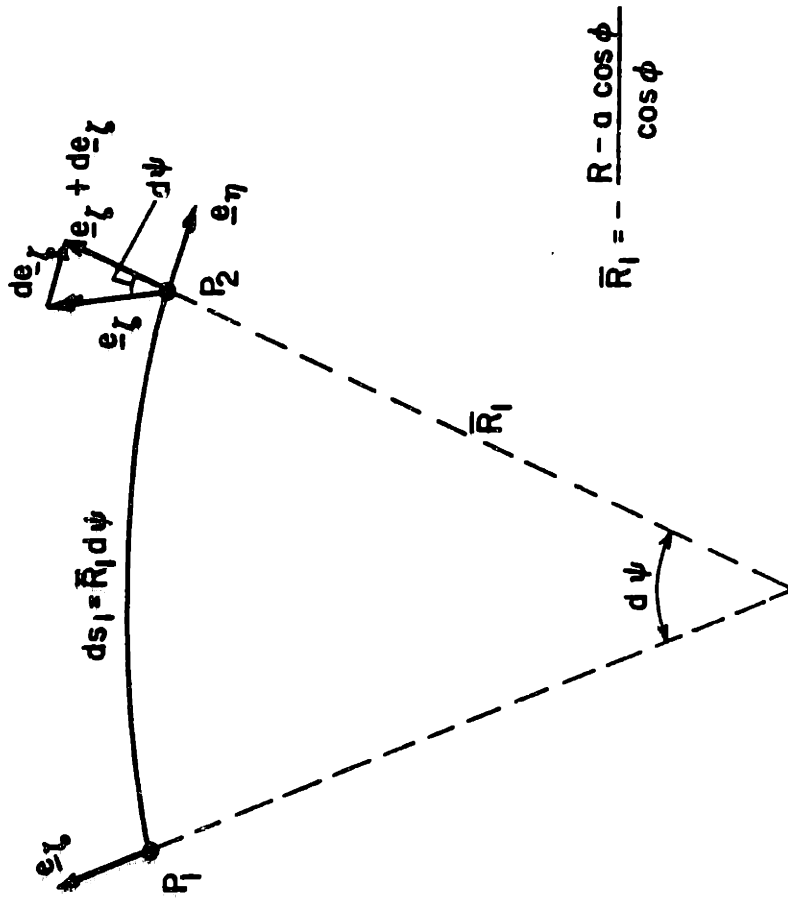
where  $\partial \Psi$  is a differential of the angular position measured at the center of curvature of  $s_1$  and  $\underline{e}_\eta$  is the unit vector tangent to  $s_1$ . Using Eq. (2.7), the angular coordinate  $\Psi$  and the first natural coordinate  $\theta$  are related by the equation

$$\partial \Psi = \frac{L_1}{\bar{R}_1} \partial \theta \quad (\text{A.2})$$

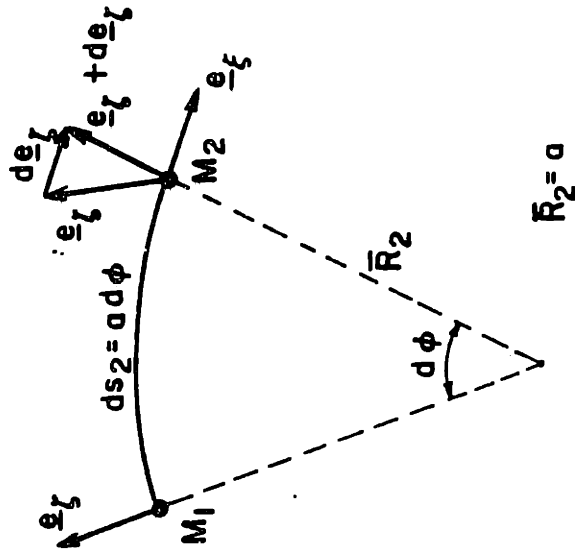
where  $L_1$  and  $\bar{R}_1$  are the Lamé parameter and the first principal curvature radius, respectively. Substituting for  $L_1$  and  $\bar{R}_1$ , see Fig. 2.2, into Eq. (A.2) and then into Eq. (A.1) we obtain

$$\frac{\partial \underline{e}_\zeta}{\partial \theta} = - \cos \phi \underline{e}_\eta \quad (\text{A.3})$$

Similarly, along the other line of principal curvature  $s_2$ , shown in Fig. A.1(b), the vector change of the normal with respect to the angular position  $\phi$  is



(a) NORMAL  $\underline{e}_\zeta$  ALONG  $s_1$



(b) NORMAL  $\underline{e}_\zeta$  ALONG  $s_2$

FIGURE A.1 The Pipe Midsurface Normal Along the Lines of Principal Coordinates.



$$\frac{\partial \underline{e}_\xi}{\partial \phi} = \underline{e}_\xi \quad (\text{A.4})$$

Consider now the evaluation of the derivatives of the unit vectors  $\underline{e}_\eta$  and  $\underline{e}_\xi$  of the pipe midsurface. First, we notice that,

$$\frac{\partial}{\partial \phi} \left( \frac{\partial \underline{r}}{\partial \theta} \right) = \frac{\partial}{\partial \theta} \left( \frac{\partial \underline{r}}{\partial \phi} \right) \quad (\text{A.5})$$

where  $\underline{r}$  is the midsurface position vector. Then, using the definition of unit vectors, Eqs. (2.9) and (2.10), in the above equation we have the following relation

$$\frac{\partial L_1}{\partial \phi} \underline{e}_\eta + L_1 \frac{\partial \underline{e}_\eta}{\partial \phi} = \frac{\partial L_2}{\partial \theta} \underline{e}_\xi + L_2 \frac{\partial \underline{e}_\xi}{\partial \theta} \quad (\text{A.6})$$

where  $L_1 = R - a \cos \phi$  and  $L_2 = a$ . Hence, combining equal terms of each side of Eq. A.6 we obtain,

$$\frac{\partial \underline{e}_\xi}{\partial \theta} = \sin \phi \underline{e}_\eta \quad (\text{A.7})$$

$$\frac{\partial \underline{e}_\eta}{\partial \phi} = 0$$

Further, consider the components of the derivative  $\frac{\partial \underline{e}_\eta}{\partial \theta}$  along the axes  $\underline{e}_\eta$ ,  $\underline{e}_\xi$  and  $\underline{e}_s$ . Since this derivative is perpendicular to the unit vector, it has obviously no component in the  $\underline{e}_\eta$  direction and its components on the remaining axes are given by

its dot product with these axes,

$$\frac{\partial \underline{e}_\eta}{\partial \theta} \cdot \underline{e}_\xi = \frac{\partial}{\partial \theta} (\underline{e}_\eta \cdot \underline{e}_\xi) - \underline{e}_\eta \cdot \frac{\partial \underline{e}_\xi}{\partial \theta} = -\sin \phi$$

and,

$$\frac{\partial \underline{e}_\eta}{\partial \theta} \cdot \underline{e}_\zeta = -\underline{e}_\eta \cdot \frac{\partial \underline{e}_\zeta}{\partial \theta} = \cos \phi$$

and therefore,

$$\frac{\partial \underline{e}_\eta}{\partial \theta} = -\sin \phi \underline{e}_\xi + \cos \phi \underline{e}_\zeta \quad (\text{A.8})$$

Similarly, the components of the derivative  $\frac{\partial \underline{e}_\xi}{\partial \phi}$  along  $\underline{e}_\eta$  and  $\underline{e}_\zeta$  axes are calculated in the same way, that is,

$$\frac{\partial \underline{e}_\xi}{\partial \phi} \cdot \underline{e}_\eta = -\underline{e}_\xi \cdot \frac{\partial \underline{e}_\eta}{\partial \phi} = 0 ; \frac{\partial \underline{e}_\xi}{\partial \phi} \cdot \underline{e}_\zeta = -\underline{e}_\xi \cdot \frac{\partial \underline{e}_\zeta}{\partial \phi} = -1$$

and therefore,

$$\frac{\partial \underline{e}_\xi}{\partial \phi} = -\underline{e}_\zeta \quad (\text{A.9})$$

Eqs. (A.3-4) and (A.7-9) form a set of formulae employed in the differentiation of vectors with given components on the local pipe midsurface axes of coordinates  $\underline{e}_\eta$ ,  $\underline{e}_\xi$  and  $\underline{e}_\zeta$ . This set of equations was used to establish Eqs. (2.12) and (2.13).